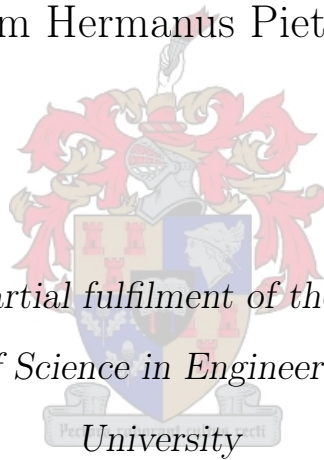


System Identification for Fault Tolerant Control of Unmanned Aerial Vehicles

by

Willem Hermanus Pietersen

*Thesis presented in partial fulfilment of the requirements for the
degree of Master of Science in Engineering at Stellenbosch*



Supervisor: Dr Iain Peddle

Department of Electrical and Electronic Engineering

March 2010

Declaration

By submitting this thesis electronically, I declare that the entirety of the work contained therein is my own, original work, that I am the owner of the copyright thereof (unless to the extent otherwise explicitly stated), and that I have not previously in its entirety or in part submitted it for obtaining any qualification.

March 2010

Copyright © 2010 Stellenbosch University

All rights reserved.

Abstract

In this project, system identification is done on the Modular Unmanned Aerial Vehicle (UAV). This is necessary to perform fault detection and isolation, which is part of the Fault Tolerant Control research project at Stellenbosch University.

The equations necessary to do system identification are developed. Various methods for system identification is discussed and the regression methods are implemented. It is shown how to accommodate a sudden change in aircraft parameters due to a fault. Smoothed numerical differentiation is performed in order to acquire data necessary to implement the regression methods.

Practical issues regarding system identification are discussed and methods for addressing these issues are introduced. These issues include data collinearity and identification in a closed loop.

The regression methods are implemented on a simple roll model of the Modular UAV in order to highlight the various difficulties with system identification. Different methods for accommodating a fault are illustrated.

System identification is also done on a full nonlinear model of the Modular UAV. All the parameters converges quickly to accurate values, with the exception of $C_{l_{\delta_R}}$, C_{n_P} and $C_{n_{\delta_A}}$. The reason for this is discussed. The importance of these parameters in order to do Fault Tolerant Control is also discussed.

An S-function that implements the recursive least squares algorithm for parameter estimation is developed. This block accommodates for the methods of applying the forgetting factor and covariance resetting. This block can be used as a stepping stone for future work in system identification and fault detection and isolation.

Opsomming

In hierdie projek word stelsel identifikasie gedoen op die Modulêre Onbemande Vliegtuig. Dit is nodig om foutopsporing en isolasie te doen wat 'n deel uitmaak van fout verdraagsame beheer.

Die vergelykings wat nodig is om stelsel identifikasie te doen is ontwikkel. Verskeie metodes om stelsel identifikasie te doen word bespreek en die regressie metodes is uitgevoer. Daar word gewys hoe om voorsiening te maak vir 'n skielike verandering in die vliegtuig parameters as gevolg van 'n fout. Reëlmatige numeriese differensiasie is gedoen om data te verkry wat nodig is vir die uitvoering van die regressie metodes.

Praktiese kwessies aangaande stelsel identifikasie word bespreek en metodes om hierdie kwessies aan te spreek word gegee. Hierdie kwessies sluit interafhanklikheid van data en identifikasie in 'n geslote lus in.

Die regressie metodes word toegepas op 'n eenvoudige rol model van die Modulêre Onbemande Vliegtuig om die verskeie kwessies aangaande stelsel identifikasie uit te wys. Verskeie metodes vir die hantering vir 'n fout word ook illustreer.

Stelsel identifikasie word ook op die volle nie-linêre model van die Modulêre Onbemande Vliegtuig gedoen. Al die parameters konvergeer vinnig na akkurate waardes, met die uitsondering van $C_{l_{\delta_R}}$, C_{n_P} and $C_{n_{\delta_A}}$. Die belangrikheid van hierdie parameters vir fout verdraagsame beheer word ook bespreek.

'n S-funksie blok vir die rekursiewe kleinste-kwadraat algoritme is ontwikkel. Hierdie blok voorsien vir die metodes om die vergeetfaktor en kovariansie herstelling te implementeer. Hierdie blok kan gebruik word vir toekomstige werk in stelsel identifikasie en foutopsporing en isolasie.

Acknowledgements

I would like to extend my gratitude to the following people:

- Dr. Iain Peddle, my supervisor, for the excellent guidance and feedback during the past two years.
- AM de Jager, for the excellent feedback on my thesis. Also for being a friend when I most needed one.
- Chris Jaquet, for all the help with Matlab plots, latex and other technical stuff.
- Pieter Muller and Marike Nel for the awesome coffee breaks during the past two years.
- Simon for being an awesome friend whom I can trust with anything.
- Marcel and the first-year guys for your support and entertainment.
- Dieter and Reinhart for providing a place to stay when the residence was closed for holidays.
- My family for their love and support.
- My fiancée, Danielle Kulenkampff, for all your love and support and all the lunch packed with love.
- Most importantly, to God, who guides me through life and gave me this opportunity of doing my Masters. Thank you God!

Contents

Declaration	i
Abstract	ii
Opsomming	iii
Acknowledgements	iv
Contents	v
List of Figures	vi
List of Tables	vii
Nomenclature	viii
1 Introduction	1
1.1 Background	1
1.2 Fault Tolerant Control Overview	2
1.3 Short History of System Identification Applied to Aircraft	5
1.4 Outline of this Document	6
2 Aircraft Model	7
2.1 Introduction	7
2.2 Definitions	7

2.2.1	Axis system definitions	8
2.2.1.1	Inertial Axis System	8
2.2.1.2	Body Axis System	8
2.2.1.3	Wind Axis System	9
2.2.2	Definition of Aircraft Control Surfaces	10
2.3	Aircraft Model Overview	11
2.4	Outer Loop Model - Point Mass Kinematics	12
2.4.1	Velocity Dynamics	12
2.4.2	Position Dynamics	14
2.4.3	Attitude Dynamics	14
2.5	Inner Loop Model - Aircraft Specific Forces and Moments	15
2.5.1	Rigid Body Rotational Dynamics	16
2.5.2	Specific Forces and Moments	19
2.6	Conclusion	22
3	System Identification Methods	23
3.1	Introduction	23
3.2	Parameter Estimation Models	23
3.2.1	Estimator for the Bayesian Model	24
3.2.2	Estimator for the Fisher Model	25
3.2.3	Estimator for the Least-Squares Model	26
3.3	Overview of Identification Methods	26
3.3.1	Batch Methods	27
3.3.1.1	The Filter-Error Method	27
3.3.1.2	Frequency Domain Methods	28
3.3.2	Real-Time Methods	28
3.3.2.1	Extended Kalman Filter	29
3.4	Regression Methods Theory	30
3.4.1	Ordinary Least Squares	31
3.4.2	Recursive Least Squares	33

3.4.3	Accommodating Changing Parameter Values	36
3.4.3.1	The Forgetting Factor	36
3.4.3.2	Covariance Resetting	37
3.5	Conclusion	37
4	Applying Regression Methods	39
4.1	Introduction	39
4.2	Setting Up the Regression Equations	39
4.3	Estimating Aerodynamic Force and Moment Coefficients	41
4.3.1	Smoothed numerical differentiation	42
4.3.1.1	Example of Fitting a Second Order Curve to Five Data Points	42
4.3.1.2	Averaging and Differential Kernels	45
4.4	Conclusion	47
5	Parameter Identifiability	48
5.1	Introduction	48
5.2	Data Collinearity	48
5.2.1	Standardised Regressors	49
5.2.2	Detection of Data Collinearity	51
5.3	Input Design	51
5.3.1	Impulse	52
5.3.2	Frequency Sweeps	53
5.3.3	Multisine Inputs	55
5.3.4	Doublets and Multisteps	59
5.4	Determining the Natural Frequency of the Aircraft Modes	62
5.4.1	The Short Period Mode	62
5.4.2	The Dutch Roll Mode	63
5.4.3	Roll Mode	64
5.5	System Identification in a Closed Loop	65

5.6	Conclusion	66
6	Simulation Results	67
6.1	Introduction	67
6.2	Simple Roll Model	68
6.2.1	Effects of Noise Filtering	69
6.2.2	Testing for Data Collinearity	73
6.2.3	Demonstrating the Effects of the Excitation Signal . . .	77
6.2.4	Effects of the forgetting factor and covariance resetting .	79
6.3	Full Nonlinear Modular UAV Model	81
6.3.1	Design of the Excitation Signals	82
6.4	Effect of Superimposing Excitation Signals	83
6.5	Conclusion	85
6.5.1	Conclusion for the Simple Roll Model	85
6.5.2	Conclusion for the Full Nonlinear Modular UAV Model .	85
6.6	Parameter Estimation Results	86
6.6.1	Estimated Parameters for the Roll Moment Coefficient .	87
6.6.2	Estimated Parameters for the Pitch Moment Coefficient .	88
6.6.3	Estimated Parameters for the Yaw Moment Coefficient .	89
6.6.4	Estimated Parameters for the Drag Force Coefficient . .	90
6.6.5	Estimated Parameters for the Side Force Coefficient . . .	91
6.6.6	Estimated Parameters for the Lift Force Coefficient . . .	92
7	Summary and Recommendations	93
7.1	Summary	93
7.2	Recommendations	95
	Appendices	96
A	Mathematical Principles and Equations	97
A.1	Moment of Inertia	97

A.2	Cross Product Transformation Matrix	98
A.3	Derivative of a Vector in a Rotating Reference Frame	98
A.4	Direction Cosine Matrix (DCM)	99
A.5	Euler Angles	99
A.6	Special Rotation Matrices	100
B	Specifications for the Modular UAV	101
B.1	Engine	101
B.2	Physical Specifications	102
B.3	Stability Derivatives	102
B.4	Control Derivatives	103
	Bibliography	104

List of Figures

1.1	A 3D model of the modular UAV	2
1.2	Fault Detection and Isolation (FDI) is performed using estimated data from system identification [1]	3
1.3	Fault Tolerant Control (FTC) architecture [1]	3
2.1	Definition of the inertial axis system	8
2.2	Definition of the body axis system	9
2.3	Definition of the wind axis system	10
2.4	Aircraft model overview [2]	11
3.1	Geometric interpretation of the least squares estimate	32
4.1	Demonstrating how to obtain the derivative of noisy data by fitting a second order curve to the last five data points	43
5.1	Impulse input	53
5.2	Linear frequency sweep input	54
5.3	Logarithmic frequency sweep input	55
5.4	Relative peak factors for a two-component multisine input	57
5.5	Multisine input with low RPF of 1.1	58
5.6	Multisine input with high RPF of 1.24	58
5.7	Doublet input	59
5.8	3-2-1-1 input	60

5.9	2-1-1 input	61
5.10	Compound doublet input	62
6.1	Measured P and filtered C_l obtained by fitting a second order curve to 40 measurements of roll rate	70
6.2	True and filtered \bar{P} obtained by fitting a second order curve to 40 measurements of roll rate	71
6.3	Measured and filtered C_l obtained by fitting a second order curve to 40 measurements of roll rate	72
6.4	Measured and filtered \bar{P} obtained by fitting a fifth order curve to the last 40 measurements of the roll rate	73
6.5	Measured and filtered C_l obtained by fitting a fifth order curve to the last 40 measurements of the roll rate	73
6.6	The standardised regressors	74
6.7	One of the standardised regressors negative demonstrating collinearity	75
6.8	The standardised regressors	76
6.9	One of the standardised regressors negative demonstrating collinearity	76
6.10	Standardised regressors demonstrating a reduction in collinearity by superimposing an excitation signal on δ_A	77
6.11	The estimated parameters over time with no excitation signal	78
6.12	The estimated parameters over time with a superimposed doublet on the aileron command	79
6.13	The estimated parameters over time with a fault at $t = 10$ and a forgetting factor of 0.98	80
6.14	The estimated parameters over time when implementing covariance resetting every five seconds	81
6.15	The doublets superimposed on the control signals in order to excite the natural modes of the Modular UAV	83
6.16	\bar{V} , α and β for the 20 second simulation time	84
6.17	Actuator deflections for the 20 second simulation time	84

6.18 Estimated parameters for the roll moment coefficient, C_l 87

6.19 Estimated parameters for the pitch moment coefficient, C_m 88

6.20 Estimated parameters for the yaw moment coefficient, C_n 89

6.21 Estimated parameters for parasitic drag C_{D_0} 90

6.22 Estimated parameters for the side force coefficient, C_y 91

6.23 Estimated parameters for the lift force coefficient, C_L 92

List of Tables

2.1	Definition of aircraft control surfaces	10
4.1	The averaging and differential kernels	46
6.1	Values used for the simple roll model of the Modular UAV	68
6.2	The values of the stability and control derivatives for the simple roll model	69
6.3	Estimated and true parameters with no excitation signal	78
6.4	Estimated and true parameters with a superimposed doublet on the aileron command	78
6.5	The values of the stability and control derivatives for the simple roll model with failed right aileron at -10 degrees	80
6.6	The values of the stability and control derivatives for the simple roll model with failed right aileron at -10 degrees	80
6.7	The values of the stability and control derivatives after implementing covariance resetting	81
6.8	Estimated and true parameters for the roll moment coefficient C_l .	87
6.9	Estimated and true parameters for the pitch moment coefficient C_m	88
6.10	Estimated and true parameters for the yaw moment coefficient C_n .	89
6.11	Estimated and true parameter for parasitic drag C_{D_0}	90
6.12	Estimated and true parameters for the side force coefficient C_y . . .	91
6.13	Estimated and true parameters for the lift force coefficient C_L . . .	92

B.1 Engine specifications 101

B.2 Physical specifications of the modular UAV 102

B.3 Stability derivatives for the Modular UAV 102

B.4 Control derivatives for the Modular UAV 103

Nomenclature

Greek Letters

α	Angle of attack
β	Sideslip angle
δ_A	Aileron deflection
δ_E	Elevator deflection
δ_R	Rudder deflection
δ_T	Throttle deflection
Φ	Roll angle
ρ	Air density
Σ	Specific acceleration vector
θ	Vector of parameters
$\hat{\theta}$	Vector of estimated parameters
Θ	Pitch angle
Ψ	Yaw angle

Lowercase Letters

\mathbf{a}	Vector of accelerometer measurements
--------------	--------------------------------------

a_x	Accelerometer measurement in the x body axis
a_y	Accelerometer measurement in the y body axis
a_z	Accelerometer measurement in the z body axis
b	Wing span
d	Number of past data values included for weighting with the forgetting factor
m	Aircraft mass
n	Order of the curve used for curve fitting
p	Number of data points used for curve fitting
s_{δ_x}	Excitation signal augmented on the actuator command denoted by x
\mathbf{y}	Vector of system outputs
\mathbf{z}	Vector of measurements

Uppercase Letters

\mathcal{R}	Aspect ratio
C_D	Aerodynamic drag coefficient
C_l	Aerodynamic roll moment coefficient
C_L	Aerodynamic lift coefficient
C_m	Aerodynamic pitching moment coefficient
C_n	Aerodynamic yaw moment coefficient
C_X	Axial aerodynamic force coefficient
C_Y	Lateral aerodynamic force coefficient

C_Z	Normal aerodynamic force coefficient
\mathbf{F}	Vector of total forces in body axis
\mathbf{F}_A	Vector of aerodynamic forces in body axis
\mathbf{F}_G	Vector of gravitational forces in body axis
\mathbf{F}_T	Vector of thrust forces in body axis
I_x	Moment of inertia about the roll axis
I_y	Moment of inertia about the pitch axis
I_z	Moment of inertia about the yaw axis
I_{xy}	Roll and pitch product of inertia
I_{xz}	Roll and yaw product of inertia
I_{yz}	Pitch and yaw product of inertia
L	Roll moment
M	Pitch moment
N	Yaw moment
P	Roll rate
Q	Pitch rate
R	Yaw rate
S	Wing area
X	Axial force
\mathbf{X}	Matrix of regressors
Y	Lateral force

Z Normal force

Subscripts

0 Trim values

B Body axis

a The augmented version

Acronyms

AVL Athena Vortex Lattice

CSIR Council for Scientific and Industrial Research

FDI Fault Detection and Isolation

FTC Fault Tolerant Control

IFAC The International Federation of Automatic Control

IMU Inertial Measurement Unit

ML Maximum Likelihood

PF Peak Factor

RPF Relative Peak Factor

SID System Identification

SU Stellenbosch University

UAV Unmanned Aerial Vehicle

VIF Variance Inflation Factor

WLS Weighted Least-Squares

Chapter 1

Introduction

1.1 Background

According to Klein [3], system identification is one of three general problems in system analysis. The three problems are as follows:

1. Simulation: given the input \mathbf{u} and the system \mathbf{S} , find the output \mathbf{y} ;
2. Control: given the system \mathbf{S} and the output \mathbf{y} , find the input \mathbf{u} ;
3. System identification: given the input \mathbf{u} and output \mathbf{y} , find the system \mathbf{S} .

This project is part of a larger joint project done by postgraduate students from Stellenbosch University (SU) and the Council for Scientific and Industrial Research (CSIR) entitled *Fault Tolerant Control (FTC) of the Modular Unmanned Aerial Vehicle (UAV)*. The aim of this larger project is to make the modular UAV capable of recovering from a single fault such as an actuator failure. The redundant design of the Modular UAV makes this possible, e.g. if an aileron fails, the flaps can be used to induce a roll moment. Figure 1.1 depicts a 3D model of the modular UAV.

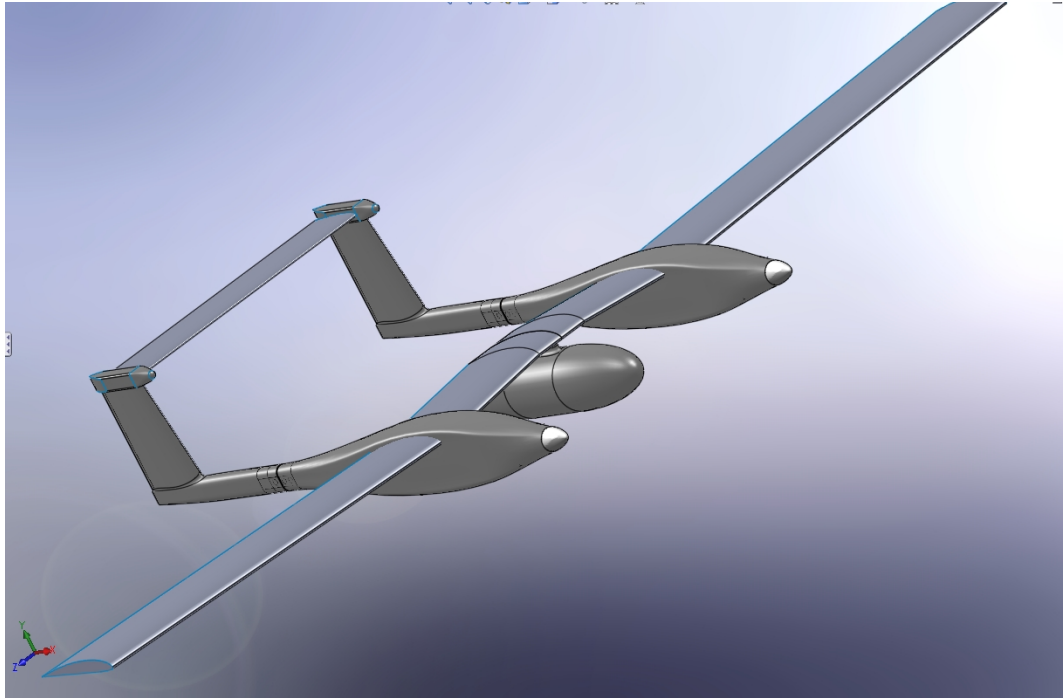


Figure 1.1: A 3D model of the modular UAV

1.2 Fault Tolerant Control Overview

Figure 1.2 serves to explain how System Identification (SID) can be used to detect the event of a fault as presented in [1]. System identification continuously provides estimated control and stability derivatives of the aircraft. Fault detection algorithms continuously monitor the estimated parameters. When a drastic change in the estimated parameters occur, a fault is detected and appropriate action can be taken to isolate this fault. This process is called Fault Detection and Isolation (FDI).

Figure 1.3 serves to explain where Fault Detection and Isolation fits into Fault Tolerant Control as presented in [1]. It can be seen that the Fault Tolerant Control system is broken down into five levels.

At the lowest level on the right of Figure 1.3 is the *Physical Aircraft Layer* with its individual actuators, natural stability, etc. A 3D model of the Modular UAV is shown in Figure 1.1. For this configuration, the Modular UAV has

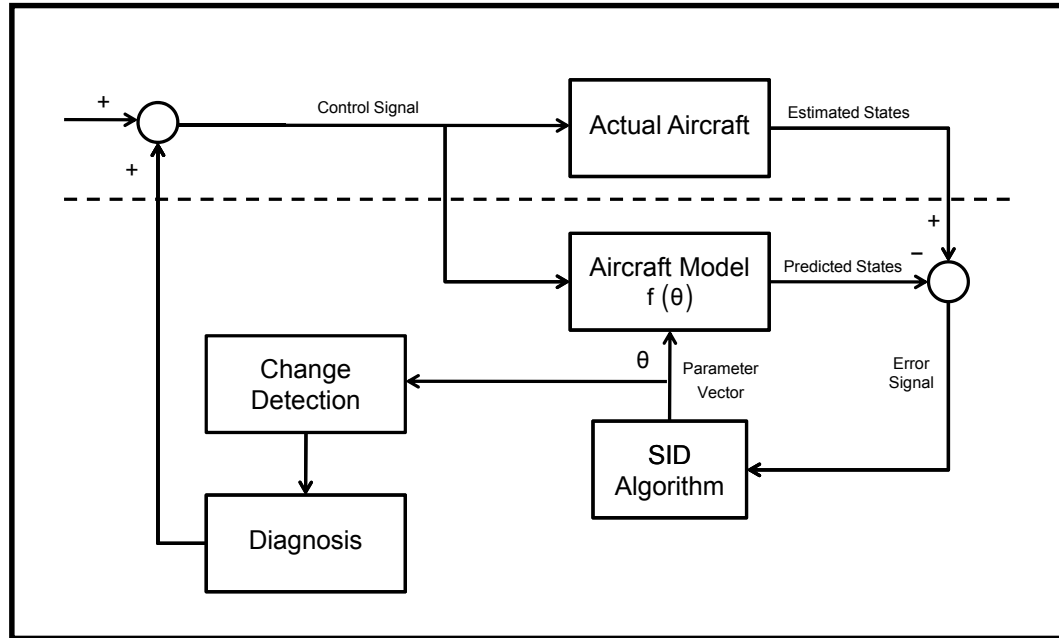


Figure 1.2: Fault Detection and Isolation (FDI) is performed using estimated data from system identification [1]

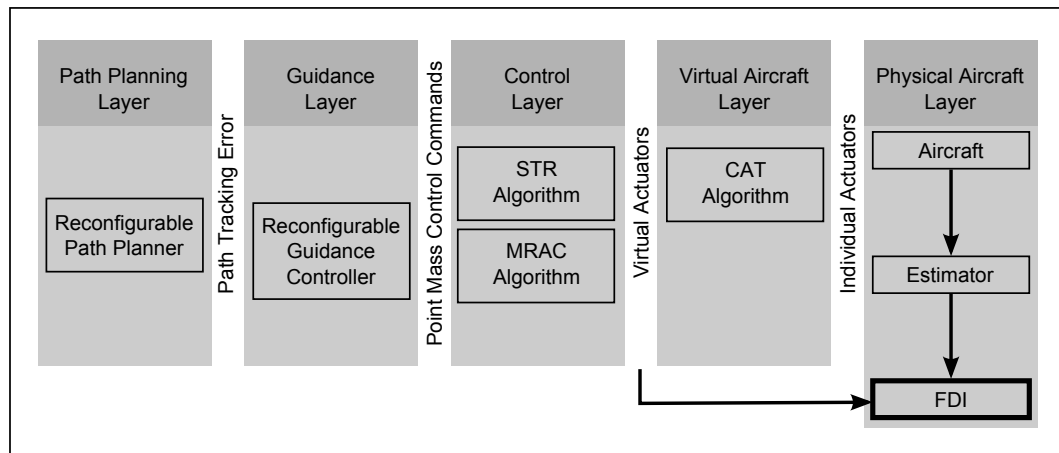


Figure 1.3: Fault Tolerant Control (FTC) architecture [1]

two fuselages, two engines, two rudders, a set of ailerons, a set of flaps and an elevator. The Fault Detection and Isolation (FDI) block can be seen at the bottom of the *Physical Aircraft Layer*. System identification algorithms are used for fault detection. For this project, the inputs used for system identification comes from the virtual actuators as shown and not on the individual

actuators, thus system identification is done on the *virtual aircraft*. The structure of the model for the virtual aircraft is known and discussed in Chapter 2, therefore from this point forward the term *system identification* only refers to the estimation of the non-dimensional stability and control derivatives (hereafter referred to as the parameters) of the aircraft. These parameters are introduced in §2.5.

The *Virtual Aircraft Layer* serves the purpose of presenting a simple, consistent abstraction of the physical aircraft to the *Control Layer*. The *Virtual Aircraft Layer* thus includes a section which converts virtual actuator commands (such as aileron, elevator, rudder and throttle) to the individual actuator commands and is reconfigurable to accommodate actuator failures. This reconfiguration process is part of the current research in Fault Tolerant Control on the modular UAV.

The *Control Layer* is responsible for augmenting the natural stability of the aircraft and presenting low level virtual kinematic actuators to the guidance layer. Previous Masters and PhD work at SU has resulted in the control algorithms shown in Figure 1.3 that are easily reconfigurable making the *Control Layer* capable of adapting to changes. Current research in this layer includes *adaptive control algorithms* for immediate handling of failures and *stall prevention* to ensure that operation is always in the linear aerodynamic region.

The *Guidance Layer* is responsible for guiding the aircraft back onto a kinematically feasible path given by the *Path Planning Layer* through the path tracking error. It then interfaces with the control layer through kinematic virtual actuators.

The outer *Path Planning Layer* can be seen on the left. It serves to provide kinematically feasible paths to the guidance layer.

1.3 Short History of System Identification Applied to Aircraft

This section is an overview of system identification applied to aircraft as presented by Klein [3].

“In 1947 one of the first approaches for obtaining static and dynamic parameters from flight data was given by Milliken [4], using frequency response data and a simple semi-graphical method for the analysis. Four years later, Greenberg [5] and Shinbrot [6] established more general and rigorous ways to determine aerodynamic parameters from transient manoeuvres. Parameter estimation methods introduced in these reports were based on ordinary and nonlinear least squares.”

“The availability of digital computers brought about dramatic improvement in aircraft aerodynamic modeling techniques in the late 1960s and 1970s. The International Federation of Automatic Control (IFAC) held a symposium on *Identification and System Parameter Estimation* in 1967. This is held every 3 years.”

“Several authors made substantial contributions in the field of system identification as applied to aircraft during the late 1960s and early 1970s, e.g. Taylor et al. [7], Mehra [8], Stepner and Mehra [9] and Gerlach [10]. These contributions were mainly in the area of development and application of various estimation techniques. Excellent theoretical and practical material on aircraft system identification is given by Maine and Iliff [11; 12], with emphasis on the output-error method. Mulder [13] addresses methods for experiment design, measured data compatibility and parameter estimation. Broad overviews of aircraft system identification methods can be found in the works by Klein [14; 15], Hamel and Jategaonkar [16], and the authors of two special issues of the *Journal of Aircraft*, on applications of system identification to

aircraft [17; 18].”

1.4 Outline of this Document

This document starts by introducing an aircraft model in Chapter 2 which derives the equations necessary for simulation and system identification. This chapter shows how the aircraft model consists of an outer loop model and an inner loop model. The outer loop model governs the point mass kinematics which can be described using Newton’s laws. The inner loop model describes the aircraft specific forces and moments.

Chapter 3 gives an overview of system identification methods available. It introduces three models relating to the uncertainties in the parameters and the measurements, and briefly discusses various system identification techniques. The regression methods are discussed in detail in §3.4.

Chapter 4 shows how the regression methods theory can be applied to aircraft. It discusses how to filter noisy measurements and also how to implement smoothed numerical differentiation, based on curve fitting.

Chapter 5 discusses the issues surrounding system identifiability, including data collinearity and input design.

Chapter 6 shows how system identification techniques were applied on a simulated model of the aircraft.

Chapter 7 concludes this document, discussing the results of system identification in simulation. It also discusses what must still be done to apply these techniques to the modular UAV airframe.

Chapter 2

Aircraft Model

2.1 Introduction

In this chapter a model of the aircraft is developed. This is done to derive the equations necessary for system identification. As mentioned earlier, system identification uses the virtual actuator commands as input to the system, thus a model of a virtual conventional aircraft is developed. The conventional aircraft is considered to have one set of ailerons, one rudder, an elevator and one motor. The model developed is later used in simulation (Chapter 6) in order to test the system identification algorithms discussed in §3.4. The aircraft model consists of an outer loop model and an inner loop model. This chapter outlines the aircraft dynamic model as presented by [2].

2.2 Definitions

The definitions presented in this section will form the groundwork for the development of a mathematical model for the UAV.

2.2.1 Axis system definitions

To model the aircraft, multiple axis systems are required. This includes an inertial reference frame and two aircraft-fixed axis systems, namely the wind and body axes. The inner and outer loop models will describe the relative motion between the axis systems.

2.2.1.1 Inertial Axis System

The inertial axis system is a fixed axis system where Newton's laws of motion will apply. The earth's surface can be used as an inertial axis system if the earth's rotation and curvature are ignored. In this project, the inertial axis system is defined to be right hand orthogonal with its centre point fixed to the earth's surface at some convenient point - usually the centre of the runway. Figure 2.1 shows the directions in which the axes are defined.

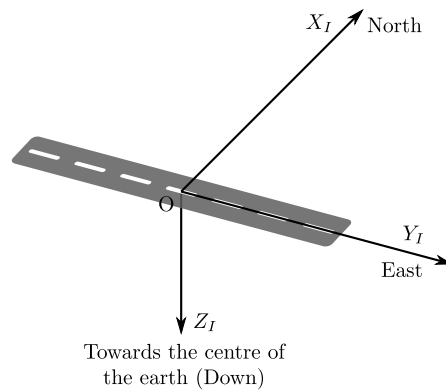


Figure 2.1: Definition of the inertial axis system

2.2.1.2 Body Axis System

The body axis system is fixed to the aircraft and rotates and translates along with it. The origin of this axis system is fixed to the aircraft's centre of mass. The X_B -axis points directly forward in the aircraft's plane of symmetry and

runs along its longitudinal reference line. The other two axes are perpendicular to the X_B -axis with the Y_B -axis running along the starboard wing of the aircraft and the Z_B -axis pointing directly down in the aircraft's plane of symmetry. The notations used in the body axes to describe the forces, moments, velocities, angular velocities and actuator commands are summarised in Figure 2.2 [19].

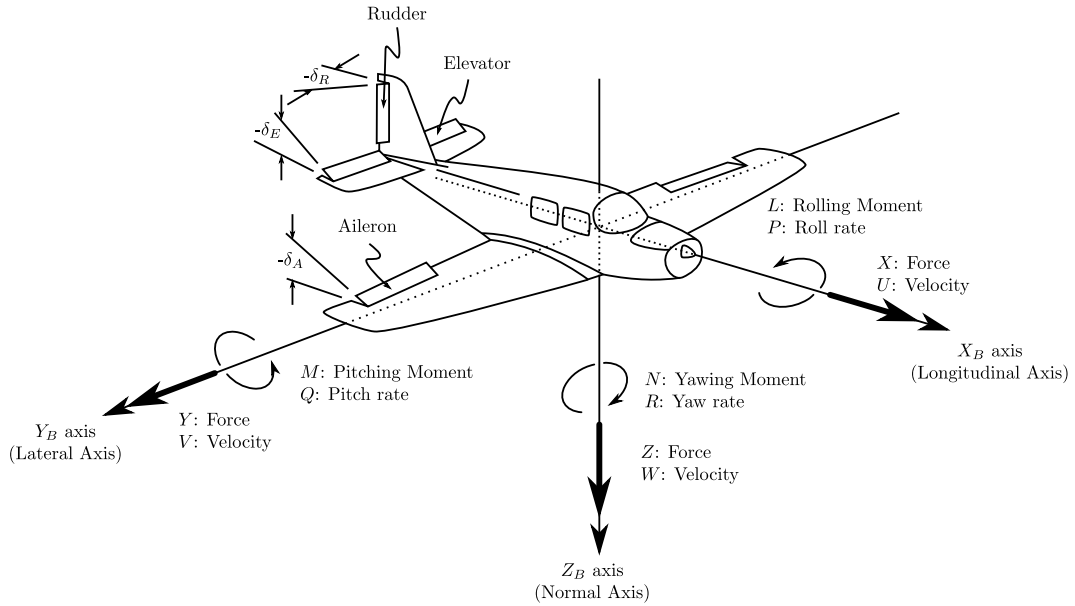


Figure 2.2: Definition of the body axis system

2.2.1.3 Wind Axis System

The wind axis system shares its origin with the body axis system at the centre of mass of the aircraft. The X_W -axis points into the direction of the oncoming free-stream velocity vector [20]. Two angles are defined to relate the orientation of the wind axes relative to the aircraft's body axes. These are the angle of attack (α) and sideslip angle (β). The wind axes are obtained by pitching the body axes negatively around the Y_B -axis by α and then positively yawing it around the Z_W -axis by β . This transformation is illustrated in Figure 2.3. The wind axis system is ideally suited for describing the aerodynamic forces

acting on the aircraft, since the forces of lift, sideslip and drag are modelled in the Z_W , Y_W and X_W directions respectively.

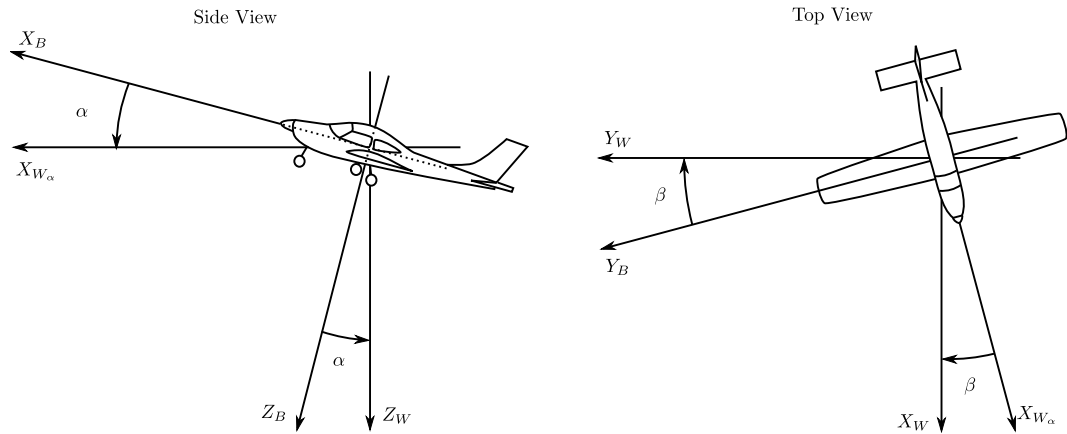


Figure 2.3: Definition of the wind axis system

2.2.2 Definition of Aircraft Control Surfaces

The virtual aircraft used in this project has three aerodynamic actuators as well as the ability to command the magnitude of the thrust vector. These actuators are listed in Table 2.1 along with their resulting effect. Refer to Figure 2.2 for their locations on the aircraft and their positive deflection directions.

Actuator	Symbol	Effect of positive deflection
Thrust Command	T_C	Positive X_B -axis Force
Elevator Deflection	δ_E	Negative Pitching Moment
Aileron Deflection	δ_A	Negative Rolling Moment
Rudder Deflection	δ_R	Negative Yawing Moment

Table 2.1: Definition of aircraft control surfaces

2.3 Aircraft Model Overview

The dynamics that describe the relative angular motion between the aircraft's body and wind axes operate at a much higher frequency than the attitude dynamics of the aircraft's wind axes relative to inertial space. It is shown by [2] how these dynamics can be split to produce models for the aircraft's point mass dynamics, and for its specific force and moment dynamics. These two models will be referred to as the *outer loop model* and the *inner loop model* respectively. Figure 2.4 illustrates this concept, with \mathbf{G}_I and \mathbf{G}_W corresponding to the gravitational acceleration vectors, coordinated in inertial and wind axes respectively. In this model the air density ρ is considered a constant under the assumption that the UAV's altitude will remain relatively constant.

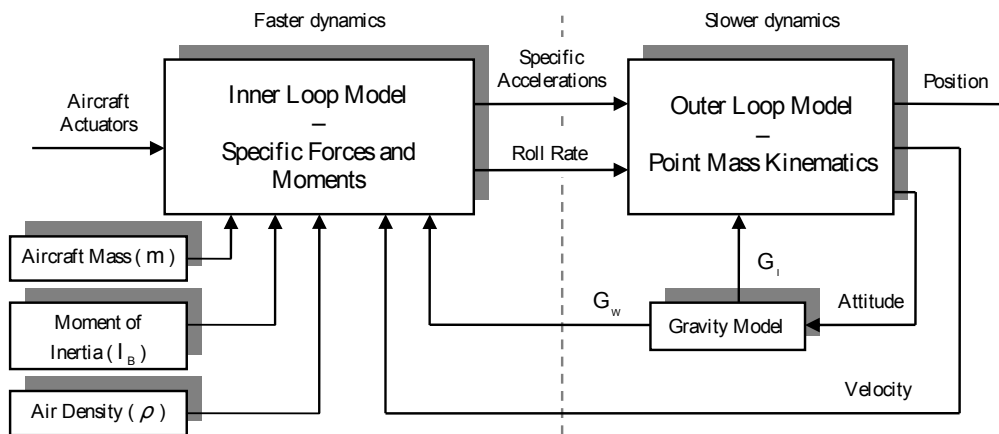


Figure 2.4: Aircraft model overview [2]

The following two sections will discuss these two models. This work is adapted from [21].

2.4 Outer Loop Model - Point Mass

Kinematics

This model describes the velocity, position and attitude of the aircraft. This model is aircraft independent and describes the motion of the aircraft's wind axis system relative to the fixed inertial axis system. It is assumed that the aircraft's specific accelerations (A_W , B_W and C_W) as well as the roll rate (P_W) are inputs to the model. The origins of these quantities will be modelled by the inner loop dynamics.

2.4.1 Velocity Dynamics

The dynamic equations describing an object's acceleration in wind axes are given by taking the time derivative of its velocity vector.

$$\left. \frac{d}{dt} \mathbf{V}^{WI} \right|_I = \mathbf{A}^{WI} \quad (2.1)$$

The total acceleration vector can be written as the sum of the specific acceleration vector ($\boldsymbol{\Sigma}$) and the gravity vector (\mathbf{G})

$$\left. \frac{d}{dt} \mathbf{V}^{WI} \right|_I = \boldsymbol{\Sigma} + \mathbf{G} \quad (2.2)$$

The specific accelerations of the aircraft will be modelled in wind axes. It is therefore more convenient to work with the velocity magnitude and the attitude of the wind axis system. The equation of Coriolis (see §A.3) can be used to transform the time derivative of a vector in a fixed inertial axis system to a rotating axis system.

$$\left. \frac{d}{dt} \mathbf{V}^{WI} \right|_W = -\boldsymbol{\omega}^{WI} \times \mathbf{V}^{WI} + \boldsymbol{\Sigma} + \mathbf{G} \quad (2.3)$$

The above equation can now be coordinated into wind axes and Eq. (A.3) can be used to simplify the cross product. The direction cosine matrix (DCM),

discussed in §A.4, is used to coordinate the gravity vector from inertial to wind axes.

$$\begin{bmatrix} \dot{\bar{V}} \\ 0 \\ 0 \end{bmatrix} = - \begin{bmatrix} 0 & -R_W & Q_W \\ R_W & 0 & -P_W \\ -Q_W & P_W & 0 \end{bmatrix} \begin{bmatrix} \bar{V} \\ 0 \\ 0 \end{bmatrix} + \begin{bmatrix} A_W \\ B_W \\ C_W \end{bmatrix} + \mathbf{DCM}^{WI} \begin{bmatrix} 0 \\ 0 \\ g \end{bmatrix} \quad (2.4)$$

Here \bar{V} is the magnitude of the aircraft's velocity vector, P_W , Q_W and R_W are its angular rates coordinated in wind axes and A_W , B_W and C_W are the components of the specific acceleration vector coordinated in wind axes. The magnitude of the gravity vector in the inertial down direction is given by g .

Eq. (2.4) can be split into three equations. The first is the dynamic equation for the velocity magnitude in wind axes and the other two are algebraic constraint equations.

$$\dot{\bar{V}} = A_W + ge_{13}^{WI} \quad (2.5a)$$

$$\begin{bmatrix} R_W \\ Q_W \end{bmatrix} = \frac{1}{\bar{V}} \begin{bmatrix} ge_{23}^{WI} \\ -ge_{33}^{WI} \end{bmatrix} + \frac{1}{\bar{V}} \begin{bmatrix} B_W \\ -C_W \end{bmatrix} \quad (2.5b)$$

where e_{xy}^{WI} corresponds to row x and column y of the \mathbf{DCM}^{WI} matrix.

The total acceleration vector of the aircraft can also be written in terms of the total force vector (\mathbf{F}^{WI}) and the mass of the aircraft (m), through Newton's second law.

$$\mathbf{A}^{WI} = \frac{1}{m} \mathbf{F}^{WI} \quad (2.6)$$

Substituting this into Eq. (2.1) and going through the same derivation process as above, will lead to a different form of the algebraic constraint equations given in Eq. (2.5b), that will be used later for the inner loop model and is given by [21]

$$R_W = \frac{1}{m\bar{V}} Y_W \quad (2.7a)$$

$$Q_W = -\frac{1}{m\bar{V}} Z_W \quad (2.7b)$$

where Y_W and Z_W correspond to the second and third components of the total force vector coordinated in wind axes.

2.4.2 Position Dynamics

In order to obtain the position dynamics, the time derivative of the position vector is taken with respect to inertial space.

$$\left. \frac{d}{dt} \mathbf{P}^{WI} \right|_I = \mathbf{V}^{WI} \quad (2.8)$$

As stated in the previous section, the velocity vector used for this model is coordinated in the aircraft's wind axes. The DCM is therefore required to coordinate the vector in inertial space.

$$\dot{\mathbf{P}}_I^{WI} = [\mathbf{DCM}^{WI}]^{-1} \mathbf{V}_W^{WI} \quad (2.9)$$

Using the orthogonal property of the DCM given by Eq. (A.7), the previous equation becomes

$$\dot{\mathbf{P}}_I^{WI} = [\mathbf{DCM}^{WI}]^T \mathbf{V}_W^{WI} \quad (2.10)$$

Simplifying this yields the position dynamics,

$$\dot{\mathbf{P}}_I^{WI} = \begin{bmatrix} e_{11}^{WI} \\ e_{12}^{WI} \\ e_{13}^{WI} \end{bmatrix} \bar{V} \quad (2.11)$$

2.4.3 Attitude Dynamics

The attitude dynamics of the wind axes allow for the dynamic calculation of the attitude states, when the angular rates coordinated in wind axes are known. The derivation of the attitude dynamics are discussed below for the Euler 3-2-1 angle sequence.

The angular rate vector can be written as the sum of the Euler angle velocities multiplied by the defined unit vector around which each one rotates. For Euler 3-2-1 this is given by

$$\boldsymbol{\omega}^{WI} = \dot{\phi}_W \mathbf{u}_1^\phi + \dot{\theta}_W \mathbf{u}_2^\theta + \dot{\psi}_W \mathbf{u}_3^\psi \quad (2.12)$$

where \mathbf{u}_i^x corresponds to the i^{th} (first, second or third) unit vector of the axis system about which the Euler angle rotation, denoted in the superscript (x), is carried out. Refer to §A.5 for more information about these rotation unit vectors. It is shown by [22] how these unit vectors can be transformed into the wind axes using single-rotation matrices. The result is taken from [21] and stated below,

$$\begin{bmatrix} P_W \\ Q_W \\ R_W \end{bmatrix} = \begin{bmatrix} 1 & 0 & -\sin \theta_W \\ 0 & \cos \phi_W & \cos \theta_W \sin \phi_W \\ 0 & -\sin \phi_W & \cos \theta_W \cos \phi_W \end{bmatrix}_{(321)} \begin{bmatrix} \dot{\phi}_W \\ \dot{\theta}_W \\ \dot{\psi}_W \end{bmatrix}_{(321)} \quad (2.13)$$

with the columns of the above 3×3 transformation matrix consisting of the three unit vectors of Eq. (2.12). By making the time derivatives of the attitude states the subject of the above equation and thereby inverting the transformation matrix, the attitude dynamics are obtained.

$$\begin{bmatrix} \dot{\phi}_W \\ \dot{\theta}_W \\ \dot{\psi}_W \end{bmatrix}_{(321)} = \begin{bmatrix} 1 & \sin \phi_W \tan \theta_W & \cos \phi_W \tan \theta_W \\ 0 & \cos \phi_W & -\sin \phi_W \\ 0 & \sin \phi_W \sec \theta_W & \cos \phi_W \sec \theta_W \end{bmatrix}_{(321)} \begin{bmatrix} P_W \\ Q_W \\ R_W \end{bmatrix} \quad (2.14)$$

2.5 Inner Loop Model - Aircraft Specific Forces and Moments

For the outer loop model derived in §2.4 it was assumed that the specific accelerations (A_W , B_W and C_W) and the roll rate (P_W) of the aircraft are inputs to the system. The inner loop model developed by [2], investigates the

origin of the specific forces and moments acting on the aircraft in order to provide the dynamic equations for these specific accelerations and rates. The inner loop model therefore encompasses all of the aircraft specific dynamics and relates the angular motion of the aircraft's body axes relative to its wind axes.

2.5.1 Rigid Body Rotational Dynamics

The rigid body rotational dynamics model the relative angular motion between the aircraft's wind and body axes, given the applied moments. From the definition of the wind axis system, its orientation relative to the body axis system is defined by two rotations as discussed in §2.2.1.3. Firstly, a negative rotation through the angle of attack (α) around the Y_B -axis and then a positive rotation through the angle of sideslip (β) around the new Z_W -axis. Therefore, the angular rate vector of the wind axes with respect to the body axes is given by the angular rates ($\dot{\alpha}$ and $\dot{\beta}$) about their respective unit vectors.

$$\boldsymbol{\omega}^{WB} = -\dot{\alpha}\mathbf{j}^B + \dot{\beta}\mathbf{k}^W \quad (2.15)$$

The angular velocity of the wind axes with respect to inertial space can be written as the sum of the angular velocity of the body axes relative to inertial space and the wind axes relative to the body axes.

$$\boldsymbol{\omega}^{WI} = \boldsymbol{\omega}^{BI} + \boldsymbol{\omega}^{WB} \quad (2.16)$$

Substituting Eq. (2.15) into Eq. (2.16) yields,

$$\boldsymbol{\omega}_B^{BI} = \dot{\alpha}\mathbf{j}_B^B - \dot{\beta}\mathbf{k}_B^W + \boldsymbol{\omega}_B^{WI} \quad (2.17)$$

with the subscripts B indicating that the vectors are now coordinated into the body axes. This equation can be rewritten using the wind to body axes coordination matrix (\mathbf{DCM}^{BW}) given by Eq. (A.9), to convert the vectors

from their native axis systems.

$$\boldsymbol{\omega}_B^{BI} = \dot{\alpha} \mathbf{j}_B^B - \dot{\beta} \mathbf{DCM}^{BW} \mathbf{k}_W^W + \mathbf{DCM}^{BW} \boldsymbol{\omega}_W^{WI} \quad (2.18)$$

Expanding the above equation yields,

$$\begin{bmatrix} P \\ Q \\ R \end{bmatrix} = \begin{bmatrix} 0 & \sin \alpha \\ 1 & 0 \\ 0 & -\cos \alpha \end{bmatrix} \begin{bmatrix} \dot{\alpha} \\ \dot{\beta} \end{bmatrix} + \begin{bmatrix} \cos \alpha \cos \beta & -\cos \alpha \sin \beta & -\sin \alpha \\ \sin \beta & \cos \beta & 0 \\ \sin \alpha \cos \beta & -\sin \alpha \sin \beta & \cos \alpha \end{bmatrix} \begin{bmatrix} P_W \\ Q_W \\ R_W \end{bmatrix} \quad (2.19)$$

By making $\dot{\alpha}$, $\dot{\beta}$ and P_W the subject of the equations and substituting the two algebraic constraints from Eq. (2.7a) and Eq. (2.7b), three equations are obtained. The first two provide the attitude dynamics of the wind axes relative to the body axes, given the body axes angular rates and wind axes forces. The third equation provides a constraint that keeps the wind axes normal vector in the aircraft's plane of symmetry.

$$\begin{bmatrix} \dot{\alpha} \\ \dot{\beta} \\ P_W \end{bmatrix} = \begin{bmatrix} -\cos \alpha \tan \beta & 1 & -\sin \alpha \tan \beta \\ \sin \alpha & 0 & -\cos \alpha \\ \cos \alpha \sec \beta & 0 & \sin \alpha \sec \beta \end{bmatrix} \begin{bmatrix} P \\ Q \\ R \end{bmatrix} + \frac{1}{m\bar{V}} \begin{bmatrix} \sec \beta & 0 \\ 0 & 1 \\ -\tan \beta & 0 \end{bmatrix} \begin{bmatrix} Z_W \\ Y_W \end{bmatrix} \quad (2.20)$$

In order to write the attitude dynamics of the wind axes in terms of the applied forces and moments, the dynamics of the angular rates in the above equation have to be obtained. Euler's law for rigid bodies states that the time derivative relative to the inertial reference frame of an object's angular momentum (\mathbf{H}), referenced to its centre of mass, is equal to the externally applied moment (\mathbf{M}) [21]

$$\mathbf{M} = \left. \frac{d}{dt} \mathbf{H} \right|_I \quad (2.21)$$

The time derivative in the above equation can be transformed to the aircraft's body axes using the equation of Coriolis, Eq. (A.5)

$$\mathbf{M} = \left. \frac{d}{dt} \mathbf{H} \right|_B + \boldsymbol{\omega}^{BI} \times \mathbf{H} \quad (2.22)$$

As stated in [2], the angular momentum vector about the centre of mass (\mathbf{H}) takes on its simplest form when coordinated into body axes, assuming the body axes are aligned with the airframe's principle axes of inertia, since in this axis system the mass distribution remains constant and is independent of the aircraft's translational and rotational motion. Coordinated in body axes this vector is given as [21]

$$\mathbf{H}_B = \mathbf{I}_B \boldsymbol{\omega}_B^{BI} \quad (2.23)$$

where \mathbf{I}_B is the moment of inertia tensor referenced to the body axis system. Due to the aircraft's symmetry, Eq. (A.2) can be used for \mathbf{I}_B . Eq. (2.22) can be coordinated into body axes and Eq. (2.23) substituted for the angular momentum vector to yield

$$\dot{\boldsymbol{\omega}}_B^{BI} = \mathbf{I}_B^{-1} \left(\mathbf{M}_B - \mathbf{S}_{\boldsymbol{\omega}_B^{BI}} \mathbf{I}_B \boldsymbol{\omega}_B^{BI} \right) \quad (2.24)$$

In the above equation, $\mathbf{S}_{\boldsymbol{\omega}_B^{BI}}$ is given by Eq. (A.4) and is a matrix used to represent the cross product. Expanding the above equations and combining it with Eq. (2.20) provides the full rigid body rotational dynamics

$$\begin{aligned} \begin{bmatrix} \dot{\alpha} \\ \dot{\beta} \end{bmatrix} &= \begin{bmatrix} -\cos \alpha \tan \beta & 1 & -\sin \alpha \tan \beta \\ \sin \alpha & 0 & -\cos \alpha \end{bmatrix} \begin{bmatrix} P \\ Q \\ R \end{bmatrix} \\ &+ \frac{1}{m\bar{V}} \begin{bmatrix} \sec \beta & 0 \\ 0 & 1 \end{bmatrix} \begin{bmatrix} Z_W \\ Y_W \end{bmatrix} \end{aligned} \quad (2.25)$$

$$\begin{bmatrix} \dot{P} \\ \dot{Q} \\ \dot{R} \end{bmatrix} = \mathbf{I}_B^{-1} \left(\begin{bmatrix} L \\ M \\ N \end{bmatrix} - \begin{bmatrix} 0 & -R & Q \\ R & 0 & -P \\ -Q & P & 0 \end{bmatrix} \mathbf{I}_B \begin{bmatrix} P \\ Q \\ R \end{bmatrix} \right) \quad (2.26)$$

with constraint,

$$P_W = \begin{bmatrix} \cos \alpha \sec \beta & 0 & \sin \alpha \sec \beta \end{bmatrix} \begin{bmatrix} P \\ Q \\ R \end{bmatrix} + \frac{1}{m\bar{V}} \begin{bmatrix} -\tan \beta & 0 \end{bmatrix} \begin{bmatrix} Z_W \\ Y_W \end{bmatrix} \quad (2.27)$$

2.5.2 Specific Forces and Moments

This section will develop the aircraft dynamic equations which will be used in system identification. It presents nondimensional lift and moment coefficients which can be expressed as a function of non-dimensional stability and control derivatives. The aim of this project is to estimate these derivatives which is unique to the specific aircraft.

This section investigates the specific forces and moments acting on the aircraft. These forces consists of aerodynamic forces and the force caused by the aircraft's thrust vector. The thrust vector represents the force caused by the engine.

$$\mathbf{F}_S = \mathbf{F}_A + \mathbf{F}_T \quad (2.28)$$

It is assumed that the direction of the thrust vector coincides with the aircraft's X_B -axis and that any moment caused by the thrust is negligibly small. It is also assumed that the inertia of the rotating blades can be ignored, thus no gyroscopic moments are introduced by the rotating blades. The aerodynamic forces of lift, drag and sideslip are all defined as being either parallel or perpendicular to the aircraft's velocity vector and therefore the wind axes are the logical choice for this model. The specific forces (X_W, Y_W and Z_W) and moments (L_W, M_W and N_W) acting on the aircraft, as given by the small incidence angle aerodynamic model [23], and coordinated in the wind axes, are

given by

$$\begin{bmatrix} X_W \\ Y_W \\ Z_W \end{bmatrix} = qS \begin{bmatrix} -C_D \\ C_y \\ -C_L \end{bmatrix} + \begin{bmatrix} \cos \alpha \cos \beta \\ -\cos \alpha \sin \beta \\ -\sin \alpha \end{bmatrix} T \quad (2.29)$$

$$\begin{bmatrix} L_W \\ M_W \\ N_W \end{bmatrix} = qS \begin{bmatrix} b & 0 & 0 \\ 0 & \bar{c} & 0 \\ 0 & 0 & b \end{bmatrix} \begin{bmatrix} C_l \\ C_m \\ C_n \end{bmatrix} \quad (2.30)$$

where q is the dynamic pressure given by

$$q = \frac{1}{2} \rho \bar{V}_a^2 \quad (2.31)$$

Here T is the magnitude of the aircraft's thrust vector, \bar{V}_a is the airspeed, ρ is the air density, S is the wing reference area, b is the wing span and \bar{c} is the mean aerodynamic chord. The aerodynamic force coefficients of *drag*, *side force* and *lift* are denoted by C_D , C_y and C_L respectively and the *roll*, *pitch* and *yaw* moment coefficients are given by C_l , C_m and C_n respectively. These coefficients can be expanded using dimensionless stability and control derivatives. Using these derivatives, the aerodynamic force and moment coefficients can be defined as the sum of various aircraft states and actuator inputs as

shown by [23],

$$C_D = C_{D_0} + \frac{C_L^2}{\pi \mathcal{R}e} \quad (2.32)$$

$$\begin{aligned} \begin{bmatrix} C_y \\ C_L \end{bmatrix} &= \begin{bmatrix} 0 \\ C_{L_0} \end{bmatrix} + \begin{bmatrix} 0 & C_{y\beta} & \frac{b}{2V} C_{yP} & 0 & \frac{b}{2V} C_{yR} \\ C_{L\alpha} & 0 & 0 & \frac{\bar{c}}{2V} C_{LQ} & 0 \end{bmatrix} \begin{bmatrix} \alpha \\ \beta \\ P \\ Q \\ R \end{bmatrix} \\ &+ \begin{bmatrix} C_{y\delta_A} & 0 & C_{y\delta_R} \\ 0 & C_{L\delta_E} & 0 \end{bmatrix} \begin{bmatrix} \delta_A \\ \delta_E \\ \delta_R \end{bmatrix} \end{aligned} \quad (2.33)$$

$$\begin{aligned} \begin{bmatrix} C_l \\ C_m \\ C_n \end{bmatrix} &= \begin{bmatrix} 0 \\ C_{m_0} \\ 0 \end{bmatrix} + \begin{bmatrix} 0 & C_{l\beta} & \frac{b}{2V} C_{lP} & 0 & \frac{b}{2V} C_{lR} \\ C_{m\alpha} & 0 & 0 & \frac{\bar{c}}{2V} C_{mQ} & 0 \\ 0 & C_{n\beta} & \frac{b}{2V} C_{nP} & 0 & \frac{b}{2V} C_{nR} \end{bmatrix} \begin{bmatrix} \alpha \\ \beta \\ P \\ Q \\ R \end{bmatrix} \\ &+ \begin{bmatrix} C_{l\delta_E} & 0 & C_{l\delta_R} \\ 0 & C_{m\delta_E} & 0 \\ C_{n\delta_E} & 0 & C_{n\delta_R} \end{bmatrix} \begin{bmatrix} \delta_A \\ \delta_E \\ \delta_R \end{bmatrix} \end{aligned} \quad (2.34)$$

with e defined as the Oswald efficiency factor and \mathcal{R} as the aspect ratio of the wing. The static lift and pitching moment coefficients are given by C_{L_0} and C_{m_0} respectively. The non-dimensional stability and control derivatives are terms of the form

$$C_{A_x} = \frac{\partial C_A}{\partial x'} \quad (2.35)$$

where

$$x' = n_c x \quad (2.36)$$

normalises x through a normalising coefficient n_c . For derivatives with respect to pitch rate this coefficient is given by $\bar{c}/2\bar{V}$ and for derivatives with respect

to roll and yaw rate this coefficient is $b/2\bar{V}$. Angles of incidence as well as control perturbation angles have a unity normalising coefficient.

The following assumptions are required to reduce the aerodynamic model to the form shown above [21]:

- Ignore the effects of main wing downwash lag on the horizontal tail as well as added mass effects as they are typically negligibly small. Therefore $C_{m_{\dot{\alpha}}} = 0$ and $C_{L_{\dot{\alpha}}} = 0$.
- Assume the aircraft is operating in pre-stall flight conditions and therefore the incidence angles are small.

The aerodynamic model presented in this section provides the forces and moments acting on the aircraft in wind axes. However, the rigid body rotational dynamics model, derived in §2.5.1 requires the aircraft's moments in body axes. The DCM^{BW} transformation matrix in Eq. (A.9) can be used to coordinate the moment vectors from wind to body axes as follows

$$\begin{bmatrix} L \\ M \\ N \end{bmatrix} = DCM^{BW} \begin{bmatrix} L_W \\ M_W \\ N_W \end{bmatrix} \quad (2.37)$$

2.6 Conclusion

This chapter outlined the derivation of a conventional aircraft model for system identification purposes. The aerodynamic and control derivative equations, Eq. (2.32) to Eq. (2.34), were developed and are used for the identification process discussed in Chapter 4. The model developed in this section is also used to assess the identification methods. This is done in Chapter 6.

Chapter 3

System Identification Methods

3.1 Introduction

This chapter starts by giving the structure of three parameter estimation models. Different identification methods based on these models are briefly discussed. The methods can be split into batch methods, where parameter estimation is done after recording of all the relevant data, and real-time methods, where the estimated parameters are updated in real-time. The regression methods are discussed in more detail at the end of this chapter, as these are the methods eventually used for assessment in Chapter 6. The reasons for using the *regression methods* are given in §3.5.

3.2 Parameter Estimation Models

Parameter estimation is usually done by minimising some cost function. In this section, the cost functions to be optimised for various estimator models are introduced.

Measurement equations can be linear or nonlinear in the parameters:

$$\mathbf{z} = \mathbf{H}\boldsymbol{\theta} + \mathbf{v} \quad (3.1)$$

or

$$\mathbf{z} = \mathbf{h}(\boldsymbol{\theta}) + \mathbf{v} \quad (3.2)$$

Schweppe [24] designated three models for the uncertainties in the parameters $\boldsymbol{\theta}$, and the measurement noise \mathbf{v} . These are the Bayesian model, the Fisher model and the least-squares model, formed as follows:

Bayesian model:

1. $\boldsymbol{\theta}$ is a vector of random variables with probability density $p(\boldsymbol{\theta})$.
2. \mathbf{v} is a random vector with probability density $p(\mathbf{v})$

Fisher model:

1. $\boldsymbol{\theta}$ is a vector of unknown constant parameters.
2. \mathbf{v} is a random vector with probability density $p(\mathbf{v})$

Least-squares model:

1. $\boldsymbol{\theta}$ is a vector of unknown constant parameters.
2. \mathbf{v} is a random vector of measurement noise.

3.2.1 Estimator for the Bayesian Model

For the Bayesian model, the probability densities $p(\boldsymbol{\theta})$ and $p(\mathbf{v})$ are assumed to be known *a priori*. The conditional probability density of parameter vector

$\boldsymbol{\theta}$, given the observation \mathbf{z} , designated by $p(\boldsymbol{\theta}|\mathbf{z})$, is related to the *a priori* probability densities by Bayes' rule:

$$p(\boldsymbol{\theta}|\mathbf{z}) = \frac{p(\mathbf{z}|\boldsymbol{\theta})p(\boldsymbol{\theta})}{p(\mathbf{z})} \quad (3.3)$$

If the vectors $\boldsymbol{\theta}$ and \mathbf{v} have Gaussian distributions and are independent, their mean values and variances are

$$\begin{aligned} E(\boldsymbol{\theta}) &= \boldsymbol{\theta}_p, & \text{Cov}(\boldsymbol{\theta}) &= \boldsymbol{\Sigma}_p \\ E(\mathbf{v}) &= \mathbf{0}, & \text{Cov}(\mathbf{v}) &= \mathbf{R} \end{aligned} \quad (3.4)$$

which can also be stated as

$$\begin{aligned} \boldsymbol{\theta} &\text{ is } \mathbb{N}(\boldsymbol{\theta}_p, \boldsymbol{\Sigma}_p) \\ \mathbf{v} &\text{ is } \mathbb{N}(\mathbf{0}, \mathbf{R}) \end{aligned} \quad (3.5)$$

The most probable estimate of the parameters is derived in [3] as

$$\hat{\boldsymbol{\theta}} = \max_{\boldsymbol{\theta}} p(\boldsymbol{\theta}|\mathbf{z}) \quad (3.6)$$

which minimises the cost function

$$J(\boldsymbol{\theta}) = \frac{1}{2}(\mathbf{z} - \mathbf{H}\boldsymbol{\theta})^T \mathbf{R}^{-1}(\mathbf{z} - \mathbf{H}\boldsymbol{\theta}) + \frac{1}{2}(\boldsymbol{\theta} - \boldsymbol{\theta}_p)^T \boldsymbol{\Sigma}_p^{-1}(\boldsymbol{\theta} - \boldsymbol{\theta}_p) \quad (3.7)$$

3.2.2 Estimator for the Fisher Model

The estimator for the Fisher model is based on the Fisher [25] estimation theory, using the concept of a likelihood function

$$\mathbb{L}(\mathbf{z}; \boldsymbol{\theta}) = p(\mathbf{z}|\boldsymbol{\theta}) \quad (3.8)$$

The most common estimator for the Fisher model is the maximum likelihood (ML) estimator, which is equal to the value of $\boldsymbol{\theta}$ that maximises $\mathbb{L}(\mathbf{z}; \boldsymbol{\theta})$ for a given \mathbf{z} . In the case of a Gaussian $p(\mathbf{z})$, where \mathbf{v} is $\mathbb{N}(\mathbf{0}, \mathbf{R})$, the likelihood function takes the form

$$\mathbb{L}(\mathbf{z}; \boldsymbol{\theta}) = [(2\pi)^N |\mathbf{R}|]^{-\frac{1}{2}} \exp \left[-\frac{1}{2}(\mathbf{z} - \mathbf{H}\boldsymbol{\theta})^T \mathbf{R}^{-1}(\mathbf{z} - \mathbf{H}\boldsymbol{\theta}) \right] \quad (3.9)$$

The maximum likelihood estimate

$$\hat{\boldsymbol{\theta}} = \max_{\boldsymbol{\theta}} \mathbb{L}(\mathbf{z}; \boldsymbol{\theta}) \quad (3.10)$$

now minimises

$$J(\boldsymbol{\theta}) = \frac{1}{2}(\mathbf{z} - \mathbf{H}\boldsymbol{\theta})^T \mathbf{R}^{-1}(\mathbf{z} - \mathbf{H}\boldsymbol{\theta}) \quad (3.11)$$

3.2.3 Estimator for the Least-Squares Model

In the least-squares model no uncertainty models for $\boldsymbol{\theta}$ and \mathbf{v} are used, i.e., there are no probability statements concerning $\boldsymbol{\theta}$ and \mathbf{v} . The best estimate of $\boldsymbol{\theta}$ comes from minimising the weighted sum of squared differences between the measured outputs and the model outputs

$$J(\boldsymbol{\theta}) = \frac{1}{2}(\mathbf{z} - \mathbf{H}\boldsymbol{\theta})^T \mathbf{R}^{-1}(\mathbf{z} - \mathbf{H}\boldsymbol{\theta}) \quad (3.12)$$

where \mathbf{R}^{-1} is a positive definite weighting matrix, chosen by judgement. Minimising $J(\boldsymbol{\theta})$ in the above equation leads to the weighted least-squares (WLS) estimator. In the case where $\mathbf{R} = \mathbf{I}$, the ordinary least-squares (OLS) estimator is obtained, with cost function

$$J(\boldsymbol{\theta}) = \frac{1}{2}(\mathbf{z} - \mathbf{H}\boldsymbol{\theta})^T (\mathbf{z} - \mathbf{H}\boldsymbol{\theta}) \quad (3.13)$$

It can be seen from Eq. (3.11) that for a linear measurement equation $\mathbf{z} = \mathbf{H}\boldsymbol{\theta} + \mathbf{v}$, the maximum likelihood estimator reduces to a least-squares estimator with weighting equal to the inverse of the noise covariance matrix.

Least-squares theory is discussed in more detail in §3.4. The application of the least-squares estimator is covered in Chapter 4.

3.3 Overview of Identification Methods

This section serves to give a short overview of different system identification methods as presented in [3]. These methods can be split up into batch methods

and real-time methods. Note that regression methods are not discussed in this section, as they are discussed in more detail in §3.4 and Chapter 4.

3.3.1 Batch Methods

Batch methods use a complete set of recorded data to perform system identification. They are also referred to as offline methods. Batch methods are often used to determine parameters from wind tunnel or ground tests in the case of aircraft. This subsection discusses a few batch methods.

3.3.1.1 The Filter-Error Method

The filter-error method uses the Fisher model discussed in §3.2.2. The model equations take the form

$$\dot{\mathbf{x}}(t) = \mathbf{A}\mathbf{x}(t) + \mathbf{B}\mathbf{u}(t) + \mathbf{B}_w\mathbf{w}(t) \quad (3.14)$$

$$\mathbf{y}(t) = \mathbf{C}\mathbf{x}(t) + \mathbf{D}\mathbf{u}(t) \quad (3.15)$$

$$\mathbf{z}(i) = \mathbf{y}(i) + \mathbf{v}(i) \quad i = 1, 2, \dots, N \quad (3.16)$$

where

$$E[\mathbf{x}(0)] = \bar{\mathbf{x}}_0 \quad E\{[\mathbf{x}(0) - \bar{\mathbf{x}}_0][\mathbf{x}(0) - \bar{\mathbf{x}}_0]^T\} = \mathbf{P}_0 \quad (3.17)$$

The random vectors $\mathbf{w}(t)$ and $\mathbf{v}(i)$ are assumed to be white with

$$\begin{aligned} E[\mathbf{w}(t)] &= \mathbf{0} & E[\mathbf{w}(t_i)\mathbf{w}^T(t_j)] &= \mathbf{Q}(t_i)\delta(t_i - t_j) \\ E[\mathbf{v}(i)] &= \mathbf{0} & E[\mathbf{v}(i)\mathbf{v}^T(j)] &= \mathbf{R}(i)\delta_{ij} \end{aligned} \quad (3.18)$$

In this method, the elements of the vector of unknown parameters $\boldsymbol{\theta}$ appear in the elements of the $\mathbf{A}, \mathbf{B}, \mathbf{B}_w, \mathbf{C}, \mathbf{D}, \mathbf{P}_0, \mathbf{Q}$ and \mathbf{R} matrices and the initial state vector $\bar{\mathbf{x}}_0$. Following the development in §3.2.2, the likelihood function for a sequence of measurements $\mathbf{Z}_N = [\mathbf{z}(1) \quad \mathbf{z}(2) \quad \dots \quad \mathbf{z}(N)]$ will be denoted

by $\mathbb{L}[\mathbf{Z}_N; \boldsymbol{\theta}]$. By successive applications of Bayes' rule, the expression for the likelihood function is given by [3] as

$$\mathbb{L}[\mathbf{Z}_N; \boldsymbol{\theta}] = \prod_{i=1}^N \mathbb{L}[z(i) | \mathbf{Z}_{i-1}; \boldsymbol{\theta}] \quad (3.19)$$

Now the parameter estimate must maximise the likelihood function.

$$\hat{\boldsymbol{\theta}} = \max_{\boldsymbol{\theta}} \mathbb{L}[\mathbf{Z}_N; \boldsymbol{\theta}] \quad (3.20)$$

The value of $\hat{\boldsymbol{\theta}}$ can now be found by using an optimisation algorithm. It is shown by [3] that it is advantageous to minimise the negative logarithm of the likelihood function, rather than to maximise the likelihood function. This is permissible because the logarithm is a monotonic function.

3.3.1.2 Frequency Domain Methods

According to Klein [3], Frequency Domain analysis has certain advantages, including physical insight in terms of frequency content, direct applicability to control system design, and a smaller number of data points for parameter estimation.

For parametric modeling in the frequency domain, two different models for uncertainty are considered, the Fisher model and the Least-Squares model. The Bayesian model introduces difficulties in formulating probability densities for complex random variables.

To apply frequency domain methods, the measured data have to be transformed into the frequency domain first which can be computationally expensive. Various frequency domain methods are discussed in [3].

3.3.2 Real-Time Methods

The real-time methods provide estimated parameters while the measurement data is acquired, making the detection of a fault in the system possible by

monitoring variations in the estimated parameters. This makes it possible to reconfigure the control system to accommodate the changed parameters.

This section will briefly discuss the extended Kalman filter which can be used to do real-time system identification. The real-time regression method, using recursive least-squares, is discussed in detail in §3.4.2.

3.3.2.1 Extended Kalman Filter

For the extended Kalman filter, the same algorithm can be used to estimate both the states and the parameters in a dynamic system model. This is demonstrated in [3] by considering the following model equations:

$$\dot{\mathbf{x}} = \mathbf{A}(\boldsymbol{\theta})\mathbf{x} + \mathbf{B}(\boldsymbol{\theta})\mathbf{u} + \mathbf{w} \quad (3.21)$$

$$\mathbf{z}(i) = \mathbf{C}(\boldsymbol{\theta})\mathbf{x}(i) + N(i) \quad i = 1, 2, \dots, N \quad (3.22)$$

$$E[\mathbf{x}(0)] = \bar{\mathbf{x}}_0 \quad E\{[\mathbf{x}(0) - \bar{\mathbf{x}}_0][\mathbf{x}(0) - \bar{\mathbf{x}}_0]^T\} = \mathbf{P}_{\mathbf{x}_0} \quad (3.23)$$

The noise sequences \mathbf{w} and \mathbf{v} are zero-mean white Gaussian noise sequences with covariance matrices \mathbf{Q} and \mathbf{R} respectively

$$\mathbf{v} \text{ is } \mathbb{N}(\mathbf{0}, \mathbf{R}) \quad \text{Cov}[\mathbf{v}(i)] = E[\mathbf{v}(i)\mathbf{v}^T(j)] = \mathbf{R}\delta_{ij} \quad (3.24)$$

$$\mathbf{w} \text{ is } \mathbb{N}(\mathbf{0}, \mathbf{Q}) \quad \text{Cov}[\mathbf{w}(i)] = E[\mathbf{w}(t_i)\mathbf{w}^T(t_j)] = \mathbf{Q}\delta(t_i - t_j) \quad (3.25)$$

For the extended Kalman filter, the state vector is augmented with parameter vector

$$\mathbf{x}_a = \begin{bmatrix} \mathbf{x} \\ \boldsymbol{\theta} \end{bmatrix} \quad (3.26)$$

This new state vector will be considered as the state vector for the extended Kalman filter. For now the unknown parameters $\boldsymbol{\theta}$ are assumed to be constant, therefore

$$\dot{\boldsymbol{\theta}} = \mathbf{0} \quad (3.27)$$

The system equations for the augmented state are then

$$\dot{\mathbf{x}}_a = \mathbf{A}_a \mathbf{x}_a + \mathbf{B}_a \mathbf{u} + \mathbf{w}_a \quad (3.28)$$

$$\mathbf{z}(i) = \mathbf{C}_a \mathbf{x}_a(i) + N(i) \quad i = 1, 2, \dots, N \quad (3.29)$$

$$E[\mathbf{x}_a(0)] = \bar{\mathbf{x}}_{a_0} \quad E\{[\mathbf{x}_a(0) - \bar{\mathbf{x}}_{a_0}][\mathbf{x}_a(0) - \bar{\mathbf{x}}_{a_0}]^T\} = \mathbf{P}_{a_0} \quad (3.30)$$

where

$$\mathbf{A}_a \equiv \begin{bmatrix} \mathbf{A}(\boldsymbol{\theta}) & \mathbf{0} \\ \mathbf{0} & \mathbf{0} \end{bmatrix} \quad \mathbf{B}_a \equiv \begin{bmatrix} \mathbf{B}(\boldsymbol{\theta}) \\ \mathbf{0} \end{bmatrix} \quad \mathbf{w}_a \equiv \begin{bmatrix} \mathbf{w} \\ \mathbf{0} \end{bmatrix} \quad \bar{\mathbf{x}}_{a_0} \equiv \begin{bmatrix} \bar{\mathbf{x}}_0 \\ \boldsymbol{\theta}_0 \end{bmatrix} \\ \mathbf{C}_a \equiv \begin{bmatrix} \mathbf{C}(\boldsymbol{\theta}) & \mathbf{0} \end{bmatrix} \quad (3.31)$$

The dynamic system for the augmented state is no longer linear, as the system matrices depend on elements of the augmented state.

The augmented state covariance matrix has four partitions corresponding to the original state error covariance, the estimated parameter error covariance and their cross variance

$$\mathbf{P}_a \equiv \begin{bmatrix} \mathbf{P}_x & \mathbf{P}_{x\boldsymbol{\theta}} \\ \mathbf{P}_{x\boldsymbol{\theta}} & \mathbf{P}_\boldsymbol{\theta} \end{bmatrix} \quad (3.32)$$

Problems can appear in convergence of the parameter estimates, due to the constraint given by Eq. (3.27) [26]. This problem can be overcome by introducing fictitious random noise \mathbf{w}_f , so that Eq. (3.27) would be replaced by

$$\dot{\boldsymbol{\theta}} = \mathbf{w}_f \quad (3.33)$$

Application of the extended Kalman filter to aircraft state and parameter estimation is covered in [26] and [27].

3.4 Regression Methods Theory

The methods used for system identification in this project are called *regression methods* and are adapted from [3]. It makes use of the least squares model

in §3.2.3 to estimate the non-dimensional aerodynamic and control derivatives presented in Chapter 2. This section introduces the ordinary least-squares estimation method, which is a batch method. The expansion to a recursive least-squares method capable of real-time parameter estimation is also introduced later in this section. Methods to accommodate changing parameters are discussed at the end of this section.

3.4.1 Ordinary Least Squares

The theory in this section is adapted from [28] and [3]. Consider the linear model equation

$$\mathbf{y} = \mathbf{X}\boldsymbol{\theta} \quad (3.34)$$

and the linear measurement equation

$$\mathbf{z} = \mathbf{X}\boldsymbol{\theta} + \mathbf{v} \quad (3.35)$$

where

$$\begin{aligned} \mathbf{z} &= \begin{bmatrix} z(1) & z(2) & \cdots & z(N) \end{bmatrix}^T = N \times 1 \text{ vector of measurements} \\ \boldsymbol{\theta} &= \begin{bmatrix} \theta_0 & \theta_1 & \cdots & \theta_n \end{bmatrix}^T = n_p \times 1 \text{ vector of unknown parameters, } n_p = n + 1 \\ \mathbf{X} &= \begin{bmatrix} \mathbf{1} & \boldsymbol{\xi}_1 & \cdots & \boldsymbol{\xi}_n \end{bmatrix} N \times n_p \text{ known matrix of ones and regressors, } N > n \\ \mathbf{v} &= \begin{bmatrix} v(1) & v(2) & \cdots & v(N) \end{bmatrix}^T = N \times 1 \text{ vector of white noise.} \end{aligned}$$

Note that N is the number of measurements taken, n is the number of regressors and n_p is the number of parameters to be estimated. The reason for introducing the vector of ones in \mathbf{X} is to accommodate the constant bias term in the measurements, thus $n_p = n + 1$.

For the least-squares model, there are no probability statements regarding $\boldsymbol{\theta}$ or \mathbf{v} , but \mathbf{v} is assumed to be zero mean and uncorrelated, with constant variance,

$$E(\mathbf{v}) = \mathbf{0} \quad E(\mathbf{v}\mathbf{v}^T) = \sigma^2 \mathbf{I} \quad (3.36)$$

The best estimation of $\boldsymbol{\theta}$ in a least-squares sense comes from minimising

$$\|\mathbf{v}\| = (v(1)^2 + v(2)^2 + \cdots + v(N)^2)^{1/2} \quad (3.37)$$

i.e. minimising the cost function

$$J(\boldsymbol{\theta}) = \frac{1}{2}(\mathbf{z} - \mathbf{X}\boldsymbol{\theta})^T(\mathbf{z} - \mathbf{X}\boldsymbol{\theta}) \quad (3.38)$$

The least squares problem can thus be interpreted as the problem of finding the constants $\theta_0, \dots, \theta_n$ such that the vector \mathbf{z} is approximated as accurately as possible by the linear combination of the vectors x^1, x^2, \dots, x^n where x^i represents the i^{th} column of the matrix \mathbf{X} . Figure 3.1 shows how this can be represented geometrically for the estimation of two parameters.

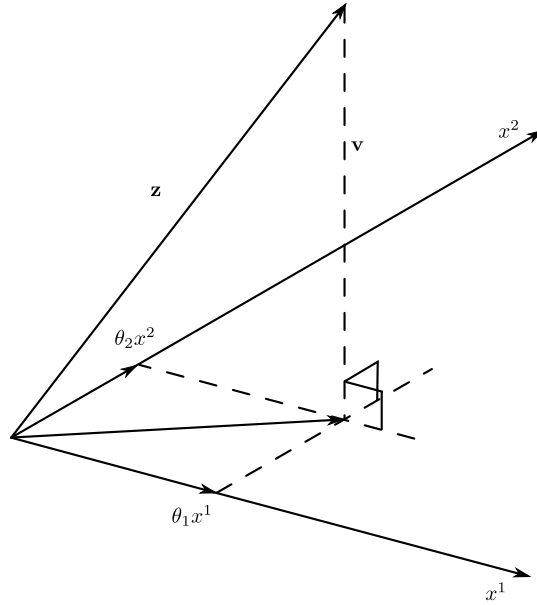


Figure 3.1: Geometric interpretation of the least squares estimate

The estimate $\hat{\boldsymbol{\theta}}$ that minimises the cost function $J(\boldsymbol{\theta})$ must satisfy

$$\frac{dJ}{d\boldsymbol{\theta}} = -\mathbf{X}^T \mathbf{z} + \mathbf{X}^T \mathbf{X} \hat{\boldsymbol{\theta}} = \mathbf{0} \quad (3.39)$$

or

$$\mathbf{X}^T \mathbf{X} \hat{\boldsymbol{\theta}} = \mathbf{X}^T \mathbf{z} \quad (3.40)$$

or

$$\mathbf{X}^T(\mathbf{z} - \mathbf{X}\hat{\boldsymbol{\theta}}) = \mathbf{0} \quad (3.41)$$

The n equations represented in Eq. (3.41) are called the normal equations. The solution of these equations for the unknown parameter vector $\boldsymbol{\theta}$ gives the formula for the least-squares estimator,

$$\hat{\boldsymbol{\theta}} = (\mathbf{X}^T \mathbf{X})^{-1} \mathbf{X}^T \mathbf{z} \quad (3.42)$$

The $n \times n$ matrix $\mathbf{X}^T \mathbf{X}$ is always symmetric. If the regressor vectors that make up the columns of \mathbf{X} are linearly independent, then $\mathbf{X}^T \mathbf{X}$ is positive definite, the eigenvalues of $\mathbf{X}^T \mathbf{X}$ are positive real numbers, the associated eigenvectors are mutually orthogonal, and $(\mathbf{X}^T \mathbf{X})^{-1}$ exists.

The covariance matrix of the parameter estimate $\hat{\boldsymbol{\theta}}$, also known as the covariance matrix of the estimation error $\hat{\boldsymbol{\theta}} - \boldsymbol{\theta}$, is given by

$$\begin{aligned} \text{Cov}(\hat{\boldsymbol{\theta}}) &\equiv E[(\hat{\boldsymbol{\theta}} - \boldsymbol{\theta})(\hat{\boldsymbol{\theta}} - \boldsymbol{\theta})^T] \\ &= E\{(\mathbf{X}^T \mathbf{X})^{-1} \mathbf{X}^T (\mathbf{z} - \mathbf{y})(\mathbf{z} - \mathbf{y})^T \mathbf{X} (\mathbf{X}^T \mathbf{X})^{-1}\} \\ &= (\mathbf{X}^T \mathbf{X})^{-1} \mathbf{X}^T E(\mathbf{v}\mathbf{v}^T) \mathbf{X} (\mathbf{X}^T \mathbf{X})^{-1} \end{aligned} \quad (3.43)$$

where the true parameter vector $\boldsymbol{\theta}$ is related to the true output vector \mathbf{y} by $\boldsymbol{\theta} = (\mathbf{X}^T \mathbf{X})^{-1} \mathbf{X}^T \mathbf{y}$. With the assumption that the measurement errors are uncorrelated and have constant variance as in Eq. (3.36), the expression for the covariance matrix of $\hat{\boldsymbol{\theta}}$ is simplified to

$$\text{Cov}(\hat{\boldsymbol{\theta}}) = E[(\hat{\boldsymbol{\theta}} - \boldsymbol{\theta})(\hat{\boldsymbol{\theta}} - \boldsymbol{\theta})^T] = \sigma^2 (\mathbf{X}^T \mathbf{X})^{-1} = \sigma^2 \mathcal{D} \quad (3.44)$$

where \mathcal{D} is defined as

$$\mathcal{D} = (\mathbf{X}^T \mathbf{X})^{-1} \quad (3.45)$$

3.4.2 Recursive Least Squares

In the previous section, the linear measurement equation was expressed as:

$$\mathbf{z} = \mathbf{X}\boldsymbol{\theta} + \mathbf{v} \quad (3.46)$$

where

$$E(\mathbf{v}) = \mathbf{0} \quad E(\mathbf{v}\mathbf{v}^T) = \sigma^2 \mathbf{I} \quad (3.47)$$

The ordinary least-squares solution based on k measurements followed from minimisation of the cost function

$$J(\boldsymbol{\theta}) = \frac{1}{2} \sum_{i=1}^k [z(i) - \mathbf{x}^T(i)\boldsymbol{\theta}]^2 \quad (3.48)$$

as

$$\boldsymbol{\theta}(k) = \mathcal{D}(k) \mathbf{X}_k^T \mathbf{Z}_k \quad (3.49a)$$

$$\text{Cov}[\hat{\boldsymbol{\theta}}(k)] = \sigma^2 \mathcal{D}(k) \quad (3.49b)$$

where

$$\mathcal{D}(k) = [\mathbf{X}_k^T \mathbf{X}_k]^{-1} \quad (3.50a)$$

$$\mathbf{X}_k^T = [\mathbf{x}(1) \quad \mathbf{x}(2) \quad \cdots \quad \mathbf{x}(k)] \quad (3.50b)$$

$$\mathbf{Z}_k = [z(1) \quad z(2) \quad \cdots \quad z(k)]^T \quad (3.50c)$$

When a new measurement $z(k+1)$ is available, the ordinary least-squares solution from Eq. (3.42) then becomes

$$\begin{aligned} \boldsymbol{\theta}(k+1) &= \mathcal{D}(k+1) \mathbf{X}_{k+1}^T \mathbf{Z}_{k+1} \\ &= \mathcal{D}(k+1) [\mathbf{X}_k^T \mathbf{Z}_k + \mathbf{x}(k+1)z(k+1)] \end{aligned} \quad (3.51)$$

where

$$\begin{aligned} \mathcal{D}(k+1) &= [\mathbf{X}_{k+1}^T \mathbf{X}_{k+1}]^{-1} \\ &= \left\{ \begin{bmatrix} \mathbf{X}_k \\ \mathbf{x}^T(k+1) \end{bmatrix}^T \begin{bmatrix} \mathbf{X}_k \\ \mathbf{x}^T(k+1) \end{bmatrix} \right\}^{-1} \\ &= [\mathbf{X}_k^T \mathbf{X}_k + \mathbf{x}(k+1)\mathbf{x}^T(k+1)]^{-1} \\ &= [\mathcal{D}^{-1}(k) + \mathbf{x}(k+1)\mathbf{x}^T(k+1)]^{-1} \end{aligned} \quad (3.52)$$

Applying the matrix inversion lemma [3] to this expression results in

$$\mathcal{D}(k+1) = \mathcal{D}(k) - \mathcal{D}(k)\mathbf{x}(k+1)[1 + \mathbf{x}^T(k+1)\mathcal{D}(k)\mathbf{x}(k+1)]^{-1}\mathbf{x}^T(k+1)\mathcal{D}(k) \quad (3.53)$$

Eq. (3.53) represents a direct update of the matrix $\mathcal{D}(k+1) = [\mathbf{X}_{k+1}^T \mathbf{X}_{k+1}]^{-1}$. Using this expression, the inversion of a $p \times p$ matrix in Eq. (3.52) has been replaced by the inversion of a scalar in Eq. (3.53), provided that $\mathcal{D}(k+1) = [\mathbf{X}_{k+1}^T \mathbf{X}_{k+1}]^{-1}$ is non-singular. This will be discussed further in Chapter 5.

Substituting Eq. (3.53) into Eq. (3.51) and using Eq. (3.49),

$$\begin{aligned} \hat{\boldsymbol{\theta}}(k+1) &= \hat{\boldsymbol{\theta}}(k) + \mathcal{D}(k)\mathbf{x}(k+1)z(k+1) \\ &\quad - \mathcal{D}(k)\mathbf{x}(k+1)[1 + \mathbf{x}^T(k+1)\mathcal{D}(k)\mathbf{x}(k+1)]^{-1} \\ &\quad \cdot [\mathbf{x}^T(k+1)\hat{\boldsymbol{\theta}}(k) + \mathbf{x}^T(k+1)\mathcal{D}(k)\mathbf{x}(k+1)z(k+1)] \end{aligned} \quad (3.54)$$

Rearranging the last two terms

$$\begin{aligned} \hat{\boldsymbol{\theta}}(k+1) &= \hat{\boldsymbol{\theta}}(k) - \mathcal{D}(k)\mathbf{x}(k+1)[1 + \mathbf{x}^T(k+1)\mathcal{D}(k)\mathbf{x}(k+1)]^{-1}\mathbf{x}^T(k+1)\hat{\boldsymbol{\theta}}(k) \\ &\quad + \mathcal{D}(k)\mathbf{x}(k+1)[1 + \mathbf{x}^T(k+1)\mathcal{D}(k)\mathbf{x}(k+1)]^{-1}\{[1 + \mathbf{x}^T(k+1) \\ &\quad \cdot \mathcal{D}(k+1)\mathbf{x}(k+1) - \mathbf{x}^T(k+1)\mathcal{D}(k)\mathbf{x}(k+1)]z(k+1)\} \end{aligned} \quad (3.55)$$

or

$$\begin{aligned} \hat{\boldsymbol{\theta}}(k+1) &= \hat{\boldsymbol{\theta}}(k) \\ &\quad + \mathcal{D}(k)\mathbf{x}(k+1)[1 + \mathbf{x}^T(k+1)\mathcal{D}(k)\mathbf{x}(k+1)]^{-1} \\ &\quad \cdot [z(k+1) - \mathbf{x}^T(k+1)\hat{\boldsymbol{\theta}}(k)] \end{aligned} \quad (3.56)$$

Therefore, the recursive least-squares estimate can be computed from the following equations:

$$\hat{\boldsymbol{\theta}}(k+1) = \hat{\boldsymbol{\theta}}(k) + \mathbf{K}(k+1)[z(k+1) - \mathbf{x}^T(k+1)\hat{\boldsymbol{\theta}}(k)] \quad (3.57a)$$

$$\mathbf{K}(k+1) = \mathcal{D}(k)\mathbf{x}(k+1)[1 + \mathbf{x}^T(k+1)\mathcal{D}(k)\mathbf{x}(k+1)]^{-1} \quad (3.57b)$$

$$\begin{aligned} \mathcal{D}(k+1) &= \mathcal{D}(k) - \mathcal{D}(k)\mathbf{x}(k+1) \\ &\quad \cdot [1 + \mathbf{x}^T(k+1)\mathcal{D}(k)\mathbf{x}(k+1)]^{-1}\mathbf{x}^T(k+1)\mathcal{D}(k) \end{aligned} \quad (3.57c)$$

To use the recursive formulae in Eq. (3.57), starting values $\hat{\boldsymbol{\theta}}(0)$ and $\mathcal{D}(0)$ must be specified. These values can be obtained by running the batch equations

(3.49a) and (3.50a) on previously recorded data. If no prior information is available, $\hat{\boldsymbol{\theta}}(0)$ can be set to the zero vector and $\mathcal{D}(0)$ can be chosen as $\mathcal{D}(0) = c\mathbf{I}$ where c is a large number, e.g., $c = 10^6$. This means that the variance of the initial parameter estimates is very large and that the starting values will thus be ignored.

3.4.3 Accommodating Changing Parameter Values

In the recursive least squares method in the previous section the parameters are assumed to be constant over time. This section discuss two ways of accommodating changing parameters. These methods are based on the recursive least squares method in the previous section

3.4.3.1 The Forgetting Factor

In this algorithm, old data in the estimation process are gradually devalued and eventually discarded. The cost function is now formulated as

$$J(\boldsymbol{\theta}) = \frac{1}{2} \sum_{i=k-d}^k \lambda^{k-i} [z(i) - \mathbf{x}^T(i)\boldsymbol{\theta}]^2 \quad 0 < \lambda \leq 1 \quad (3.58)$$

where d is the number of past values included weighted by powers of λ , which is called the forgetting factor. The estimation algorithm that minimises the cost function in Eq. (3.58) can be developed in a manner similar to the recursive least squares in the previous section. The resulting equations are given by [3] as

$$\hat{\boldsymbol{\theta}}(k+1) = \hat{\boldsymbol{\theta}}(k) + \mathbf{K}(k+1)[z(k+1) - \mathbf{x}^T(k+1)\hat{\boldsymbol{\theta}}(k)] \quad (3.59a)$$

$$\mathbf{K}(k+1) = \mathcal{D}(k)\mathbf{x}(k+1)[\lambda + \mathbf{x}^T(k+1)\mathcal{D}(k)\mathbf{x}(k+1)]^{-1} \quad (3.59b)$$

$$\mathcal{D}(k+1) = \frac{1}{\lambda} \{ \mathcal{D}(k) - \mathcal{D}(k)\mathbf{x}(k+1) \cdot [\lambda + \mathbf{x}^T(k+1)\mathcal{D}(k)\mathbf{x}(k+1)]^{-1} \mathbf{x}^T(k+1)\mathcal{D}(k) \} \quad (3.59c)$$

For $\lambda = 1$, Eq. (3.59) reduces to the recursive least-squares equations, Eq. (3.57). For $\lambda \ll 1$, a large weighting is placed on recent data by rapidly fading out older data. Typical values of λ are chosen in the range $0.9 \leq \lambda < 1.0$.

3.4.3.2 Covariance Resetting

As mentioned in §3.4.2, if no prior knowledge of the parameters exist, $\mathcal{D}(0)$ can be chosen as $\mathcal{D}(0) = c\mathbf{I}$ where c is a large number, e.g., $c = 10^6$. The covariance resetting concept refers to periodical resetting of the covariance matrix to $\mathcal{D} = c\mathbf{I}$ where c is a large number, e.g., $c = 10^6$. This ensures that no data recorded before the resetting is taken into account for the estimation process. The estimated parameter values can be updated every time just before the resetting occurs, ensuring accurate parameter estimation. It may happen that the parameters change between two resetting events. In this case the estimated parameters might be inaccurate between the two resetting events.

3.5 Conclusion

This chapter discussed various parameter estimation techniques. The regression methods were discussed in more detail, as they are used in the simulation chapter (Chapter 6). The reasons that the regression methods were chosen, is given below:

- The regression methods are based on the least-squares model, which assumes that the parameter vector $\boldsymbol{\theta}$ is a vector of unknown constant parameters and the measurement noise vector \mathbf{v} is a vector of uncorrelated white noise. This is applicable, because the measurement noise on the sensors used on the Modular UAV is assumed to be white, uncorrelated noise.

- The aerodynamic and control derivative equations, Eq. (2.32) to Eq. (2.34), can easily be manipulated to fit the regression equation, Eq. (3.35).
- The regression methods accommodate changing parameters, which is in line with the aim of the larger project of Fault Tolerant Control of the Modular UAV.

Chapter 4

Applying Regression Methods

4.1 Introduction

This chapter starts by showing how the regression methods discussed in Chapter 3 can be applied to the aerodynamic and control derivative equations derived in Chapter 2. It then continues by discussing how the aerodynamic moment coefficients can be estimated from noisy data using curve fitting.

4.2 Setting Up the Regression Equations

The regression methods theory discussed in §3.4 can be used to estimate the non-dimensional stability and control derivatives of the aircraft. First, the aerodynamic and control derivative equations, Eq. (2.32) to Eq. (2.34), are manipulated to fit the measurement equation, Eq. (3.35) and split into lateral motion

$$C_y = C_{y_\beta}\beta + C_{y_P}\bar{P} + C_{y_R}\bar{R} + C_{y_{\delta_A}}\delta_A + C_{y_{\delta_R}}\delta_R \quad (4.1a)$$

$$C_l = C_{l_0} + C_{l_\beta}\beta + C_{l_P}\bar{P} + C_{l_R}\bar{R} + C_{l_{\delta_A}}\delta_A + C_{l_{\delta_R}}\delta_R \quad (4.1b)$$

$$C_n = C_{n_0} + C_{n_\beta}\beta + C_{n_P}\bar{P} + C_{n_R}\bar{R} + C_{n_{\delta_A}}\delta_A + C_{n_{\delta_R}}\delta_R \quad (4.1c)$$

and longitudinal motion

$$C_L = C_{L_0} + C_{L_\alpha}\alpha + C_{L_Q}\bar{Q} + C_{L_{\delta_E}}\delta_E \quad (4.2a)$$

$$C_D = C_{D_0} + \frac{C_L^2}{\pi\bar{R}e} \quad (4.2b)$$

$$C_m = C_{m_0} + C_{m_\alpha}\alpha + C_{m_Q}\bar{Q} + C_{m_{\delta_E}}\delta_E \quad (4.2c)$$

where \bar{P} , \bar{Q} and \bar{R} are the non-dimensional roll, pitch and yaw rates respectively, given by

$$\bar{P} = \frac{b}{2\bar{V}}P$$

$$\bar{Q} = \frac{\bar{c}}{2\bar{V}}Q$$

$$\bar{R} = \frac{b}{2\bar{V}}R$$

Eqns. (4.1) and (4.2) each are in the form of the measurement equation, Eq. (3.35) if it is assumed that the aircraft state parameters (α, β, P, Q and R) and the control deflections (δ_A, δ_E and δ_R) can be fully measured. The aerodynamic force and moment coefficients on the left side of the previous equations are considered *virtual* measurements. The following section discusses how to determine these virtual measurements.

As mentioned, Eqns. (4.1) and (4.2) each are in the form of the measurement equation, thus each of these six equations can be fit into the measurement equation. To make this clear, an example is given where Eq. (4.1b) is separated into a measurement vector, parameter vector and a matrix of regressors.

Example of using least squares to estimate the nondimensional roll parameters

For the roll equation, Eq. (4.1b),

$$C_l = C_{l_0} \times 1 + C_{l_\beta}\beta + C_{l_P}\bar{P} + C_{l_R}\bar{R} + C_{l_{\delta_A}}\delta_A + C_{l_{\delta_R}}\delta_R \quad (4.4)$$

the least squares variables with N measurements are given by:

$$\mathbf{z} = \begin{bmatrix} C_l(1) & C_l(2) & \cdots & C_l(N) \end{bmatrix}^T \quad (4.5)$$

$$\mathbf{X} = \begin{bmatrix} 1 & \beta(1) & \bar{P}(1) & \bar{R}(1) & \delta_A(1) & \delta_R(1) \\ 1 & \beta(2) & \bar{P}(2) & \bar{R}(2) & \delta_A(2) & \delta_R(2) \\ \vdots & \vdots & \vdots & \vdots & \vdots & \vdots \\ 1 & \beta(N) & \bar{P}(N) & \bar{R}(N) & \delta_A(N) & \delta_R(N) \end{bmatrix} \quad (4.6)$$

$$\boldsymbol{\theta} = \begin{bmatrix} C_{l_0} & C_{l_\beta} & C_{l_P} & C_{l_R} & C_{l_{\delta_A}} & C_{l_{\delta_R}} \end{bmatrix}^T \quad (4.7)$$

4.3 Estimating Aerodynamic Force and Moment Coefficients

The dependent variable values on the left sides of the preceding equations and the C_L term in Eq. (4.2b) can be computed from Eq. (2.29) and Eq. (2.30)

$$C_X = \frac{1}{\bar{q}S}(ma_x - T) \quad (4.8a)$$

$$C_y = \frac{ma_y}{\bar{q}S} \quad (4.8b)$$

$$C_Z = \frac{ma_z}{\bar{q}S} \quad (4.8c)$$

$$C_L = -C_Z \cos \alpha + C_X \sin \alpha \quad (4.8d)$$

$$C_D = -C_X \cos \alpha - C_Z \sin \alpha \quad (4.8e)$$

$$C_l = \frac{1}{\bar{q}Sb} \left[I_x \dot{P} + (I_z - I_y)QR \right] \quad (4.8f)$$

$$C_m = \frac{1}{\bar{q}S\bar{c}} \left[I_y \dot{Q} + (I_x - I_z)PR \right] \quad (4.8g)$$

$$C_n = \frac{1}{\bar{q}Sb} \left[I_z \dot{R} + (I_y - I_x)PQ \right] \quad (4.8h)$$

where a_x , a_y and a_z are the accelerometer measurements. The accelerometers measure the *specific acceleration* of the aircraft and can be related to the applied forces

$$\mathbf{a} = \boldsymbol{\Sigma} = \frac{(\mathbf{F}_A + \mathbf{F}_T)}{m} \quad (4.9)$$

where \mathbf{F}_A is the aerodynamic force and \mathbf{F}_T is the thrust force.

The values of S , \bar{c} , b , I_x , I_y and I_z are considered known constants. It can be seen that these dependent variables are independent of the attitude of the aircraft. To estimate the angular accelerations (\dot{P}, \dot{Q} and \dot{R}) in Eqns. (4.8f), (4.8g) and (4.8h) respectively, smoothed numerical differentiation has to be done on the noisy gyroscope measurements P , Q and R . This is discussed in the following section.

4.3.1 Smoothed numerical differentiation

As mentioned earlier, to do system identification using regression methods, the derivatives of the angular rates of the aircraft must be calculated. Normal Euler differentiation is not an option, since the rate measurements are corrupted with noise and normal differentiation will amplify the noise. Smoothed numerical differentiation can be done by fitting a curve on the last number of data points. The derivative of the data can then be estimated as the derivative of the curve at its centre point. This concept is explained by an example in the following section where the derivative is obtained by fitting a second order curve to five data points.

4.3.1.1 Example of Fitting a Second Order Curve to Five Data Points

This section discusses how the derivatives of the angular rates can be obtained by fitting a second order curve to the last five data points and then using the curve's derivative. This process is demonstrated in Figure 4.1. Note that the third (middle) data point is considered to be at $t = 0$. The derivative is obtained by taking the derivative of the curve at this point. This implies that a two sample delay is introduced, as the derivative at time $t = 0$ can only be estimated after the last data point is sampled at time $t = 2\Delta t$.

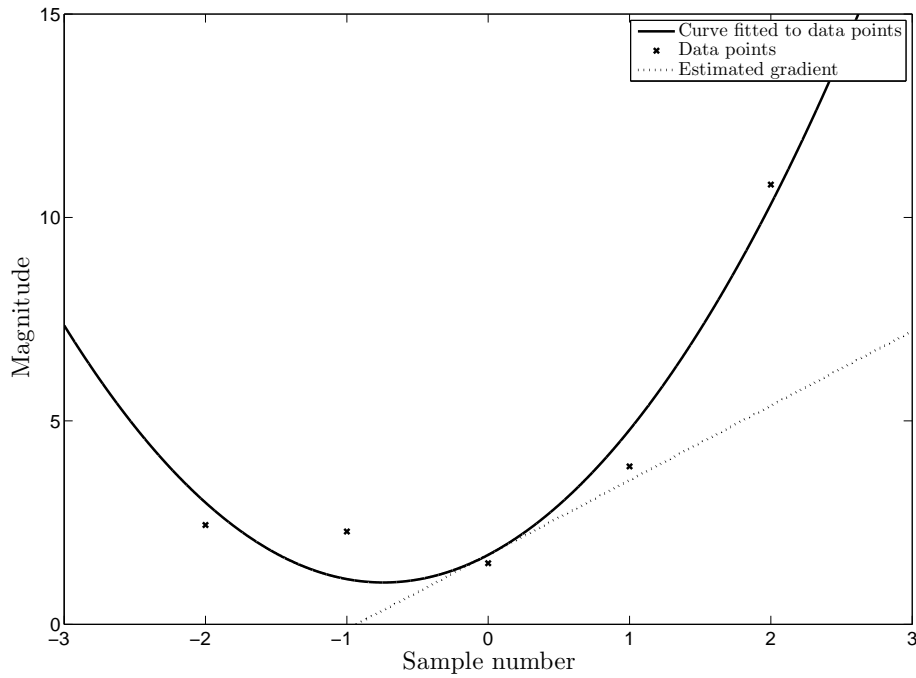


Figure 4.1: Demonstrating how to obtain the derivative of noisy data by fitting a second order curve to the last five data points

It is assumed that the last five measurement points lie on a parabola described by

$$y = a_0 + a_1 t + a_2 t^2 \quad (4.10)$$

If $z(i)$ is the i^{th} measurement taken at time $i\Delta t$, then the equations applicable for the last five data points are

$$a_0 + a_1(-2\Delta t) + a_2(-2\Delta t)^2 = z(i-2) \quad (4.11a)$$

$$a_0 + a_1(-\Delta t) + a_2(-\Delta t) = z(i-1) \quad (4.11b)$$

$$a_0 = z(i) \quad (4.11c)$$

$$a_0 + a_1(\Delta t) + a_2(\Delta t) = z(i+1) \quad (4.11d)$$

$$a_0 + a_1(2\Delta t) + a_2(2\Delta t)^2 = z(i+2) \quad (4.11e)$$

which can be written as

$$\begin{bmatrix} 1 & -2\Delta t & 4(\Delta t)^2 \\ 1 & -\Delta t & (\Delta t)^2 \\ 1 & 0 & 0 \\ 1 & \Delta t & (\Delta t)^2 \\ 1 & 2\Delta t & 4(\Delta t)^2 \end{bmatrix} \begin{bmatrix} a_0 \\ a_1 \\ a_2 \end{bmatrix} = \begin{bmatrix} z(i-2) \\ z(i-1) \\ z(i) \\ z(i+1) \\ z(i+2) \end{bmatrix} \quad (4.12)$$

There are five equations for three unknowns, so the least-squares solution from Eq. (3.42) applies:

$$\hat{\boldsymbol{\theta}} = (\mathbf{X}^T \mathbf{X})^{-1} \mathbf{X}^T \mathbf{z} \quad (4.13)$$

where

$$\mathbf{X} = \begin{bmatrix} 1 & -2\Delta t & 4(\Delta t)^2 \\ 1 & -\Delta t & (\Delta t)^2 \\ 1 & 0 & 0 \\ 1 & \Delta t & (\Delta t)^2 \\ 1 & 2\Delta t & 4(\Delta t)^2 \end{bmatrix}$$

$$\hat{\boldsymbol{\theta}} = \begin{bmatrix} a_0 \\ a_1 \\ a_2 \end{bmatrix}$$

$$\mathbf{z} = \begin{bmatrix} z(i-2) \\ z(i-1) \\ z(i) \\ z(i+1) \\ z(i+2) \end{bmatrix}$$

This produces the resulting normal equations:

$$5a_0 + 10(\Delta t)^2 a_2 = \sum_{k=i-2}^{i+2} z(k) \quad (4.14a)$$

$$10\Delta t a_1 = \sum_{k=i-2}^{i+2} kz(k) \quad (4.14b)$$

$$10a_0 + 34(\Delta t)^2 a_2 = \sum_{k=i-2}^{i+2} k^2 z(k) \quad (4.14c)$$

which gives the least squares estimate of a_0

$$\hat{a}_0 = \frac{34}{70} \sum_{k=i-2}^{i+2} z(k) - \frac{1}{7} \sum_{k=i-2}^{i+2} k^2 z(k) \quad (4.15)$$

which is the smoothed value of $z(i)$.

The derivative of Eq. (4.10) yields

$$\dot{y} = a_1 + 2a_2 t \quad (4.16)$$

which, at time $t = 0$, gives the smoothed derivative

$$\dot{z}(i) = \hat{a}_1 = \frac{1}{10\Delta t} \sum_{k=i-2}^{i+2} kz(k) \quad (4.17)$$

4.3.1.2 Averaging and Differential Kernels

This section serves to generalise the derivation in the previous section to be applicable to higher order curves fitted on more data points by using filter kernels. Using a filter kernel replaces the need to calculate Eq. (4.15) and Eq. (4.17) for every new data point, but has exactly the same result.

In the previous section an expression is presented for the smoothed average and differential using curve fitting on the last five data points on a parabola. Other expressions can be developed by fitting a higher order curve on more data points, provided that the amount of data points is more than twice the order of the curve. The average and differential expressions can be represented

by a filter kernel. This kernel can be multiplied by a column vector of the last few data points. For example, for the five data points in the previous section, the average can be expressed as

$$\bar{P} = \begin{bmatrix} -0.086 & 0.343 & 0.486 & 0.343 & -0.086 \end{bmatrix} \begin{bmatrix} P(t - 4\Delta t) \\ P(t - 3\Delta t) \\ P(t - 2\Delta t) \\ P(t - \Delta t) \\ P(t) \end{bmatrix} \quad (4.18)$$

and the differential can be expressed as

$$\dot{P} = \begin{bmatrix} -0.2 & -0.1 & 0 & 0.1 & 0.2 \end{bmatrix} / \Delta t \begin{bmatrix} P(t - 4\Delta t) \\ P(t - 3\Delta t) \\ P(t - 2\Delta t) \\ P(t - \Delta t) \\ P(t) \end{bmatrix} \quad (4.19)$$

Table 4.1 shows the kernels for higher order curves and for data points equal to twice the order of the curve plus one. Note that, to save space, only half of the kernels are given in Table 4.1, as the averaging kernel is symmetrical and the differential kernel is negatively symmetrical. The first line for each order of curve gives the averaging kernel and the second line the differential kernel.

Order	Half of Kernel
2	$\begin{bmatrix} -0.085714 & 0.34286 & 0.48571 \end{bmatrix}$ $\begin{bmatrix} -0.2 & -0.1 & 0 \end{bmatrix}$
3	$\begin{bmatrix} -0.095238 & 0.14286 & 0.28571 & 0.33333 \end{bmatrix}$ $\begin{bmatrix} -0.10714 & -0.071429 & -0.035714 & 0 \end{bmatrix}$
4	$\begin{bmatrix} -0.090909 & 0.060606 & 0.16883 & 0.23377 & 0.25541 \end{bmatrix}$ $\begin{bmatrix} -0.066667 & -0.05 & -0.033333 & -0.016667 & 0 \end{bmatrix}$
5	$\begin{bmatrix} -0.083916 & 0.020979 & 0.10256 & 0.16084 & 0.1958 & 0.20746 \end{bmatrix}$ $\begin{bmatrix} -0.045455 & -0.036364 & -0.027273 & -0.018182 & -0.0090909 & 0 \end{bmatrix}$

Table 4.1: The averaging and differential kernels

4.4 Conclusion

This chapter discussed how the regression methods can be applied to the aerodynamic and control derivative equations in Eqns. (4.1) and (4.2). It also shows how to estimate the aerodynamic force and moment coefficients. The aerodynamic moment coefficients are calculated from the derivatives of the angular rates of the aircraft. The measurements of the angular rates can be noisy, thus a method was introduced to estimate the derivatives by using curve fitting. This method can be implemented by using the differential and averaging kernels discussed. This introduces a lag in the estimated aerodynamic moment coefficients. This implies that all the measured data should be filtered to in such a way that the same amount of lag is introduced.

The actuator deflections can be obtained by passing the actuator commands through a servo model, which takes the slew rates of the actuators into account. The actuator deflections do not need to be filtered, as they are not corrupted with measurement noise. This deflection must then be delayed with the same amount as the lag introduced by filtering.

The delays introduced by filtering causes a delay in the estimated parameters, i.e. the parameters estimates updated now are actually parameter estimates for a couple of sample periods back.

Chapter 5

Parameter Identifiability

5.1 Introduction

The previous chapter discussed how regression methods can be implemented to perform system identification on the model of the aircraft presented in Chapter 2. However, it is not always possible to identify the parameters. This can happen if two or more regressors are linearly dependent due to a lack of excitation or a control law that produces a control signal that is highly correlated with one of the other regressors.

This chapter discusses how to test for data collinearity and how data collinearity can be prevented by superimposing an excitation signal on the control signal.

5.2 Data Collinearity

If a regressor in Eq. (3.35) is equal to a linear combination of one or more of the other regressors, then the involved regressors are linearly dependent. This means that many different weighted combinations of these linearly dependent

regressors will result in the same variation in the dependent variable, thus the minimum error in Eq. (3.37)

$$\|\mathbf{v}\| = (v(1)^2 + v(2)^2 + \dots + v(N)^2)^{1/2} \quad (5.1)$$

is only unique if the matrix $\mathbf{X}^T \mathbf{X}$ is non-singular (e.g. it has full rank) and the estimated parameters are given by Eq. (3.42)

$$\hat{\boldsymbol{\theta}} = (\mathbf{X}^T \mathbf{X})^{-1} \mathbf{X}^T \mathbf{z} \quad (5.2)$$

Various degrees of data collinearity can exist. If the regressors are almost linearly dependent, $(\mathbf{X}^T \mathbf{X})^{-1}$ exists, but the estimate of the parameters $\hat{\boldsymbol{\theta}}$, might not be accurate because of the noise in the system. In order to detect data collinearity, the regressors must be standardised as done in [3]. This is shown in the following subsection. §5.2.2 shows how to detect data collinearity using the standardised regressors.

5.2.1 Standardised Regressors

Several scaling techniques exist. The one discussed in this section is known as *unit length scaling*. The equations for the transformed regressors and response variable are

$$\xi_j^*(i) = \frac{\xi_j(i) - \bar{\xi}_j}{\sqrt{S_{jj}}} \quad \begin{array}{l} i = 1, 2, \dots, N \\ j = 1, 2, \dots, n \end{array} \quad (5.3)$$

$$z^*(i) = \frac{z(i) - \bar{z}}{\sqrt{S_{zz}}} \quad i = 1, 2, \dots, N \quad (5.4)$$

where

$$S_{jj} = \sum_{i=1}^N [\xi_j(i) - \bar{\xi}_j]^2 \quad (5.5)$$

is the centered sum of squares for the regressor ξ_j , and

$$S_{zz} = \sum_{i=1}^N [z(i) - \bar{z}]^2 \quad (5.6)$$

is the centered sum of squares for the response \mathbf{z} . With this scaling, each new regressor $\boldsymbol{\xi}_j^*$ has mean value

$$\bar{\xi}_j^* = 0 \quad j = 1, 2, \dots, n \quad (5.7)$$

and length

$$\|\boldsymbol{\xi}_j^*\| = \sqrt{\sum_{i=1}^N [\xi_j^*(i)]^2} = 1 \quad j = 1, 2, \dots, n \quad (5.8)$$

The regression model with scaled regressors now takes the form

$$z^*(i) = \theta_1^* \xi_1^*(i) + \theta_2^* \xi_2^*(i) + \dots + \theta_n^* \xi_n^*(i) + v(i) \quad j = 1, 2, \dots, n \quad (5.9)$$

Note that the constant bias term θ_0 is omitted because the regressors and the response variable are now centered, with their mean values removed.

Using vector and matrix notation as in Eq. (3.42), the least-squares estimator becomes

$$\hat{\boldsymbol{\theta}}^* = (\mathbf{X}^{*T} \mathbf{X}^*)^{-1} \mathbf{X}^{*T} \mathbf{z}^* \quad (5.10)$$

where

$$\mathbf{X}^* = \begin{bmatrix} \boldsymbol{\xi}_1^* & \boldsymbol{\xi}_2^* & \dots & \boldsymbol{\xi}_n^* \end{bmatrix} \quad (5.11)$$

The $\mathbf{X}^{*T} \mathbf{X}^*$ matrix then takes the form of a correlation matrix

$$\mathbf{X}^{*T} \mathbf{X}^* = \begin{bmatrix} 1 & r_{12} & r_{13} & \dots & r_{1n} \\ r_{21} & 1 & r_{23} & \dots & r_{2n} \\ \vdots & & & & \vdots \\ r_{n1} & r_{n2} & r_{n3} & \dots & 1 \end{bmatrix} \quad (5.12)$$

where

$$r_{jk} = \frac{\sum_{i=1}^N [\xi_j(i) - \bar{\xi}_j][\xi_k(i) - \bar{\xi}_k]}{\sqrt{S_{jj}S_{kk}}} \quad j, k = 1, 2, \dots, n \quad (5.13)$$

is the simple pair-wise correlation between $\boldsymbol{\xi}_j$ and $\boldsymbol{\xi}_k$ [3].

The parameters in the vector $\boldsymbol{\theta}^*$ are called standardised parameters and relate to the original parameters by

$$\theta_j = \theta_j^* \sqrt{\frac{S_{zz}}{S_{jj}}} \quad j = 1, 2, \dots, n \quad (5.14)$$

$$\hat{\theta}_0 = \bar{z} - \sum_{j=1}^n \hat{\theta}_j^* \bar{\xi}_j \quad (5.15)$$

5.2.2 Detection of Data Collinearity

Many procedures have been developed to detect collinearity [3]. A simple procedure for assessing collinearity is to examine the standardised regressor correlation matrix $\mathbf{X}^{*T} \mathbf{X}^*$. A high correlation coefficient can indicate a possible collinearity problem. A good rule of thumb is that collinearity might cause problems in the parameter estimation process for any pairwise regressor correlation with absolute value greater than 0.9 [3].

If a pairwise regressor correlation has an absolute value greater than 0.9, the estimated parameters might not be accurate. This can be prevented by designing an input in such a way that collinearity is not a problem anymore. In the case where the data is acquired from a system in a closed loop, an excitation signal can be superimposed on the control signal. This is discussed in the next section.

5.3 Input Design

When conducting a test flight, it is important to excite the natural modes of the aircraft. There are two general approaches. The first is to design the input assuming no *a priori* knowledge of the parameters is available. The goal in that case is to design an input in such a way that the system is excited over a broad frequency range. These inputs include frequency sweeps, impulse inputs and multisine inputs. The second approach, which will be used in this project,

is to use *a priori* knowledge about the aircraft. The goal in this case is to design the inputs to excite the aircraft at or near the *a priori* estimates of the natural frequencies for the dynamic modes. This will ensure that a good excitation is obtained by using the least amount of energy and time. §5.4 discusses how these frequencies can be estimated.

There are many different input forms that can be used for flight-test manoeuvres. Some of these are discussed below. The inputs shown are perturbations from the trim value and can be superimposed on the input signal.

5.3.1 Impulse

The impulse is a simple input that excites a wide frequency range. It is simply a spike or sudden bump, often called a stick rap [3]. Figure 5.1 shows the impulse and its power spectrum. Note that the impulse is not a perfect impulse, but has a finite width. The power spectrum is wideband, but with low amplitude. The impulse can also be two-sided to help return the aircraft to its initial condition. Theoretically, the impulse can be used to collect modelling data when there is no *a priori* information, but this is often impractical because of the low input energy.

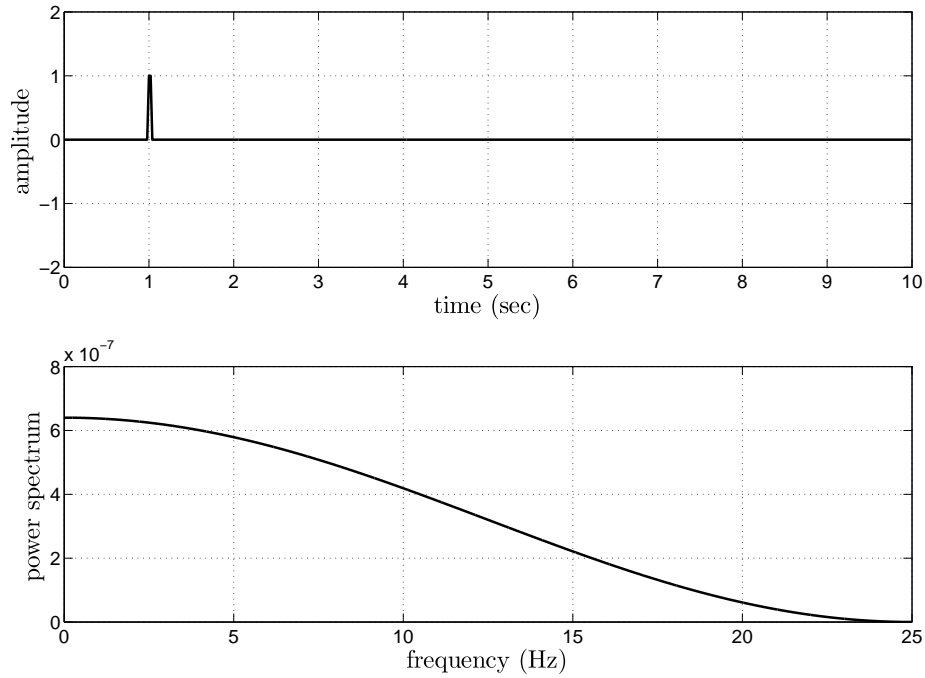


Figure 5.1: Impulse input

5.3.2 Frequency Sweeps

The frequency sweep is more commonly used when there is little or no *a priori* information [3]. The idea is to apply a continuous sinusoid with the frequency increasing in time, so that the frequency of the input covers the frequency band of interest. The linear frequency sweep can be described mathematically by [3]

$$\begin{aligned} u(i) &= \sin[\varphi(i)] & i &= 0, 2, 3, \dots, N-1 \\ \varphi(i) &= \omega_0 t(i) + \frac{1}{2}(\omega_1 - \omega_0) \frac{[t(i)]^2}{T} & i &= 0, 2, 3, \dots, N-1 \end{aligned} \quad (5.16)$$

where $t(i) = i\delta t$, T is the manoeuvre time, $T = (N-1)\delta t$, and $[\omega_0, \omega_1]$ rad/s is the frequency band. Figure 5.2 shows the linear frequency sweep.

Frequency sweeps are often used to collect data for generating a bode plot. The abscissa of the Bode plot is a logarithmic scale. This means that using the linear frequency sweep defined in Eq. (5.16) gives sparse frequency content at

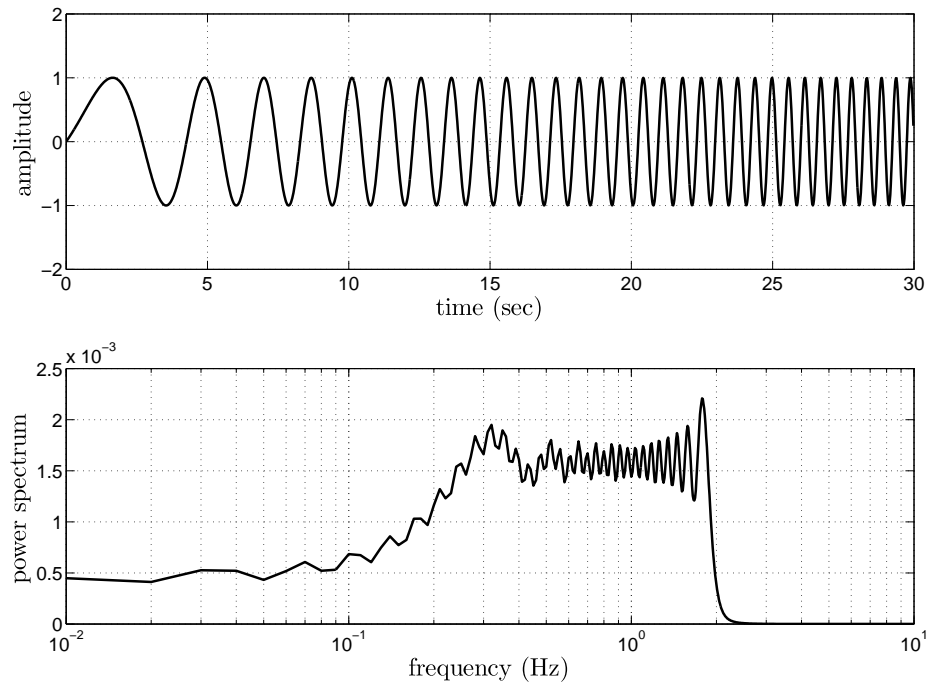


Figure 5.2: Linear frequency sweep input

the lower frequencies. This can be avoided by using a logarithmic frequency sweep, which can be implemented by using Eq. (5.16) with

$$\varphi(i) = \omega_0 t(i) + c_2(\omega_1 - \omega_0) \left[\frac{T}{c_1} e^{c_1 t(i)/T} - t(i) \right] \quad i = 0, 2, 3, \dots, N - 1 \quad (5.17)$$

where $c_1 = 4$ and $c_2 = 0.0187$ have been found to work well in practice [29]. Figure 5.3 shows the logarithmic frequency sweep for the frequency band stretching from 0.1 Hz to 2 Hz.

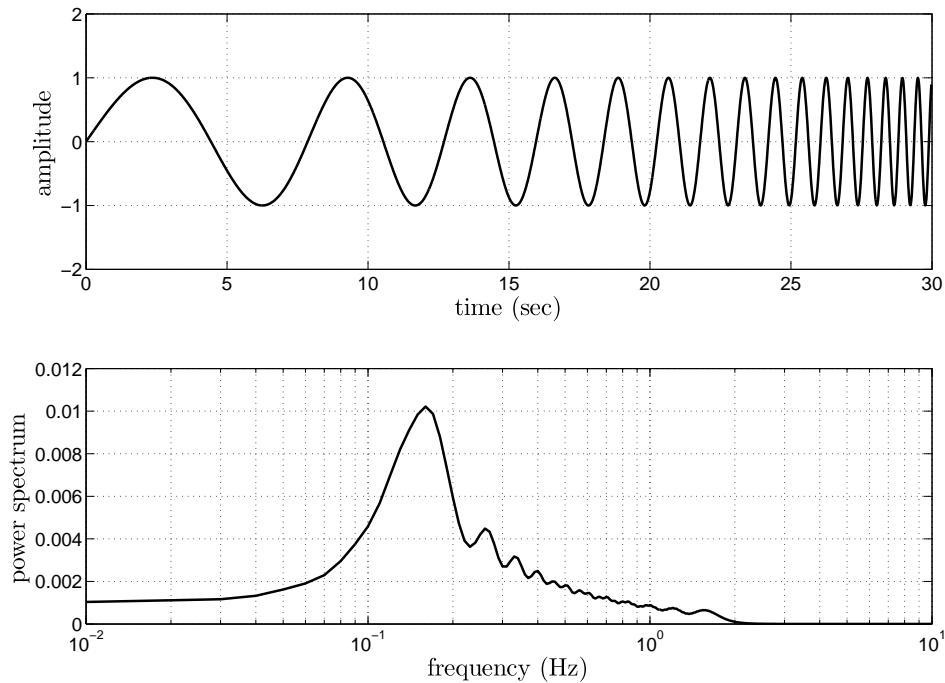


Figure 5.3: Logarithmic frequency sweep input

5.3.3 Multisine Inputs

Multisine inputs is a summation of multiple sine waves with various frequencies, amplitudes and phase angles. The frequencies are chosen to span the frequency band of interest and the amplitudes to achieve a specific power distribution through the frequency band. The phase angles can be chosen arbitrarily, often in such a way as to ensure that the signal equals zero at the start. The time length of excitation can be chosen to ensure that the excitation signal ends in a zero as well. This means that the perturbed signal will have no sharp edges at the beginning and at the end of the perturbation.

One type of multisine input that is used in aircraft system identification consists of the sum of multiple harmonic sinusoids with individual phase lags.

The input takes the form

$$u(i) = \sum_{k=1}^M A_k \cos\left(\frac{2\pi kt(i)}{T} + \phi_k\right) \quad i = 0, 1, 2, \dots, N-1 \quad (5.18)$$

where M is the total number of available harmonically related frequencies, T is the time length of the excitation and ϕ_k are phase angles for each of the harmonic components. ϕ_k can be chosen to produce a low peak factor (PF), defined by

$$\text{PF}(\mathbf{u}) = \frac{[\max(\mathbf{u}) - \min(\mathbf{u})]/2}{\sqrt{(\mathbf{u}^T \mathbf{u})/N}} \quad (5.19)$$

where $\mathbf{u} = [u_0, u_1, \dots, u_{N-1}]^T$, or

$$\text{PF}(\mathbf{u}) = \frac{[\max(\mathbf{u}) - \min(\mathbf{u})]/2}{\text{rms}(\mathbf{u})} \quad (5.20)$$

A single sinusoidal component has $\text{PF} = \sqrt{2}$, so the relative peak factor (RPF), defined by

$$\text{RPF} = \frac{\text{PF}}{\sqrt{2}} \quad (5.21)$$

quantifies the peak factor of \mathbf{u} relative to the peak factor of a single sinusoid.

The relative peak factor is a measure of efficiency of an input for parameter estimation purposes, in terms of the amplitude range of the input divided by a measure of the input energy [3]. Lower peak factors are more desirable for parameter estimation, where the aim is to excite the system with a variety of frequencies without driving the input too far from the trim condition.

Figure 5.4 shows the RPF of a multisine input consisting of two sinusoids phase-shifted by ϕ_1 and ϕ_2 respectively. It can be seen that a minimum RPF exists for multiple phase combinations. It is possible to choose the phase in such a way that the input begins and ends at zero magnitude.

Schroeder [30] has shown that a phase-shifted sum of sinusoids, often referred to as a Schroeder sweep, provides an input with good frequency content and a low peak factor. For a uniform power spectrum, the Schroeder sweep input results from Eq. (5.18) with

$$\begin{aligned} A_k &= \sqrt{P/M} \\ \phi_1 &= 0 \\ \phi_k &= \phi_{k-1} - \frac{\pi k^2}{M} \quad k = 2, 3, \dots, M \end{aligned} \quad (5.22)$$

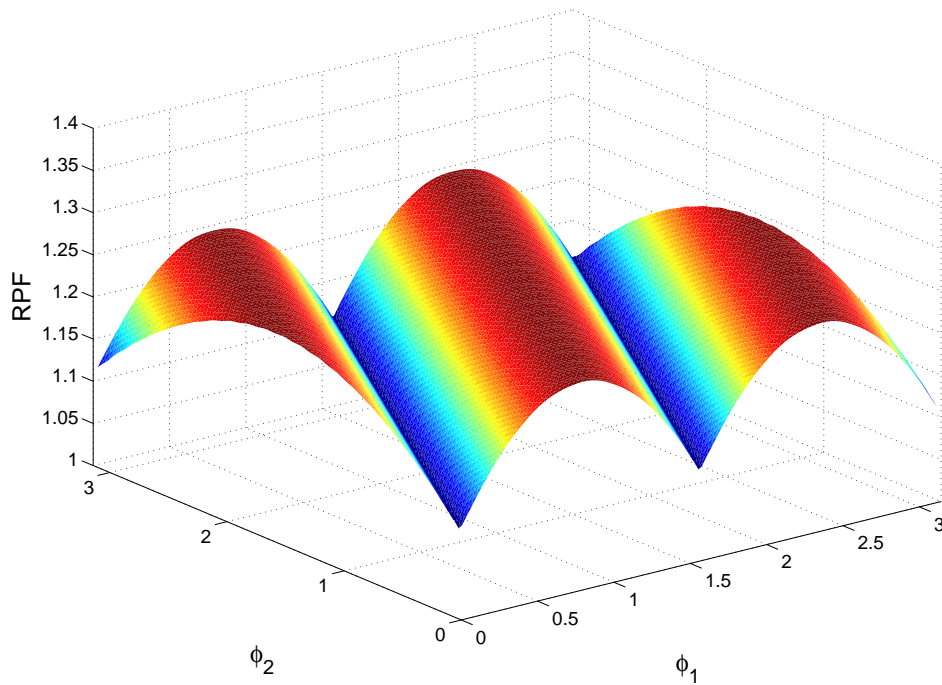


Figure 5.4: Relative peak factors for a two-component multisine input

where P is the total desired input power. Comparisons of the Schroeder sweep with linear and logarithmic frequency sweep inputs have indicated that the Schroeder sweep is generally the superior input for dynamic modeling in the frequency domain [31]. The Schroeder sweep has been used successfully in practical aircraft system identification problems [32; 33].

Figure 5.5 and Figure 5.6 show multisine inputs with the corresponding power spectrums for a low and high RPF respectively.

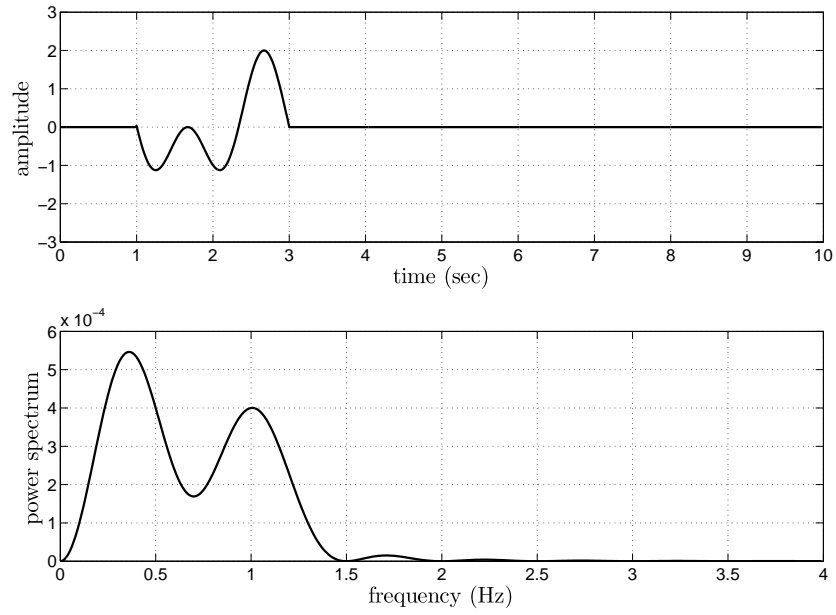


Figure 5.5: Multisine input with low RPF of 1.1

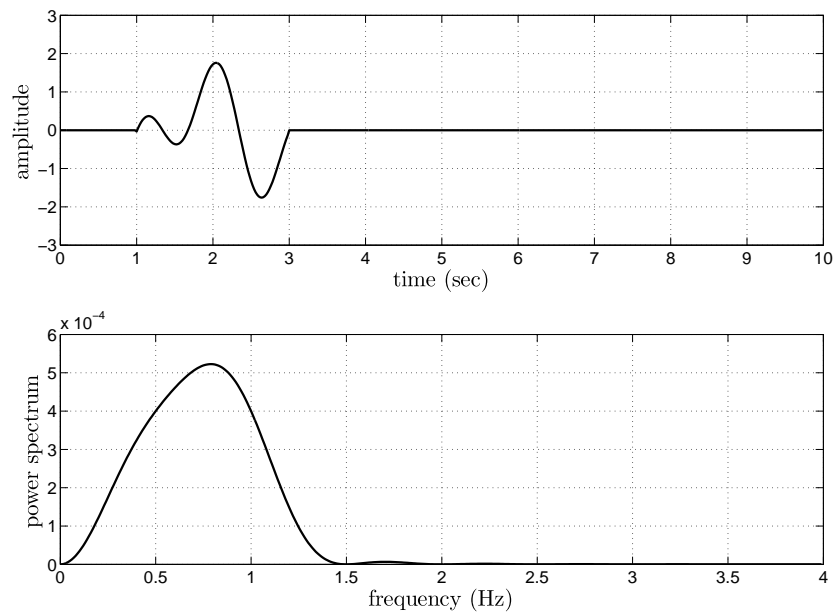


Figure 5.6: Multisine input with high RPF of 1.24

5.3.4 Doublets and Multisteps

Doublets are two-sided pulses as shown in Figure 5.7. For the doublet shown, the dominant frequency is just a bit less than 0.5 Hz. The reason for this is that only a single isolated doublet is used, not a train of doublets. The length of the doublet can be adjusted to fit the expected natural frequency of the system.

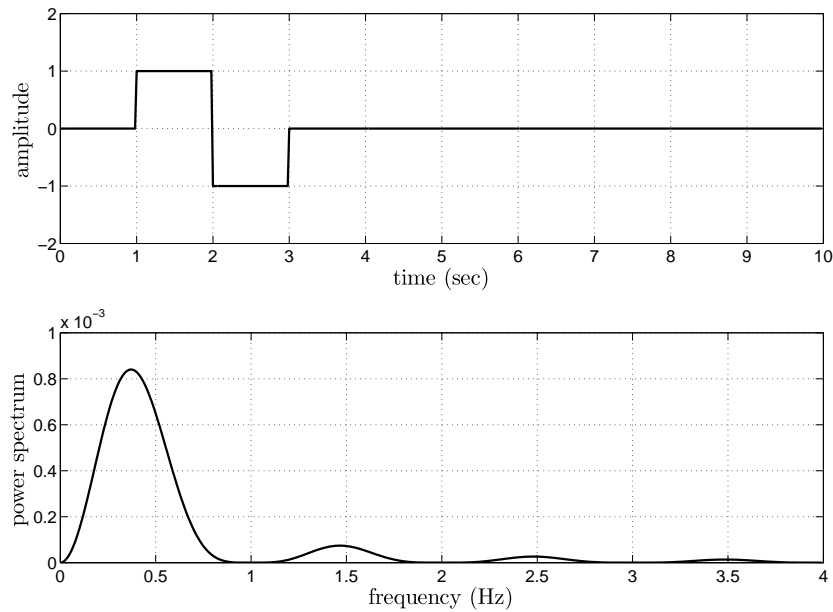


Figure 5.7: Doublet input

Note that the square edges of the doublet input produce a wider frequency spectrum than the single spike that would be obtained with a pure sine wave at the same basic frequency. The square-wave form is therefore useful for purposes of system identification. The amplitude of the doublet is chosen in such a way as to obtain a good signal-to-noise ratio at the output, but not large enough to violate the small-angle assumption in the model.

More pulses with different widths can be added to the doublet. A common input for aircraft system identification is called the 3-2-1-1 [3]. This input

consists of multiple alternating pulses with widths in the ratio 3-2-1-1 as shown in Figure 5.8. The width of the 2 pulse is selected to correspond to half the period of the expected natural frequency (0.5 Hz in the Figure 5.8). The 3 and 1 pulses widen the frequency band on both sides of the expected natural frequency, resulting in a relatively wideband input. Comparing Figure 5.7 and Figure 5.8, it can be seen that the 3-2-1-1 has a much richer frequency content than a doublet.

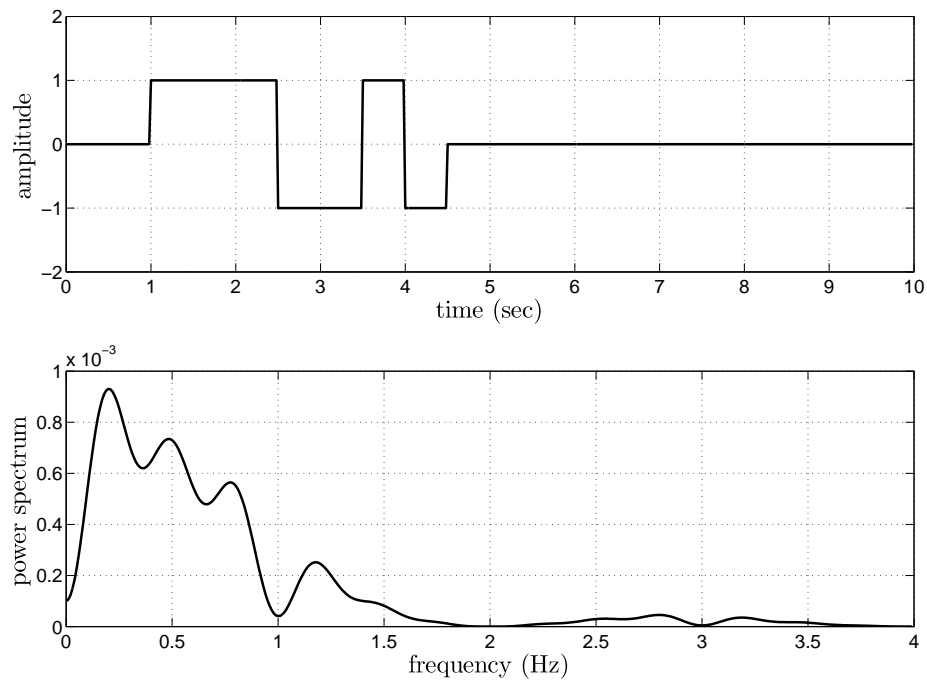


Figure 5.8: 3-2-1-1 input

The 3-2-1-1 input is sometimes difficult to use because the 3 pulse is long and tends to drive the aircraft off its current flight condition [3]. To address this, a 2-1-1 input can be used instead. Figure 5.9 shows that the pulse widths are chosen in a ratio 2-1-1. The following choice for the 1 pulse has been found to work well [3]:

$$1 \text{ pulse width} = \frac{0.7}{2f_n} \quad (5.23)$$

where f_n is the expected natural frequency in Hz for the dominant mode.

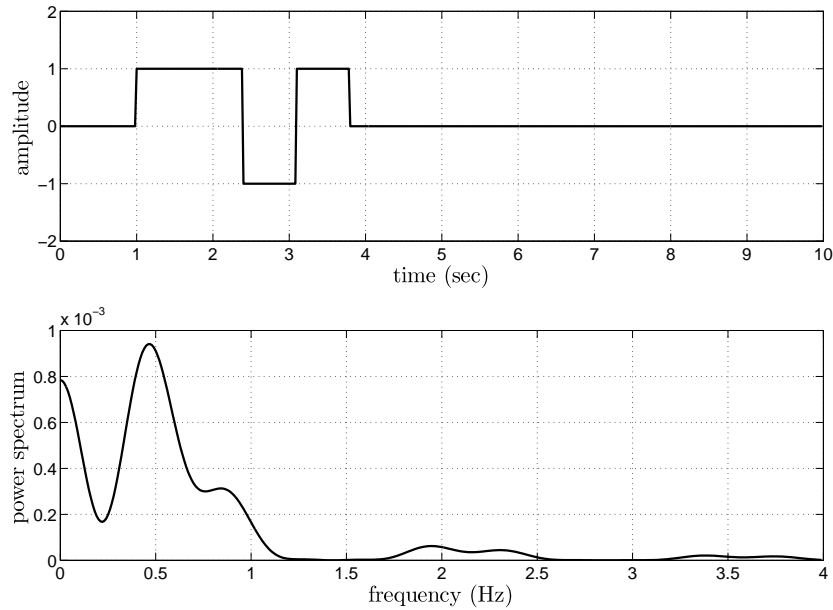


Figure 5.9: 2-1-1 input

It is possible to design an input signal consisting of multiple steps with various amplitudes. Allowing different input amplitudes for each pulse expands the possibilities for input spectra using a multistep input form.

Another practical approach is to use an input perturbation consisting of multiple doublets with different durations as shown in Figure 5.10. Comparing this with Figure 5.7, it can be seen that this approach provides more input power over a wider frequency band.

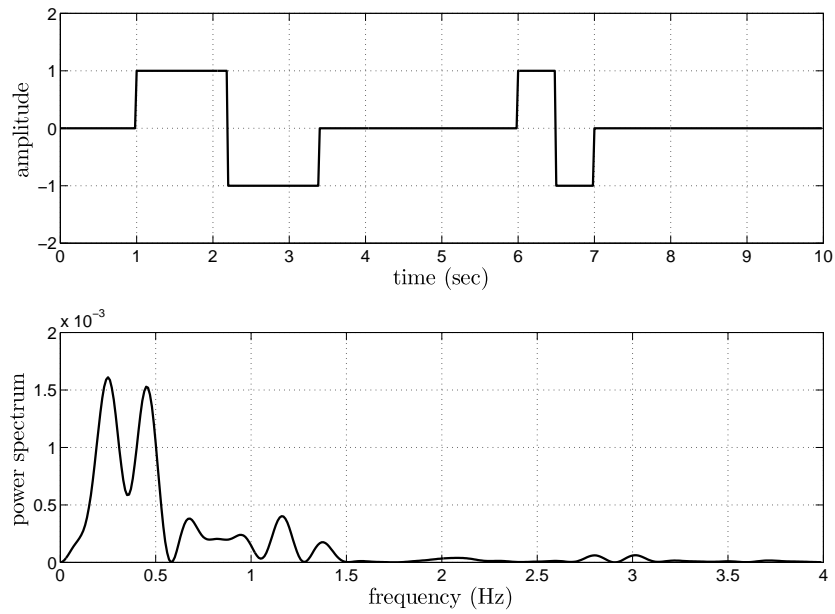


Figure 5.10: Compound doublet input

5.4 Determining the Natural Frequency of the Aircraft Modes

In order to design an excitation signal as discussed in §5.3, an estimate of the natural frequency of the applicable mode of the aircraft is needed. This section discusses how an estimate of this frequency can be obtained for the Short Period mode, the Dutch Roll mode and the Roll mode.

5.4.1 The Short Period Mode

The standard characteristic equation for the normal dynamics (Short Period mode) poles is given by [2]

$$p(s) = s^2 + \left(\frac{L_\alpha}{m\bar{V}} - \frac{M_Q}{I_y} \right) s - \left(\frac{L_\alpha}{m\bar{V}} \frac{M_Q}{I_y} + \frac{M_\alpha}{I_y} \right) \quad (5.24)$$

which is in the form

$$p(s) = s^2 + 2\omega_n\zeta s + \omega_n^2 \quad (5.25)$$

thus the natural frequency of the normal dynamics can be estimated as

$$\omega_{n(\text{normal})} = \sqrt{-\left(\frac{L_\alpha}{m\bar{V}}\frac{M_Q}{I_y} + \frac{M_\alpha}{I_y}\right)} \quad (5.26)$$

where

$$\begin{aligned} L_\alpha &= qSC_{L_\alpha} \\ M_Q &= qS\bar{c}\frac{\bar{c}}{2\bar{V}}C_{m_Q} \\ M_\alpha &= qS\bar{c}C_{m_\alpha} \end{aligned} \quad (5.27)$$

and

$$q = \frac{1}{2}\rho\bar{V}^2 \quad (5.28)$$

Thus, expanding Eq. (5.26) using Eq. (5.27) and Eq. (5.28) yields

$$\omega_{n(\text{normal})} = \bar{V}\sqrt{-\left(\frac{(\rho S\bar{c})^2 C_{L_\alpha} C_{m_Q}}{8mI_y} + \frac{\rho S\bar{c}C_{m_\alpha}}{2I_y}\right)} \quad (5.29)$$

For $\rho = 1.0588$ (air density in Pretoria) [34] and the Modular UAV parameters presented in Chapter B, this reduces to

$$\omega_{n(\text{normal})} = 0.1953 \times \bar{V} \quad (5.30)$$

Note that the natural frequency is linearly dependent on \bar{V} , thus the natural frequency changes with airspeed. Assuming that the air density is a constant, it can be seen that the natural frequency only changes with airspeed. This means that the input signals must be designed in flight using the current airspeed and approximate values of C_{L_α} , C_{m_Q} and C_{m_α} .

5.4.2 The Dutch Roll Mode

The standard characteristic equation for the Dutch Roll mode poles is given by [2]

$$p(s) = s^2 - \left(\frac{Y_\beta}{m\bar{V}} + \frac{N_R}{I_z}\right)s + \left(\frac{Y_\beta}{m\bar{V}}\frac{N_R}{I_z} + \frac{N_\beta}{I_z}\right) \quad (5.31)$$

which is in the form

$$p(s) = s^2 + 2\omega_n\zeta s + \omega_n^2 \quad (5.32)$$

thus the natural frequency of the Dutch Roll mode can be estimated as

$$\omega_{n(\text{Dutch Roll})} = \sqrt{\left(\frac{Y_\beta}{m\bar{V}} \frac{N_R}{I_z} + \frac{N_\beta}{I_z}\right)} \quad (5.33)$$

where

$$\begin{aligned} Y_\beta &= qSC_{y_\beta} \\ N_R &= qSb \frac{b}{2\bar{V}} C_{n_R} \\ N_\beta &= qSbC_{n_\beta} \end{aligned} \quad (5.34)$$

and

$$q = \frac{1}{2}\rho\bar{V}^2 \quad (5.35)$$

Thus, expanding Eq. (5.33) using Eq. (5.34) and Eq. (5.35) yields

$$\omega_{n(\text{Dutch Roll})} = \bar{V} \sqrt{\left(\frac{(\rho S b)^2 C_{y_\beta} C_{n_R}}{8mI_z} + \frac{\rho S b C_{n_\beta}}{2I_z}\right)} \quad (5.36)$$

For $\rho = 1.0588$ (air density in Pretoria) [34] and the Modular UAV parameters presented in Chapter B, this reduces to

$$\omega_{n(\text{Dutch Roll})} = 0.0453 \times \bar{V} \quad (5.37)$$

5.4.3 Roll Mode

The roll dynamics are given by [2] as

$$\dot{P} = \left[\frac{L_P}{I_x}\right] P + \left[\frac{L_{\delta_A}}{I_x}\right] \delta_A + \left[\frac{L_{\delta_R}}{I_x}\right] \delta_R \quad (5.38)$$

Applying the Laplace transform yields

$$sP(s) = \left[\frac{L_P}{I_x}\right] P(s) + \frac{\left[\frac{L_{\delta_A}}{I_x}\right] \delta_A + \left[\frac{L_{\delta_R}}{I_x}\right] \delta_R}{s} \quad (5.39)$$

or

$$P(s) = \frac{\left[\frac{L\delta_A}{I_x}\right] \delta_A + \left[\frac{L\delta_R}{I_x}\right] \delta_R}{s^2 - \frac{L_P}{I_x}} \quad (5.40)$$

thus, the characteristic equation for the Roll mode poles is given by

$$p(s) = s^2 - \frac{L_P}{I_x} \quad (5.41)$$

Thus, the natural frequency of the roll mode is given by

$$\omega_{n(\text{Roll mode})} = \sqrt{-\frac{L_P}{I_x}} \quad (5.42)$$

where

$$L_P = qSb\frac{b}{2\bar{V}}C_{l_P} \quad (5.43)$$

and

$$q = \frac{1}{2}\rho\bar{V}^2 \quad (5.44)$$

Expanding Eq. (5.42) using Eq. (5.43) and Eq. (5.44) yields

$$\omega_{n(\text{Roll mode})} = \sqrt{-\frac{\rho\bar{V}Sb^2C_{l_P}}{4I_x}} \quad (5.45)$$

5.5 System Identification in a Closed Loop

In some cases, the control system can cause data collinearity. Take, for instance, the control law

$$\delta_E(i) = K\alpha(i) \quad (5.46)$$

where K is some constant. This control law will cause the δ_E and α regressors to be collinear. This problem can be overcome by superimposing an excitation signal on the δ_E actuator as discussed earlier. The control law now becomes

$$\delta_E(i) = K\alpha(i) + s_{\delta_E}(i) \quad (5.47)$$

where s_{δ_E} is the excitation signal superimposed on the actuator. This superimposed signal will disturb the aircraft for a short duration. The aircraft can then recover from the disturbance.

5.6 Conclusion

This section discussed how to detect data collinearity and how to prevent it by designing an input to excite the natural modes of the aircraft. The derivation of expressions for the natural frequencies of the modes of the aircraft was shown. The input signal can be designed to excite this specific frequency. It was also shown how the designed excitation signal can be superimposed on the control signal if the aircraft inputs are determined by some control law.

Chapter 6

Simulation Results

6.1 Introduction

In this chapter, the following topics regarding system identification are presented:

- Effects of differential filtering.
- Effects of the forgetting factor.
- Effects of resetting of the covariance matrix.
- Detection of data collinearity.
- Effects of identification in a closed loop.

System identification is done on a simple roll model in order to highlight the topics mentioned. Later, system identification is done on the full nonlinear Modular UAV model.

6.2 Simple Roll Model

This section is included to highlight the topics mentioned above. The reference and excitation signal, and values for curve fitting, the forgetting factor and resetting period of the covariance matrix are chosen in such a way that the effect of the topics mentioned above is made clear. A sampling period of $T = 0.02$ s is used throughout this chapter.

The roll dynamics of the aircraft in this model is given by

$$\dot{P} = \frac{\bar{q}}{I_x} S b C_l \quad (6.1)$$

where

$$\bar{q} = \frac{1}{2} \rho \bar{V}^2 \quad (6.2)$$

The values of the variables in the above equations are given in Table 6.1

Variable	Description	Value	Units
I_x	Moment of inertia around the x -axis	16.534	$\text{kg} \cdot \text{m}^2$
S	Wing reference area	1.44	m^2
b	Wingspan	4.0	m
ρ	Air density	1.2	kg/m^3
\bar{V}	Airspeed	22.0	m/s^2

Table 6.1: Values used for the simple roll model of the Modular UAV

The aircraft roll coefficient, C_l , is given by,

$$C_l = C_{l_0} + C_{l_p} \bar{P} + C_{l_{\delta_A}} \delta_A \quad (6.3)$$

where

$$\bar{P} = \frac{b}{2\bar{V}} P \quad (6.4)$$

and the values of the parameters are given in Table 6.2. These values are the estimated values of the parameters of the Modular UAV.

Variable	Value
C_{l_0}	0.0
C_{l_p}	-0.621899
$C_{l_{\delta_A}}$	-0.327280

Table 6.2: The values of the stability and control derivatives for the simple roll model

Excitation and control of the system

A simple Proportional/Integral (PI) controller is used to control the system. The roll rate reference, $P_{\text{reference}}$, is a simple sinusoid with a frequency of 1 rad/s and an amplitude of 0.5 rad/s.

Noise in the system

White noise is introduced on the measurement of the roll rate P . The standard deviation of the noise is chosen as 0.02 rad/s [34].

Servo slew rate

A servo slew rate of 60 degrees per second [34] is introduced on the aileron command.

6.2.1 Effects of Noise Filtering

As mentioned in §4.3.1, the measured roll rate needs to be differentiated in order to produce the dependent variable C_l . From Eq. (6.1), the value of C_l can be calculated as

$$C_l = \frac{\dot{P}I_x}{\bar{q}Sb} \quad (6.5)$$

The method used for differentiation as discussed in §4.3.1 fits a curve to the last p data points. The number of data points and the order of the curve is adjustable. The filtering however, introduces a lag into the identification

process. More lag is introduced when a higher number of data points is used. This is demonstrated by Figure 6.1 which shows measured values of P and the filtered C_l obtained by fitting a fifth order curve to the last 40 data points.

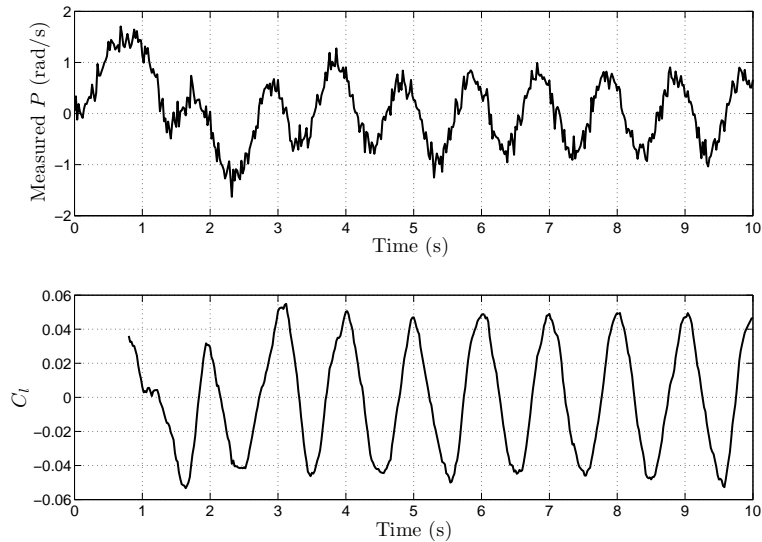


Figure 6.1: Measured P and filtered C_l obtained by fitting a second order curve to 40 measurements of roll rate

The regressors must be filtered as well. The regressors are also filtered by fitting a curve to data points as discussed in §4.3.1. The size of the filter kernel must be the same size as the filter kernel used to differentiate. This is necessary in order to introduce the same amount of lag for the regressors as for the dependent variable. The δ_A regressor is not filtered, as no measurement noise is present. It is important though, to take in account the slew rate of the servo. After the control signal δ_A is adjusted to account for the servo slew rate, it is time shifted to account for the lag introduced by filtering P .

The higher the number of data points used for curve fitting, the smoother the result will be. However, if the amount of data points is too high, the filter will start to change the measured dynamics of the aircraft. This is demonstrated in Figure 6.2 and Figure 6.3 which shows the true and calculated \bar{P}

and C_l respectively. In this case the filtered values are obtained by fitting a second order curve to the last 40 data points. Note that the filtered values are time-shifted to be in phase with the true values in order to make the difference clear.

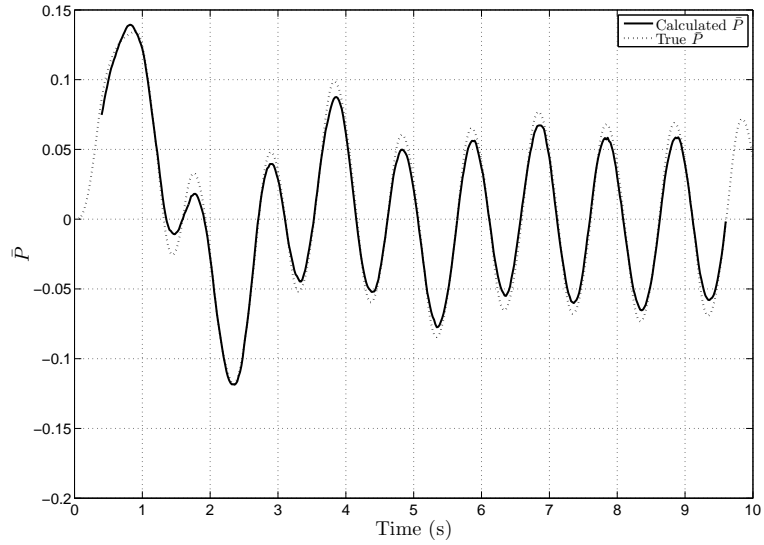


Figure 6.2: True and filtered \bar{P} obtained by fitting a second order curve to 40 measurements of roll rate

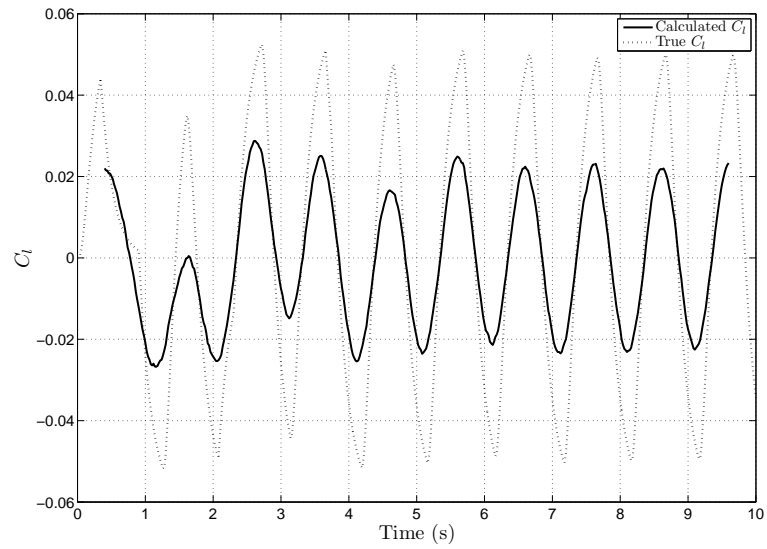


Figure 6.3: Measured and filtered C_l obtained by fitting a second order curve to 40 measurements of roll rate

This problem can be overcome by increasing the order of the curve fitted to the data points. A fifth order curve fitted to the last 40 data points have been found to work well. This is demonstrated by Figure 6.4 and Figure 6.5 which shows the true and filtered values for \bar{P} and C_l respectively.

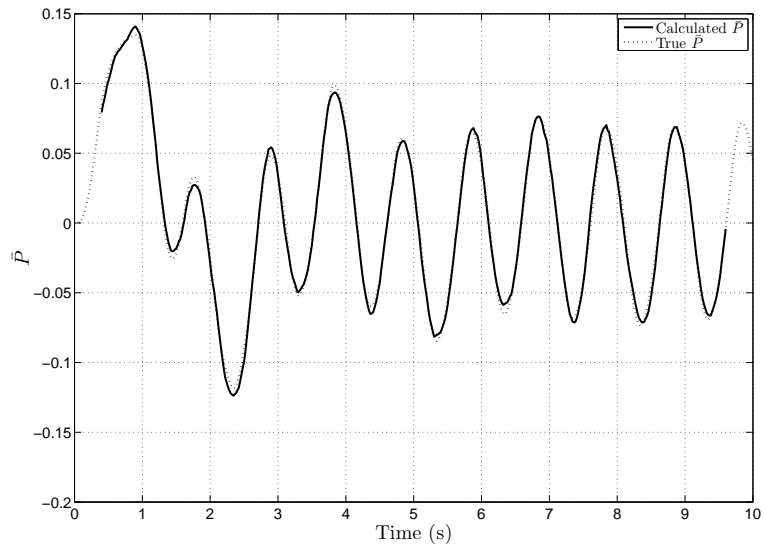


Figure 6.4: Measured and filtered \bar{P} obtained by fitting a fifth order curve to the last 40 measurements of the roll rate

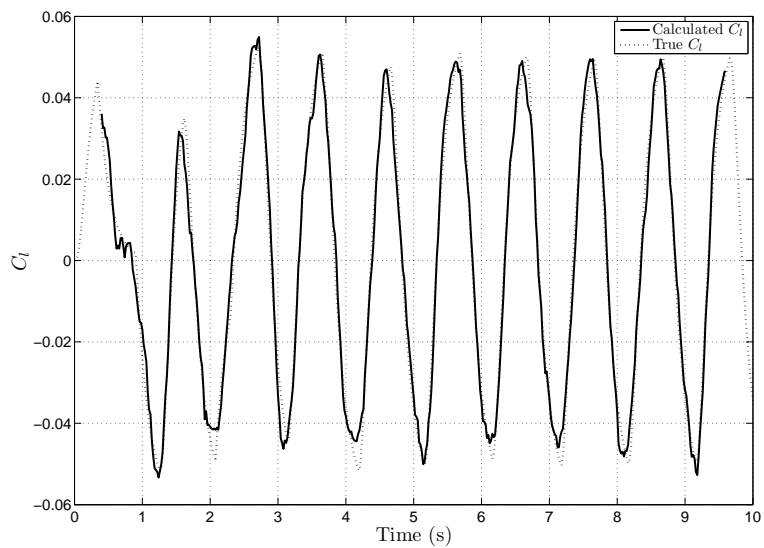


Figure 6.5: Measured and filtered C_l obtained by fitting a fifth order curve to the last 40 measurements of the roll rate

6.2.2 Testing for Data Collinearity

The previous section discussed how the regressors can be obtained by filtering measurements. In this section, the regressors obtained by fitting a fifth order

curve to 40 data points is used.

To test for data collinearity, the regressors must first be standardised as discussed in §5.2.1. Figure 6.6 shows the standardised regressors. The collinearity of these two regressors is made clear by plotting the negative of the standardised \bar{P} with the standardised δ_A as in Figure 6.7. For these plots the correlation matrix is given by

$$\mathbf{X}^{*T} \mathbf{X}^* = \begin{bmatrix} 1.0000 & -0.7463 \\ -0.7463 & 1.0000 \end{bmatrix} \quad (6.6)$$

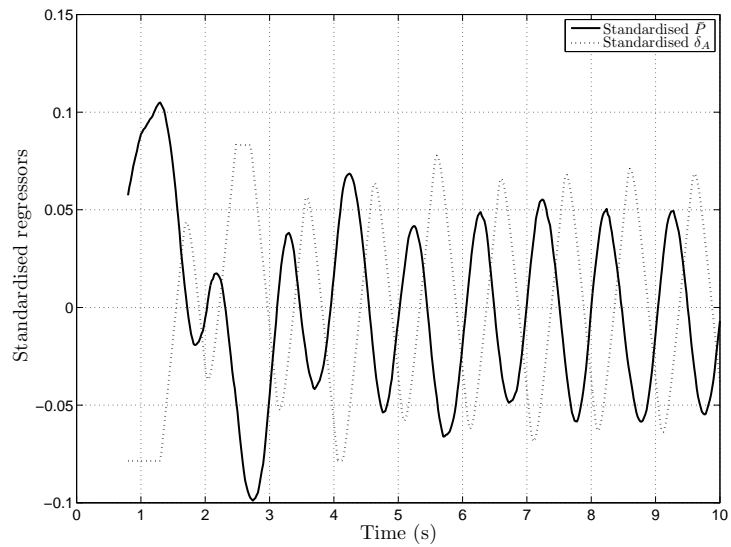


Figure 6.6: The standardised regressors

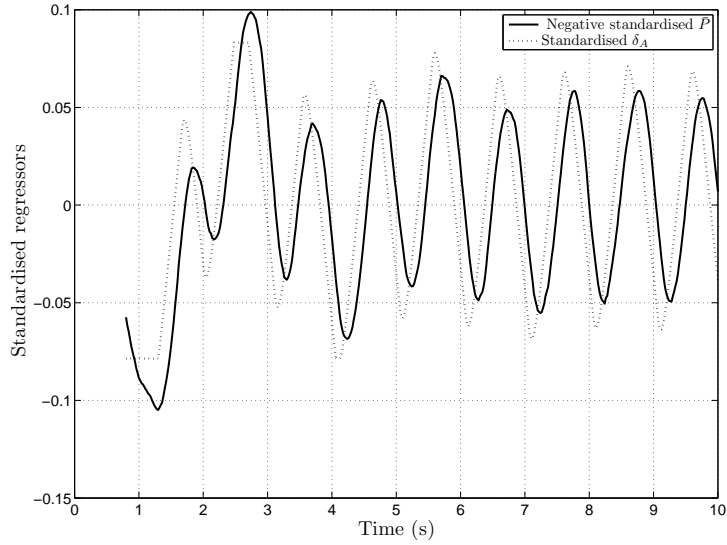


Figure 6.7: One of the standardised regressors negative demonstrating collinearity

An example where a high correlation coefficient exist is obtained by lowering the frequency of the reference roll rate to 0.2 Hz. The standardised regressors are now given in Figure 6.8. The correlation is made more clear again by plotting the negative of the standardised \bar{P} with the standardised δ_A as in Figure 6.9. For these plots the correlation matrix is given by

$$\mathbf{X}^{*T} \mathbf{X}^* = \begin{bmatrix} 1.0000 & -0.9795 \\ -0.9795 & 1.0000 \end{bmatrix} \quad (6.7)$$

The correlation matrix contains pairwise regression correlation with absolute value greater than 0.9. This indicates that collinearity might cause problems in parameter estimation as discussed in §5.2.2.

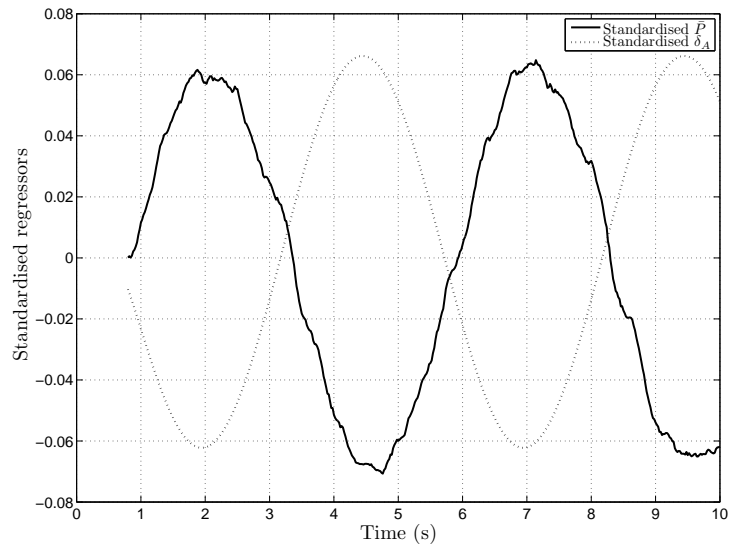


Figure 6.8: The standardised regressors

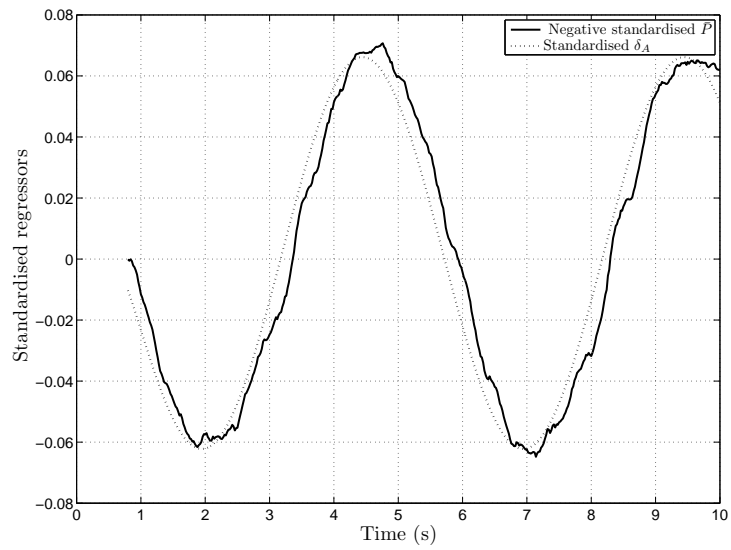


Figure 6.9: One of the standardised regressors negative demonstrating collinearity

The collinearity in the previous example can be reduced by superimposing an excitation signal on the δ_A command as discussed in §5.3. This is demonstrated by superimposing two doublets with amplitude of 0.5 rad and period of 1 second at $t = 3$ s and $t = 5$ s on the aileron command. The resulting

standardised regressors are shown in Figure 6.10. The correlation matrix for this case is given by

$$\mathbf{X}^{*T} \mathbf{X}^* = \begin{bmatrix} 1.0000 & -0.9256 \\ -0.9256 & 1.0000 \end{bmatrix} \quad (6.8)$$

Note that the control system tries to counter the disturbance in δ_A in order to track the reference roll rate.

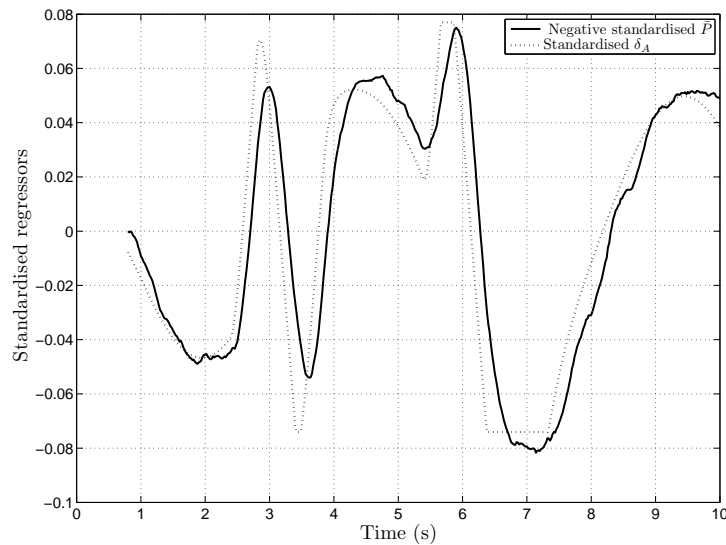


Figure 6.10: Standardised regressors demonstrating a reduction in collinearity by superimposing an excitation signal on δ_A

6.2.3 Demonstrating the Effects of the Excitation Signal

In order to demonstrate the effects of an excitation signal superimposed on the δ_A command, the amplitude of the reference roll rate is reduced to 1 rad/s. Parameter estimation is then done without the excitation and then compared with the results with excitation. Figure 6.11 shows the estimated parameters over time when no excitation signal is superimposed on δ_A . The estimated parameters at $t = 10$ s, are given in Table 6.3

Variable	Estimated value	True value
C_{l_0}	-0.0005	0.0
C_{l_p}	-0.5757	-0.621899
$C_{l_{\delta_A}}$	-0.3072	-0.327280

Table 6.3: Estimated and true parameters with no excitation signal

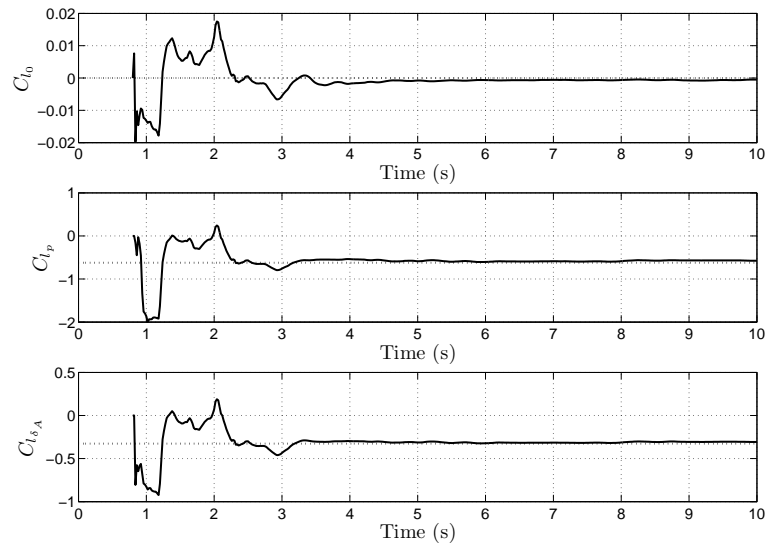


Figure 6.11: The estimated parameters over time with no excitation signal

For Table 6.4 and Figure 6.12 a doublet was superimposed on the aileron command at $t = 2$ seconds. It can be seen that the estimated parameters converges faster to more accurate values, due to the excitation signal.

Variable	Estimated value	True value
C_{l_0}	-0.0004	0.0
C_{l_p}	-0.6293	-0.621899
$C_{l_{\delta_A}}$	-0.3342	-0.327280

Table 6.4: Estimated and true parameters with a superimposed doublet on the aileron command

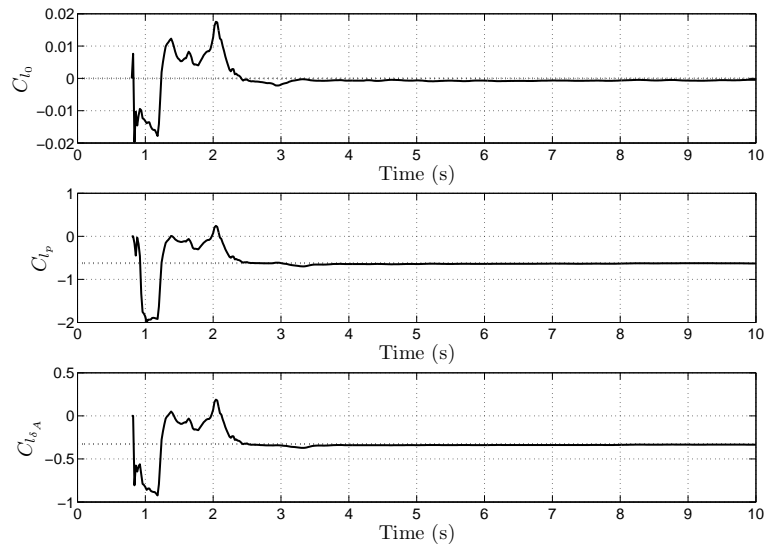


Figure 6.12: The estimated parameters over time with a superimposed doublet on the aileron command

6.2.4 Effects of the forgetting factor and covariance resetting

To account for changing parameters, a forgetting factor can be introduced to prevent old data to be taken into account as discussed in §3.4.2. The other way of achieving this is to reset the covariance matrix every few seconds. When the diagonal values of the covariance matrix are high, the parameter values have a low certainty. This causes the parameter values to change drastically as seen in the left side of Figure 6.11 and Figure 6.12 in the previous section.

To demonstrate the effects of the forgetting factor, a fault is introduced at $t = 10$ seconds. The fault used is a right aileron getting stuck at -10 degrees. This changes the parameters to those shown in Table 6.5. Note that the C_{l_0} term is not zero any more and that the $C_{l_{\delta_A}}$ term has halved. The C_{l_p} remained unchanged.

A forgetting factor of 0.98 has been found to work well. The results are shown in Figure 6.13. The estimated parameters at $t = 20$ s are shown in

Variable	Value
C_{l_0}	-0.028600
C_{l_p}	-0.621899
$C_{l_{\delta_A}}$	-0.163640

Table 6.5: The values of the stability and control derivatives for the simple roll model with failed right aileron at -10 degrees

Table 6.6

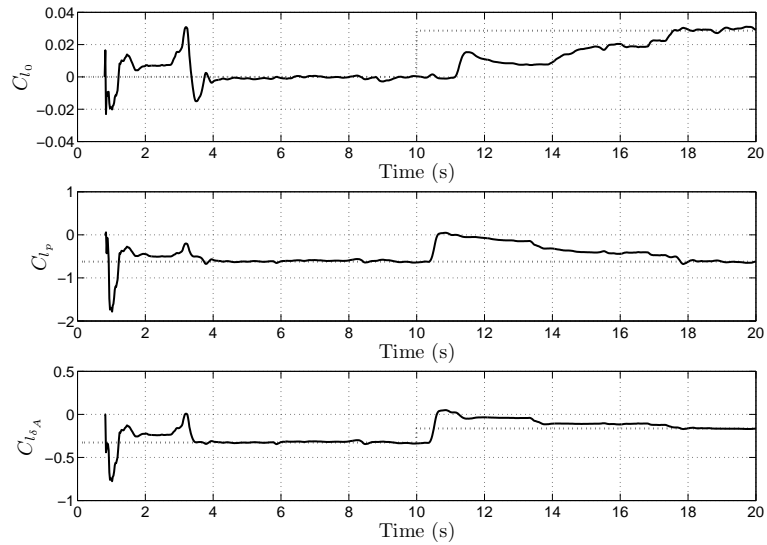


Figure 6.13: The estimated parameters over time with a fault at $t = 10$ and a forgetting factor of 0.98

Variable	Estimated value	True value
C_{l_0}	-0.0292	-0.028600
C_{l_p}	-0.6199	-0.621899
$C_{l_{\delta_A}}$	-0.1652	-0.163640

Table 6.6: The values of the stability and control derivatives for the simple roll model with failed right aileron at -10 degrees

Figure 6.14 shows the results of the estimated parameters over time when the covariance matrix is reset every five seconds. It can be seen that after

each reset, the parameters converges fast to accurate values. The estimated parameters after 20 seconds are shown in Table 6.7.

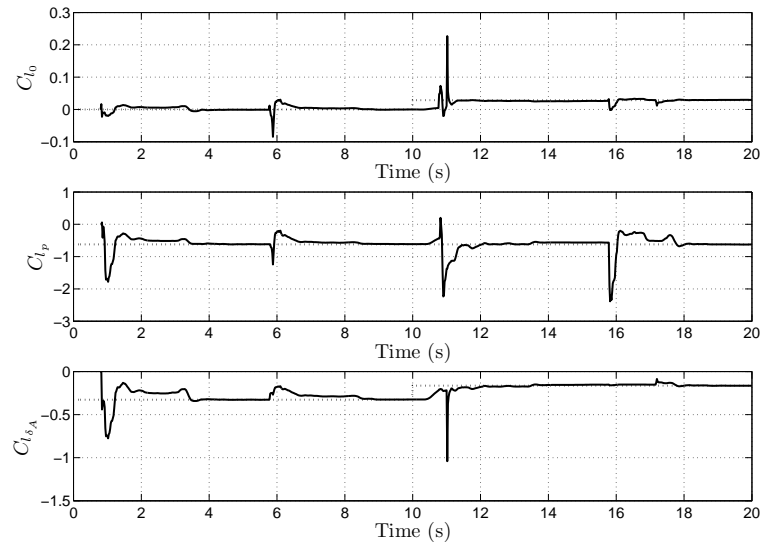


Figure 6.14: The estimated parameters over time when implementing covariance resetting every five seconds

Variable	Estimated value	True value
C_{l_0}	-0.0294	-0.028600
C_{l_p}	-0.6222	-0.621899
$C_{l_{\delta_A}}$	-0.1643	-0.163640

Table 6.7: The values of the stability and control derivatives after implementing covariance resetting

6.3 Full Nonlinear Modular UAV Model

In this chapter, system identification is done on the full nonlinear modular UAV model as presented in Chapter 2. The values for the parameters is given in Chapter B. It is assumed that the air density $\rho = 1.0588 \text{ kg/m}^3$ (Air density in Pretoria) [34]. It is also assumed that all the regressors can be measured accurately. The control system developed by Blaauw [34] and Gaum [21] is

used to keep the aircraft in a straight and level flight condition at an airspeed of $\bar{V} = 22$ m/s.

To excite natural modes of the aircraft, excitation signals for each of the actuators are designed in accordance with §5.4. This is discussed in the following section.

6.3.1 Design of the Excitation Signals

To design the excitation signals, the natural frequencies of the modes of the aircraft discussed in §5.4 must first be calculated. Using Eqns. (5.30), (5.37) and (5.45) with the parameter values of the Modular UAV given in Chapter B and with an airspeed of $\bar{V} = 22$ m/s, the following natural frequencies are obtained:

$$\omega_{n(\text{normal})} = 4.2974 \text{ rad/s} \quad (6.9a)$$

$$\omega_{n(\text{Dutch Roll})} = 0.9974 \text{ rad/s} \quad (6.9b)$$

$$\omega_{n(\text{Roll mode})} = 2.2464 \text{ rad/s} \quad (6.9c)$$

These frequencies can be transformed into time periods by applying

$$T = \frac{2\pi}{\omega_n} \quad (6.10)$$

which yields

$$T_{(\text{normal})} = 1.4621 \text{ s} \quad (6.11a)$$

$$T_{(\text{Dutch Roll})} = 6.2997 \text{ s} \quad (6.11b)$$

$$T_{(\text{Roll mode})} = 2.7969 \text{ s} \quad (6.11c)$$

A doublet signal (discussed in §5.3.4) is used to excite the dynamics of the aircraft. The reason that the *doublet* is used is because it is a short disturbance in the system, designed to excite a specific frequency band.

An amplitude of 5 degrees is used for the doublets. This will ensure that a decent amount of excitation is provided, but the aircraft still operates in the linear region. This will be demonstrated later.

The period of the elevator doublet is set equal to $T_{(\text{normal})}$, the period of the rudder doublet is set equal to $T_{(\text{Dutch Roll})}$ and the period of the aileron doublet is set equal to $T_{(\text{Roll mode})}$. The three excitation signals is then distributed arbitrarily over 20 seconds as shown in Figure 6.15.

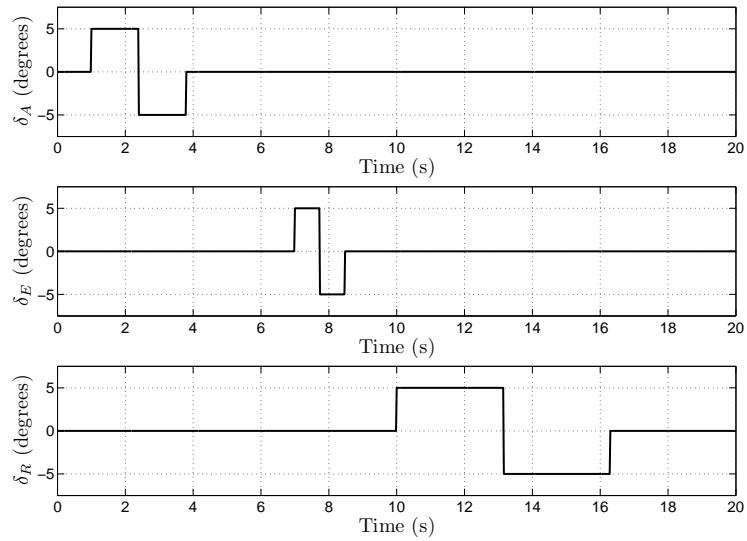


Figure 6.15: The doublets superimposed on the control signals in order to excite the natural modes of the Modular UAV

6.4 Effect of Superimposing Excitation Signals

Superimposing the excitation signals designed in the previous section causes a disturbance in the system. The control system aims to counter this disturbance as shown in Figure 6.16 and Figure 6.17. According to Basson [35], the Modular UAV will start going into stall at an angle of attack $\alpha = 15$ de-

degrees. It can be seen in Figure 6.16 that α stays well in the boundaries of safe operation.

Figures and values of the estimated parameters are shown after the conclusion.

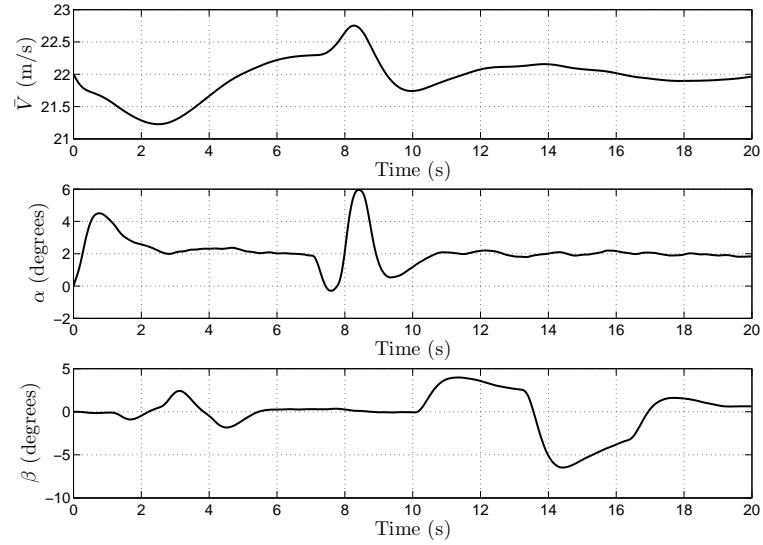


Figure 6.16: \bar{V} , α and β for the 20 second simulation time

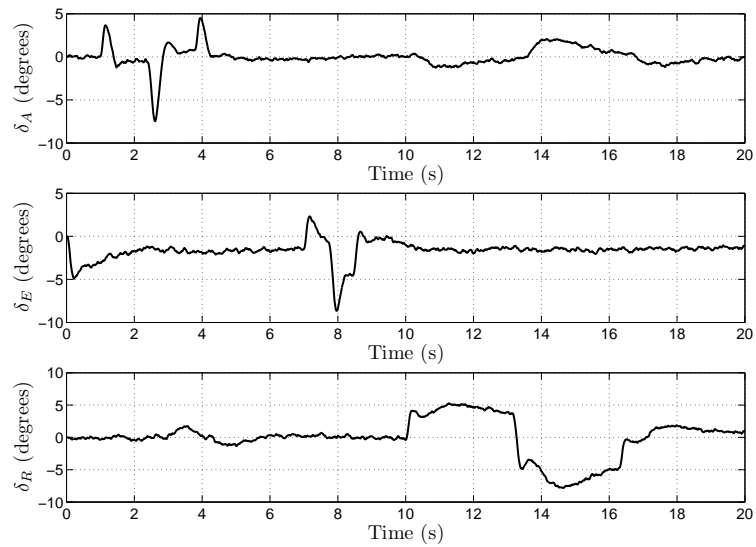


Figure 6.17: Actuator deflections for the 20 second simulation time

6.5 Conclusion

6.5.1 Conclusion for the Simple Roll Model

This chapter showed how system identification can be done on the simple roll model using regression methods. It is shown that smoothed numeric differentiation using the concept of curve fitting can be successfully implemented to determine the derivative of the roll rate. This works well by fitting a fifth order curve to the last 40 data points.

It is shown that the estimation process yields more accurate values when an excitation signal is superimposed on the aileron command.

It is also shown that a forgetting factor can be implemented to accommodate a fault during flight. A forgetting factor of 0.98 works well and the results were shown. However, covariance resetting converges faster to more accurate values of the parameters.

If the necessary processing power is available, multiple parameter estimation algorithms can be processed in parallel, with the covariance of each being reset

at different times. This will enhance the tempo at which accurate estimated parameter becomes available.

6.5.2 Conclusion for the Full Nonlinear Modular UAV Model

This section discusses the results after parameter estimation was done on the full nonlinear Modular UAV model. The results are shown in §6.6. It can be seen that all the parameters converge quickly to accurate values, with the exception of $C_{l_{\delta_R}}$, C_{n_P} and $C_{n_{\delta_A}}$.

The reason that $C_{l_{\delta_R}}$ does not converge to an accurate value can be explained by a high correlation factor of 0.9302 between β and δ_R . This value is found in $[\mathbf{X}^{*T} \mathbf{X}^*]_{(5,1)}$ in Eq. (6.12).

The reason that C_{n_P} and $C_{n_{\delta_A}}$ does not converge is because they have so little effect on the aircraft dynamics, compared to the other parameters.

The parameters mentioned are not that important in order to apply Fault Tolerant Control on the Modular UAV, as they are minor contributors to the aerodynamic forces and moments.

6.6 Parameter Estimation Results

This section shows the figures that demonstrates how the parameters were estimated over time. It also shows the values of the final estimated parameters after 20 seconds of simulation. The correlation matrix $\mathbf{X}^{*T} \mathbf{X}^*$ calculated by using standardised regressors are shown for each of the six cases. This is done after the conclusions to make the document easier to read. §6.5 discusses the results in this section.

6.6.1 Estimated Parameters for the Roll Moment Coefficient

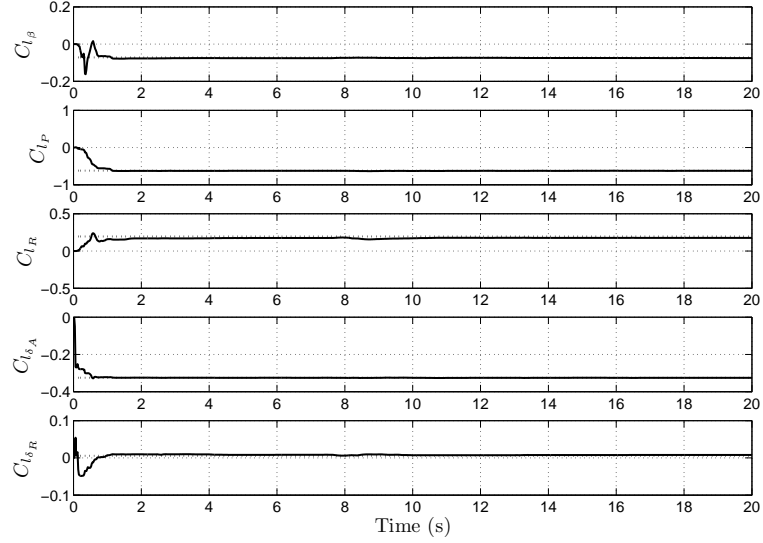


Figure 6.18: Estimated parameters for the roll moment coefficient, C_l

$$\mathbf{X}^{*T} \mathbf{X}^* = \begin{bmatrix} 1.0000 & 0.2291 & -0.0170 & -0.5239 & 0.9302 \\ 0.2291 & 1.0000 & -0.1953 & -0.7042 & 0.1522 \\ -0.0170 & -0.1953 & 1.0000 & 0.2647 & -0.1153 \\ -0.5239 & -0.7042 & 0.2647 & 1.0000 & -0.4858 \\ 0.9302 & 0.1522 & -0.1153 & -0.4858 & 1.0000 \end{bmatrix} \quad (6.12)$$

Variable	Estimated value	True value
$C_{l_{\beta}}$	-0.0749	-0.0715
C_{l_P}	0.6258	0.6219
C_{l_R}	0.1757	0.1946
$C_{l_{\delta_A}}$	-0.3255	-0.3254
$C_{l_{\delta_R}}$	0.0080	0.0056

Table 6.8: Estimated and true parameters for the roll moment coefficient C_l

6.6.2 Estimated Parameters for the Pitch Moment Coefficient

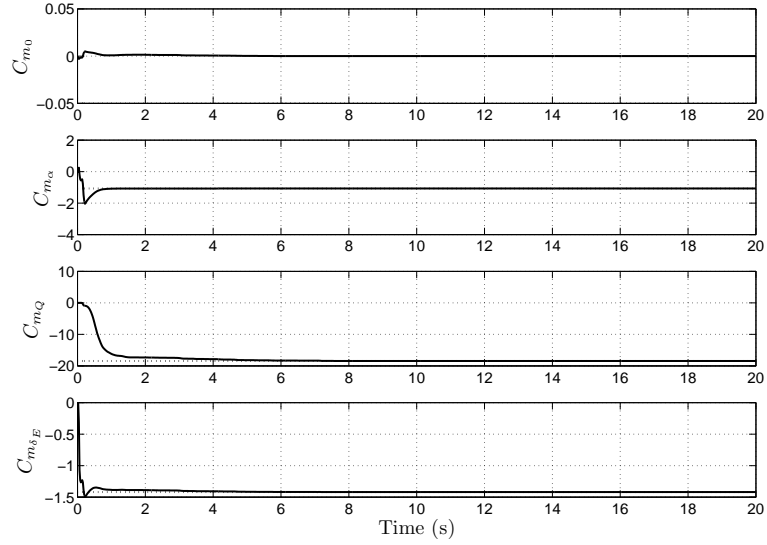


Figure 6.19: Estimated parameters for the pitch moment coefficient, C_m

$$\mathbf{X}^{*T} \mathbf{X}^* = \begin{bmatrix} 1.0000 & 0.7410 & -0.4780 \\ 0.7410 & 1.0000 & -0.8309 \\ -0.4780 & -0.8309 & 1.0000 \end{bmatrix} \quad (6.13)$$

Variable	Estimated value	True value
C_{m_0}	0.0000	-0.0500
C_{m_α}	-1.0695	-1.0695
C_{m_Q}	-18.4426	-18.4426
$C_{m_{\delta_E}}$	-1.4193	-1.4193

Table 6.9: Estimated and true parameters for the pitch moment coefficient C_m

6.6.3 Estimated Parameters for the Yaw Moment Coefficient

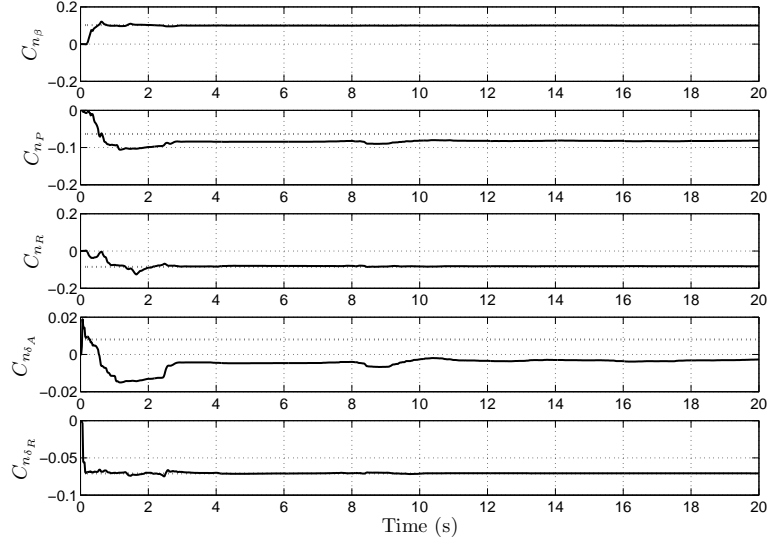


Figure 6.20: Estimated parameters for the yaw moment coefficient, C_n

$$\mathbf{X}^{*T} \mathbf{X}^* = \begin{bmatrix} 1.0000 & 0.2291 & -0.0170 & -0.5239 & 0.9302 \\ 0.2291 & 1.0000 & -0.1953 & -0.7042 & 0.1522 \\ -0.0170 & -0.1953 & 1.0000 & 0.2647 & -0.1153 \\ -0.5239 & -0.7042 & 0.2647 & 1.0000 & -0.4858 \\ 0.9302 & 0.1522 & -0.1153 & -0.4858 & 1.0000 \end{bmatrix} \quad (6.14)$$

Variable	Estimated value	True value
$C_{n\beta}$	0.0999	0.1022
C_{nP}	-0.0815	-0.0636
C_{nR}	-0.0819	-0.0853
$C_{n\delta_A}$	-0.0027	0.0080
$C_{n\delta_R}$	-0.0708	-0.0709

Table 6.10: Estimated and true parameters for the yaw moment coefficient C_n

6.6.4 Estimated Parameters for the Drag Force Coefficient

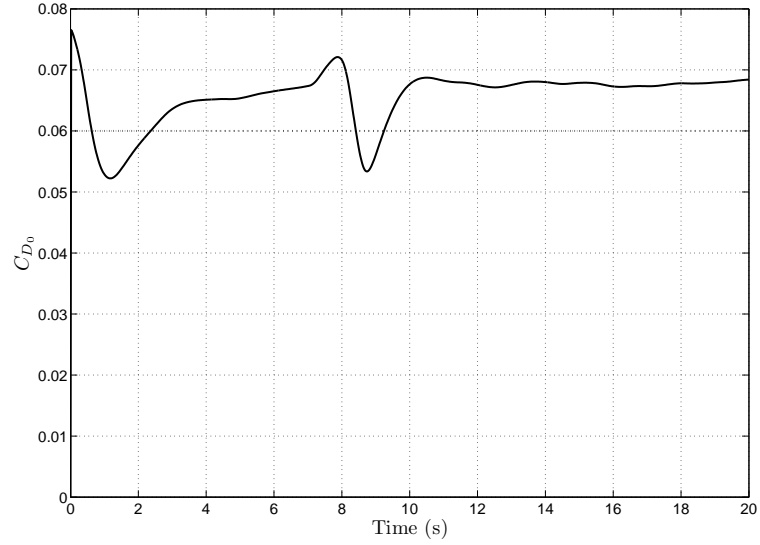


Figure 6.21: Estimated parameters for parasitic drag C_{D_0}

$$\mathbf{X}^{*T} \mathbf{X}^* = \begin{bmatrix} 1.0000 \end{bmatrix} \quad (6.15)$$

Variable	Estimated value	True value
C_{D_0}	0.0684	0.0600

Table 6.11: Estimated and true parameter for parasitic drag C_{D_0}

6.6.5 Estimated Parameters for the Side Force Coefficient

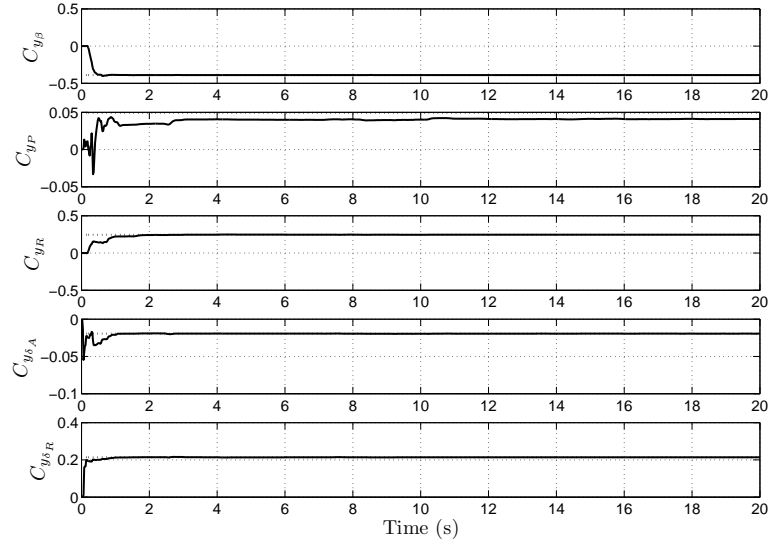


Figure 6.22: Estimated parameters for the side force coefficient, C_y

$$\mathbf{X}^{*T} \mathbf{X}^* = \begin{bmatrix} 1.0000 & 0.2291 & -0.0170 & -0.5239 & 0.9302 \\ 0.2291 & 1.0000 & -0.1953 & -0.7042 & 0.1522 \\ -0.0170 & -0.1953 & 1.0000 & 0.2647 & -0.1153 \\ -0.5239 & -0.7042 & 0.2647 & 1.0000 & -0.4858 \\ 0.9302 & 0.1522 & -0.1153 & -0.4858 & 1.0000 \end{bmatrix} \quad (6.16)$$

Variable	Estimated value	True value
$C_{y\beta}$	-0.3895	-0.3894
C_{yP}	0.0411	0.0493
C_{yR}	0.2458	0.2440
$C_{y\delta A}$	-0.0194	-0.0194
$C_{y\delta R}$	0.2138	0.2138

Table 6.12: Estimated and true parameters for the side force coefficient C_y

6.6.6 Estimated Parameters for the Lift Force Coefficient

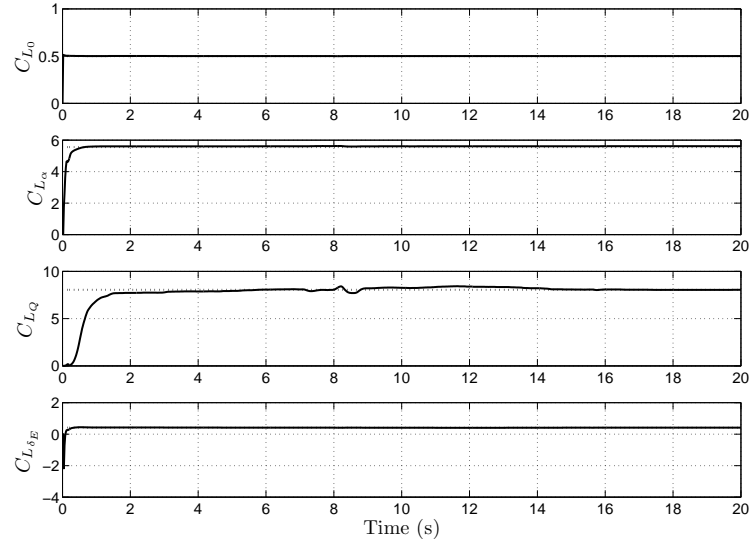


Figure 6.23: Estimated parameters for the lift force coefficient, C_L

$$\mathbf{X}^{*T} \mathbf{X}^* = \begin{bmatrix} 1.0000 & -0.7410 & -0.4780 \\ -0.7410 & 1.0000 & 0.8309 \\ -0.4780 & 0.8309 & 1.0000 \end{bmatrix} \quad (6.17)$$

Variable	Estimated value	True value
C_{L_0}	0.5002	0.5000
C_{L_α}	5.6159	5.5579
C_{L_Q}	8.0485	8.0470
$C_{L_{\delta_E}}$	0.4108	0.4104

Table 6.13: Estimated and true parameters for the lift force coefficient C_L

Chapter 7

Summary and Recommendations

7.1 Summary

This project showed how system identification can be implemented on a conventional UAV in order to do Fault Tolerant Control. A model for the UAV was presented, which contains the equations necessary for system identification. Different identification methods were considered in Chapter 3. This includes methods for accommodating a sudden change in the parameters at the event of a fault. The regression methods were chosen for the following reasons:

- The regression methods are based on the least-squares model, which assumes that the parameter vector θ is a vector of unknown constant parameters and the measurement noise vector v is a vector of uncorrelated white noise. This is applicable, because the measurement noise on the sensors used on the Modular UAV is assumed to be white, uncorrelated noise.
- The aerodynamic and control derivative equations presented in Chapter 2 can easily be manipulated to fit the regression equation presented in Chapter 3.

- The regression methods accommodate change in the parameters, which is in line with the aim of the larger project of Fault Tolerant Control of the Modular UAV.

Chapter 4 discussed how the regression methods can be implemented to the model presented in Chapter 2. This requires smoothed numerical differentiation, as the regression methods require the derivatives of the noisy angular rate measurements of the aircraft. It was discussed how smoothed numerical differentiation can be done using the concept of *curve fitting*.

Issues concerning system identification were discussed in Chapter 5 and methods for solving these problems were introduced. This involves superimposing excitation signals on the actuator commands of the aircraft. The design of the excitation signals to stimulate the natural modes of the aircraft were discussed.

Chapter 6 showed how system identification can successfully be implemented on the simple roll model. The results of different methods for accommodating a change in parameters at the event of a fault was also shown.

System identification was done on the full nonlinear model of the Modular UAV. Excitation signals was superimposed on the actuators while the control system was instructed to keep the aircraft in straight and level flight. It was shown that the disturbance caused by these excitation signals does not take the aircraft out of the linear flight envelope.

It was shown that all the parameters converge quickly to accurate values, with the exception of $C_{l_{\delta_R}}$, C_{n_P} and $C_{n_{\delta_A}}$. The reasons that these parameters did not converge to accurate values was given in §6.5.2 and it was discussed that these parameters are not that important to do Fault Tolerant Control on the Modular UAV.

An S-function block that uses the recursive least squares algorithm for parameter estimation was developed. This block accommodates for the methods

of applying the forgetting factor and covariance resetting and can be used in future system identification work.

7.2 Recommendations

Recommendations of what future work should include are given below:

- System identification in this project was done on the *virtual aircraft layer* as discussed in Chapter 1. Future work should expand the identification process to use the *individual actuators* in the *physical aircraft layer*
- Constant detection of data collinearity should be done in real-time. If the degree of collinearity is too high, an excitation signal must be superimposed on the relevant actuator command.
- Optimal filter design should be done in real-time in order to acquire more accurate measurements, i.e. different measurements should be filtered with different filters.
- Fault Detection and Isolation (FDI) algorithms should be developed. These algorithms should monitor the estimated parameters and notify the controllers if any fault is detected.
- A study should be done to quantify the accuracy at which different parameters should be estimated in order to do Fault Tolerant Control.

Appendices

Appendix A

Mathematical Principles and Equations

A.1 Moment of Inertia

The moment of inertia tensor coordinated in body axes is given by:

$$\mathbf{I}_B = \begin{bmatrix} I_x & -I_{xy} & -I_{xz} \\ -I_{xy} & I_y & -I_{yz} \\ -I_{xz} & -I_{yz} & I_z \end{bmatrix} \quad (\text{A.1})$$

Due to symmetry in the aircraft, the I_{xy} and I_{yz} cross products of inertia will be zero. The I_{xz} cross product will not be zero, but for most aircraft it will be relatively small and can also be ignored. Cross products are generally also difficult to measure. The moment of inertia tensor for most conventional aircraft is therefore given by

$$\mathbf{I}_B = \begin{bmatrix} I_x & 0 & 0 \\ 0 & I_y & 0 \\ 0 & 0 & I_z \end{bmatrix} \quad (\text{A.2})$$

A.2 Cross Product Transformation Matrix

When two vectors \mathbf{J} and \mathbf{K} are coordinated in the same axis system A , their cross product can be written in terms of their coordinate vectors as follows

$$\mathbf{J}_A \times \mathbf{K}_A = \mathbf{S}_{J_A} \mathbf{K}_A \quad (\text{A.3})$$

where the \mathbf{S}_{J_A} matrix is defined as

$$\mathbf{S}_{J_A} = \begin{bmatrix} 0 & -Z_A & Y_A \\ Z_A & 0 & -X_A \\ -Y_A & X_A & 0 \end{bmatrix} \quad (\text{A.4})$$

with X_A, Y_A and Z_A the components of \mathbf{J} coordinated in axis system A .

A.3 Derivative of a Vector in a Rotating Reference Frame

When the time derivative of a vector is described in one axis system, but a transformation is necessary to describe it in another axis system that rotates relative to the first, the equation of Coriolis is used. Coriolis provides the relationship necessary to relate the time derivative of a vector from one of these axis systems to the other. Verbally this relationship is stated as follows: An object's motion, as viewed from axis system A , is equal to its motion as viewed from axis system B , which can rotate relative to A , plus the resulting motion caused by the angular velocity of the rotation of B relative to A . Mathematically this can be expressed as follows [36]

$$\left. \frac{d}{dt} \mathbf{R} \right|_A = \left. \frac{d}{dt} \mathbf{R} \right|_B + \boldsymbol{\omega}^{BA} \times \mathbf{R} \quad (\text{A.5})$$

A.4 Direction Cosine Matrix (DCM)

The direction cosine matrix is a 3×3 matrix that can be used to transform a vector from one axis system to another. The rows of the \mathbf{DCM}^{BA} consist of the unit vectors of axis system B , coordinated in axis system A . Using this, a vector coordinated in axis system A can be transformed to be coordinated in axis system B .

$$\mathbf{V}_B = \mathbf{DCM}^{BA} \mathbf{V}_A \quad (\text{A.6})$$

Because the \mathbf{DCM} matrix consists of three orthogonal unit vectors, it is an orthogonal matrix. The inverse of an orthogonal matrix is given by its transpose. [37]

$$\mathbf{DCM}^{AB} = [\mathbf{DCM}^{BA}]^{-1} = [\mathbf{DCM}^{BA}]^T \quad (\text{A.7})$$

The reverse transform from axis system B to A is therefore given by

$$\mathbf{V}_A = [\mathbf{DCM}^{BA}]^T \mathbf{V}_B \quad (\text{A.8})$$

A.5 Euler Angles

Euler angles are an intuitive way of describing the attitude of one axis system with regards to another. This is done by three rotations of the first axis system, in order, around three different axes. To use Euler angles to transform axis system A to B , the following sequence of rotations should be carried out in order [38], with the notation, \mathbf{u}_i^A representing the i^{th} (first, second or third) unit vector of axis system A .

1. Rotate A through the ψ angle about its \mathbf{u}_a^A unit vector to obtain axis system A_1 .
2. Rotate A_1 through the Θ angle about its $\mathbf{u}_b^{A_1}$ unit vector to obtain axis system A_2 .

3. Rotate A_2 through the ϕ angle about its $\mathbf{u}_c^{A_2}$ unit vector to obtain axis system A_3 .

The selected values a , b and c determine the axes to rotate about for each of the three rotations. By varying the values of these variables, various Euler rotation sequences can be defined, with the restriction that two consecutive rotations cannot be around the same unit vector [39]. The most commonly used is Euler 3-2-1 [21]. Referring to the above sequence, it can be seen that 3-2-1 will lead to a rotation sequence of yaw, pitch and then roll.

A.6 Special Rotation Matrices

The coordination matrix used to transform a vector from the wind to body axis system is given by [21]

$$\mathbf{DCM}^{BW} = \begin{bmatrix} \cos \alpha \cos \beta & -\cos \alpha \sin \beta & -\sin \alpha \\ \sin \beta & \cos \beta & 0 \\ \sin \alpha \cos \beta & -\sin \alpha \sin \beta & \cos \alpha \end{bmatrix} \quad (\text{A.9})$$

Appendix B

Specifications for the Modular UAV

This chapter gives all the specifications for the Modular UAV

B.1 Engine

Variable	Description	Value	Units
τ	Time constant	0.4	s
T_{\max}	Maximum thrust	150.0	N
T_{\min}	Minimum thrust	0.0	N
	Dynamic thrust multiplier	0.75	

Table B.1: Engine specifications

B.2 Physical Specifications

Variable	Description	Value	Units
m	Aircraft mass	26.0	kg
b	Wingspan	4.0	m
S	Wing reference area	1.44	m ²
e	Wing efficiency factor	0.85	
I_x	Moment of inertia	16.53436	kg · m ²
I_y	Moment of inertia	11.58287	kg · m ²
I_z	Moment of inertia	13.67195	kg · m ²

Table B.2: Physical specifications of the modular UAV

B.3 Stability Derivatives

Variable	Value
C_{L_0}	26.0
C_{D_0}	0.06
C_{L_α}	5.557928
C_{L_Q}	8.046991
C_{y_β}	-0.389444
C_{y_P}	0.049295
C_{y_R}	0.244026
C_{m_0}	-0.05
C_{m_α}	-1.069455
C_{m_Q}	-18.442581
C_{l_β}	-0.071508
C_{l_P}	-0.621899
C_{l_R}	0.194571
C_{n_β}	0.102214
C_{n_P}	-0.063578
C_{n_R}	-0.085316

Table B.3: Stability derivatives for the Modular UAV

B.4 Control Derivatives

Variable	Value
$C_{L\delta_E}$	0.4104
$C_{m\delta_E}$	-1.4193
$C_{y\delta_A}$	-0.0194
$C_{l\delta_A}$	-0.3254
$C_{n\delta_A}$	0.0080
$C_{y\delta_R}$	0.2138
$C_{l\delta_R}$	0.0056
$C_{n\delta_R}$	-0.0709

Table B.4: Control derivatives for the Modular UAV

Bibliography

- [1] Peddle, I.: Fault tolerant control: Overview and research at Stellenbosch university. 2009.
- [2] Peddle, I.K.: *Acceleration Based Manoeuvre Flight Control System for Unmanned Aerial Vehicles*. Ph.D. thesis, University of Stellenbosch, 2008.
- [3] Klein, V. and Morelli, E.A.: *Aircraft System Identification: Theory and Practice*. American Institute of Aeronautics and Astronautics, Inc., 2006.
- [4] Milliken, W.: Progress in stability and control research. *Journal of the Aeronautic Sciences*, vol. 14, pp. 494–519, September 1947.
- [5] Greenberg, H.: A survey of methods for determining stability parameters of an airplane from dynamic flight measurements. Tech. Rep., NASA TN 2340, 1951.
- [6] Shinbrot, M.: A least squares curve fitting method with application of the calculation of stability coefficients from transient-response data. Tech. Rep., NACA TN 2341, 1951.
- [7] Taylor, L.W., I.K. and Powers, B.: A comparison of Newton-Raphson and other methods for determining stability derivatives from flight data. *AIAA Paper*, pp. 69–315, 1969.
- [8] Mehra, R.: Maximum likelihood identification of aircraft parameters. In: *Proceedings of the Joint Automatic Control Conference*. June 1970.

- [9] Stepner, D. and Mehra, R.: Maximum likelihood identification and optimal input design for identifying aircraft stability and control derivatives. Tech. Rep., NASA CR-2200, 1973.
- [10] Gerlach, O.: The determination of stability derivatives and performance characteristics from dynamic maneuvers. Tech. Rep., Society of Automotive Engineers, Paper 700236, 1970.
- [11] Maine, R. and Iliff, K.: Identification of dynamic systems, theory and formulation. Tech. Rep., NASA RP 1138, 1985.
- [12] Maine, R. and Iliff, K.: Application of parameter estimation to aircraft stability and control, the output error approach. Tech. Rep., NASA RP 1168, 1986.
- [13] Mulder, J.: Design and evaluation of dynamic flight test manoeuvres. Tech. Rep., Delft Univ. of Technology, Dept. of Aerospace Engineering, Report LR-497, 1986.
- [14] Klein, V.: Estimation of aircraft aerodynamic parameters from flight data. *Progress in Aerospace Sciences*, vol. 26, no. 1, pp. 1–77, 1989.
- [15] Klein, V.: Identification evaluation methods. *Parameter Identification, AGARD-LS-104, Paper 2*, 1972.
- [16] Hamel, P. and Jategaonkar, R.: Evolution of flight vehicle system identification. *Journal of Aircraft*, vol. 33, pp. 9–28, Jan - Feb 1996.
- [17] *Journal of Aircraft*, vol. 41, No. 4, July - Aug, 2004.
- [18] *Journal of Aircraft*, vol. 42, Jan - Feb, 2005.
- [19] Koen, M.: Modelling and simulation of an rpv for flight control system design purposes.

- [20] Nasa history web page. 2009.
Available at: <http://history.nasa.gov/SP-367/appendc.htm>
- [21] Gaum, D.R.: *Aggressive Flight Control Techniques for a Fixed-Wing Unmanned Aerial Vehicle*. Master's thesis, University of Stellenbosch, 2009.
- [22] Peddle, I.K.: *Autonomous Flight of a Model Aircraft*. Master's thesis, University of Stellenbosch, 2005.
- [23] Etkin, B. and Reid, L.D.: *Dynamics of Flight: Stability and Control*. John Wiley & Sons, Ltd., 1996.
- [24] Schweppe, F.: *Uncertain Dynamic Systems*. Prentice-Hall, Upper Saddle River, NJ, 1973.
- [25] Fisher, R.: On an absolute criterion for fitting frequency curves. *Messenger of Mathematics*, vol. 41, pp. 155–160, 1912.
- [26] Jategaonkar, R. and Plaetschke, E.: Estimation of aircraft parameters using filter error methods and extended kalman filter. Tech. Rep., DFVLR Forschungsbericht 88-15, 1988.
- [27] Garcia-Velo, J. and Walker, B.: Aerodynamic parameter estimation for high-performance aircraft using extended kalman filter. Tech. Rep., AIAA Paper 95-3500, 1995.
- [28] Anton, H. and Rorres, C.: *Elementary Linear Algebra*. John Wiley & Sons, Ltd., 2005.
- [29] Tischler, M.: Frequency-response identification of xv-15 tilt-rotor aircraft dynamics. Tech. Rep., NASA, 1987.
- [30] Schroeder, M.: Synthesis of low-peak-factor signals and binary sequences with low autocorrelation. *IEEE Transactions on Information Theory*, vol. IT-18, No. 1, pp. 85–89, 1970.

- [31] Young, P. and Patton, R.: Comparison of test signals for aircraft frequency domain identification. *Journal of Guidance, Control, and Dynamics*, vol. 13, No. 3, pp. 430–438, 1990.
- [32] Bosworth, J. and Burken, J.: Tailored excitation for multivariable stability-margin measurement applied to the x-31a nonlinear simulation. *AIAA*, 1997.
- [33] Klein, V. and Murphy, P.: Aerodynamic parameters of high performance aircraft estimated from wind tunnel and flight test data. *System Identification for Integrated Aircraft Development and Flight Testing*, 1999.
- [34] Blaauw, D.: *Flight Control System for a Variable Stability Blended Wing-Body Unmanned Aerial Vehicle*. Master's thesis, University of Stellenbosch, 2009.
- [35] Basson, M.: *Stall Prevention Control of Fixed-Wing Unmanned Aerial Vehicles*. Master's thesis, University of Stellenbosch, 2010.
- [36] Blakelock, J.: *Automatic Control of Aircraft and Missiles, second edition*. John Wiley & Sons, 1991.
- [37] Lay, D.: *Linear Algebra and Its Applications, third edition*. Pearson Education Inc, 2003.
- [38] Kriel, S.: *A Comparison of Control Systems for the Flight Transition of VTOL Unmanned Aerial Vehicles*. Master's thesis, Stellenbosch University, 2008.
- [39] Diebel, J.: *Representing Attitude: Euler Angles, Unit Quaternions and Rotation Vector*. Stanford University, 2006.